Exploring Giant Planets and their Potential Moons in the Habitable Zone

Undergraduate Honours Thesis

Submitted in partial fulfillment of the requirements of
USQ Honours Thesis

By

Michelle L. Hill
ID No. 0061103417

Under the supervision of:

Prof. Stephen Kane
&
Prof. Brad Carter

UNIVERSITY OF SOUTHERN QUEENSLAND, COMPUTATIONAL ENGINEERING AND SCIENCE RESEARCH CENTRE
July 2018

Declaration of Authorship

I, Michelle L. Hill, declare that this Undergraduate Honours Thesis titled, 'Exploring Giant Planets and their Potential Moons in the Habitable Zone' and the work presented in it are my own. I confirm that:

- This work was done wholly or mainly while in candidature for a research degree at this University.
- Where any part of this thesis has previously been submitted for a degree or any other qualification at this University or any other institution, this has been clearly stated.
- Where I have consulted the published work of others, this is always clearly attributed.
- Where I have quoted from the work of others, the source is always given. With the exception of such quotations, this thesis is entirely my own work.
- I have acknowledged all main sources of help.
- Where the thesis is based on work done by myself jointly with others, I have made clear exactly what was done by others and what I have contributed myself.

Signed: _____

Date: _____

Certificate

This is to certify that the thesis entitled, "*Exploring Giant Planets and their Potential Moons in the Habitable Zone*" and submitted by Michelle L. Hill ID No. 0061103417 in partial fulfillment of the requirements of USQ Honours Thesis embodies the work done by her under our supervision.

Supervisor
Prof. Stephen Kane
Adjunct Professor,
University of Southern Queensland,
Computational Engineering and Science
Research Centre, Toowoomba, Queensland
4350, Australia
University of California, Riverside,
Department of Earth Sciences, CA 92521,
USA
Date:

Co-Supervisor
Prof. Brad Carter
Professor,
University of Southern Queensland,
Computational Engineering and Science
Research Centre, Toowoomba, Queensland
4350, Australia
Date:

UNIVERSITY OF SOUTHERN QUEENSLAND, COMPUTATIONAL ENGINEERING AND SCIENCE RESEARCH CENTRE

Abstract

Bachelor of Science (Hons.)

Exploring Giant Planets and their Potential Moons in the Habitable Zone

by Michelle L. Hill

The recent discovery of a disturbance in the orbital period of a transiting exoplanet observed with the *Kepler* space telescope has provided the first observational hints of a giant satellite orbiting a planet, or an *exomoon*. The detection and study of exomoons offers new ways to understand the formation and evolution of planetary systems, and widens the search for signs of life out in the universe. This thesis thus provides proposed exoplanet target lists to search for detectable exomoons and perform more detailed follow-up studies. Improved orbital parameters compared to previous studies have been calculated to aid exomoon searches, and relevant habitable zone boundaries have been added. The list of planets has initially been refined to select exoplanets circular orbits contained within either the optimistic habitable zone (OHZ) or the conservative habitable zone (CHZ). Taking a giant planet mass to be $0.02 M_J$ (Jupiter masses), 121 giant planets in the OHZ and 88 giant planets in the CHZ are found. The eccentricity of each planet's orbit are then taken into account. In total 61 giant planets eccentric orbits have been found to remain in the OHZ while 26 giant planets eccentric orbits remain in the CHZ. Each of the 121 giant planets radial velocity curves are run through *RadVel* (Fulton et al. 2018) to confirm the orbital solution and look for linear trends to determine if there are indications for additional companions; potentially either additional planets in orbit or satellites. Of the 121 giant planets tested, 51 show indications of orbital companions. The potential exomoon properties of each giant planet have been calculated and tabulated for future imaging missions, with the results including the Hill radius, Roche limit and expected angular separation of any potentially detectable exomoon.

Acknowledgements

I would first like to thank my thesis advisor's Prof. Stephen Kane and Prof. Brad Carter. Prof. Kane has always made the time to be available for video conferencing whenever I ran into a trouble spot or had a question about my research or writing and I am indebted to him for his guidance. Additionally, Prof. Carter was always quick to respond to emails and provide advice and encouragement during the project. I would like to thank them both sincerely for their time and help throughout the year.

I would also like to acknowledge Prof. Stephen Marsden and Prof. Rob Wittenmyer for being the examiners of this thesis, I am grateful to them for their very valuable comments on the introductory seminar, literature review and draft thesis throughout the year which helped lead to the completion of this thesis.

I would also like to thank the honours coordinators Joanna Turner and Linda Galligan for their continued support and assistance throughout the year. Without their administrative help this thesis could not have been successfully completed.

Finally, I must express my very profound gratitude to my parents and to my partner Ayo for providing me with unfailing support and continuous encouragement throughout my years of study and through the process of researching and writing this thesis. This accomplishment would not have been possible without them. Thank you.

Michelle Hill

Contents

List of Figures

List of Tables

Glossary

CHZ	conservative habitable zone. iii, 8, 10, 19, 20, 22, 25, 52, 54, 56, 60, 61, 65
HZ	habitable zone. 2, 8–10, 12–15, 19, 20, 24–26, 50, 52, 61–65, 68, 69
MAP	maximum a posteriori. 22, 53, 56–60
MCMC	Markov Chain Monte Carlo. 22, 53, 55
OHZ	optimistic habitable zone. iii, 8–10, 19, 20, 22, 25, 52, 57–59, 61, 65
RV	radial velocity. 3–6, 8, 15, 17, 18, 22, 61, 62, 65, 67

Chapter 1

Introduction

1.1 Introduction

The field of exoplanets is relatively young, with the detection of the first exoplanet less than 30 years ago. The first extra-solar planet was found around a pulsar star in 1992 (Wolszczan & Frail 1992), and then another orbiting a sun-like star was found in 1995 (Mayor & Queloz 1995). From these recent beginnings the field has grown quickly, with 3726 confirmed planets to date and over 2000 more candidates awaiting confirmation (NASA Exoplanet Archive 2018). While the progress of this number was initially quite slow due to the difficult process of discovering planets, with each new telescope erected on the ground or launched into space our resolution has improved and we have been able to detect many more planets than ever before. These planets orbiting stars outside our Solar system have already provided clues to many of questions regarding the origin and prevalence of life. They have provided further understanding of the formation and evolution of the planets within our Solar system, and influenced an escalation in the area of research into what constitutes a habitable planet that could support life.

While a main goal in the detections of exoplanets has been to find Earth like planets; planets of a similar size, distance from their star and composition as Earth, the hunt for exoplanets has

revealed examples of many different planetary systems that has caused us to revise our ideas as to what could be a potentially habitable world. Included in this are the giant exoplanets discovered in what is called the habitable zone (HZ) of their star, the region around a star where water, if it exists, can exist in a liquid state on the surface of a planet (Kasting, Whitmire, & Reynolds 1993). These giant planets are likely gas giants and thus are not considered habitable on their own, but they could possibly host large rocky, or terrestrial, exomoons which would also exist in the habitable zone and could themselves be ideal candidates for holding life given the right conditions (see Figure 1.1). In fact an exomoon may be considered to be even more habitable than Earth.

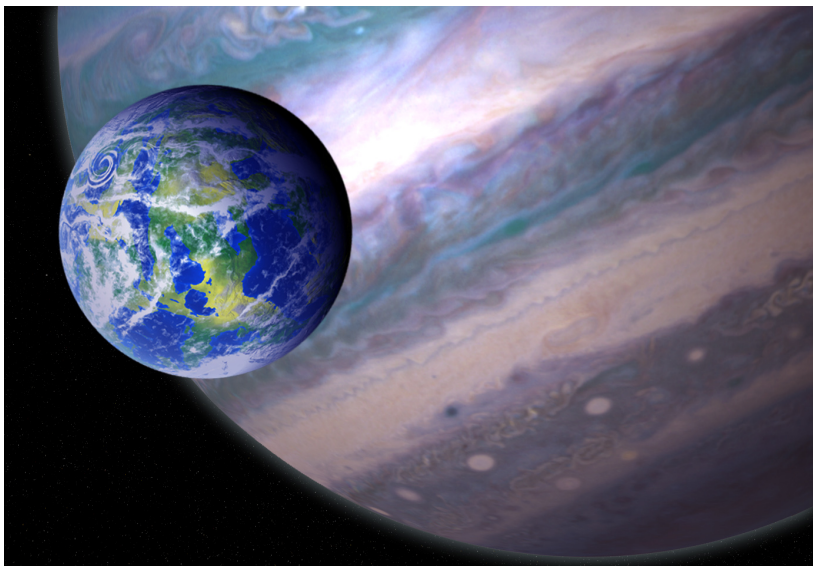

FIGURE 1.1: *An artistic impression of an Earth-like satellite orbiting a gas giant in the habitable zone of its star. Giant planets in the habitable zone could possibly host large rocky, or terrestrial, exomoons which would also exist in the habitable zone and could themselves be ideal candidates for holding life (NASA GSFC: Friedlander, J & Griswold, B 2018, pers. comm., 16 April).*

It was proposed by Heller (2012) that exomoons may be considered to have an even greater potential to hold life than that of Earth-like terrestrial planets. The thermal and reflected radiation from the host planet and the tidal effects on an exomoon can help increase the outer range of the HZ, creating a wider temperate zone in which a stable satellite may exist (Scharf 2006). The extra protection of the giant host planets magnetosphere can also increase the

likelihood that a large exomoon will hold on to its atmosphere, another essential ingredient to life as we know it (Heller & Zuluaga 2013).

This great potential for exomoons has for a long time motivated many others in the hunt for the first exomoon including Dr David Kipping and the HEK, or Hunt for Exomoons with Kepler team. [e.g. Kipping et al. 2012, 2013, 2013, 2014, 2015]. Last year the HEK team found the first potential signature of a planetary companion, Exomoon Candidate Kepler-1625b I (Teachey, Kipping & Schmitt 2017). Preliminary research indicates that Kepler-1625b is likely a Jupiter-sized planet with approximately ten times Jupiter's mass, orbited by a moon roughly the size of Neptune. Though this discovery is yet to be confirmed, it is the first real evidence of any such satellite and indicates the beginning of a new phase in the search for exoplanets.

This project contributes to the hunt for exomoons by providing a well refined list of the best radial velocity (RV) giant planets with the potential to hold large terrestrial exomoons, a giant planet being a planet with $\geq 0.02 M_J$. While there is a general consensus that the boundary between terrestrial and gaseous planets likely lies close to 1.6 Earth radii ($R_\oplus$) [e.g. Weiss & Marcy 2014, Rodgers 2015, Wolfgang, Rodgers & Ford 2016], $3R_\oplus$ is used as the cutoff to account for uncertainties in the stellar and planetary parameters and prevent the inclusion of potentially terrestrial planets in the list, as well as planets too small to host detectable exomoons. Using the mass-radius relation from Chen & Kipping (2016) this corresponds to a mass lower limit of $0.02 M_J$. Each giant planet included in this thesis has had their RV data analysed and their orbital parameters and planetary properties refined using the latest datasets. With the growing number of known exoplanets and the diversity of exoplanetary orbits, it is becoming an increasing challenge to maintain a procedure through which one can perform efficient target selection. So throughout the target list selection a method was developed, presented in Section 3, to systematically choose the best habitable zone planet candidates for follow up observations.

In Section 2 of this thesis the background of exoplanets is explored further, then an outline of methods are provided in Section 3. The results of the newly calculated orbital solutions of each RV giant planet residing in the habitable zone of its star are presented in Section 4, along with the Hill radius and Roche limit of the planet, the angular separation of any potential exomoon from its host planet, the results from testing the radial velocity data of each giant for linear trends with the RadVel program, and lastly a table outlining the telescope observation strategy. In Section 5 the calculations from Section 4 are discussed along with their implications for exomoons and proposals for observational prospects of the planets and potential moons are given. Then lastly concluding remarks and future plans are provided in Section 6.

Chapter 2

Literature Review

2.1 Exoplanets

2.1.1 Detection Methods

In the beginning of the hunt for exoplanets the primary method of detection was called the radial velocity RV method which involves detecting extremely small movements of the positions of the stars caused by the gravitational pull of the orbiting planet (Yaqoob 2011). The motion of a single planet in orbit around a star causes the star to undergo a reflex motion about the star-planet barycenter (Perryman 2011). This motion is detected through spectroscopy; observations of the spectrum of light emitted by a star. If the wavelength of characteristic spectral lines in the spectrum of the star increase and decrease regularly over a period, this indicates the presence of an orbiting body. The period of motion indicates the period of orbit of the planet. The size of the motion is related to the mass of the object orbiting the star, as well as the mass of the star and distance between the star and orbiting body. For a given star and distance, the more massive the orbiting object, the larger the reflex motion of the host star.

The first exoplanet found using this technique was a Jupiter sized planet with an orbital period of just 4.23 days (Mayor & Queloz 1995). The size and close proximity of the planet's orbit made it an ideal candidate for detection as this produced a relatively large movement of the star that was observable by our then relatively limited observational techniques. It is this ability to determine the mass (or at least a mass lower limit of $m \sin i$ if the inclination of the planets orbit is not known) of an object that continues to make RV detections and follow up observations particularly important. Without the mass of a planet, many orbital parameters cannot be constrained, and the likely structure and composition of an exoplanet would be impossible to determine. Thus this project uses only the data from those planets with properly constrained masses obtained through RV detection.

Another method of detection which is used primarily for multi-planet systems is timing variation. Here the periodic oscillation of the host star about the barycenter between itself and an already detected planet will show evidence of another orbiting body through the existence of additional periodic time signatures on the known planets orbit. Changes in the RV and astrometric position (perceived position in the sky as determined from Earth) of the known planet's orbit can provide evidence of another planetary body orbiting and can even give an estimated mass of the new planet or planets (Perryman 2011, Kipping et al. 2013, 2013). Timing variation is the method used primarily by the HEK team in the hunt for exomoons; by detecting the slight variations in transit depth of a transiting planet the existence of a orbiting satellite can be exposed.

The transit method is currently the most fruitful method of detection. It involves the very slight variation in the luminosity of a star when a planet passes directly in front of it from our line of sight as shown in Figure 2.1. Transits provide direct evidence for the radius of the planet. The larger the planet, the greater the amount of star light being blocked during a transit and so the transit light curve will provide evidence for the size of planet. This information is another of the key pieces needed to understand the likely structure and composition of an

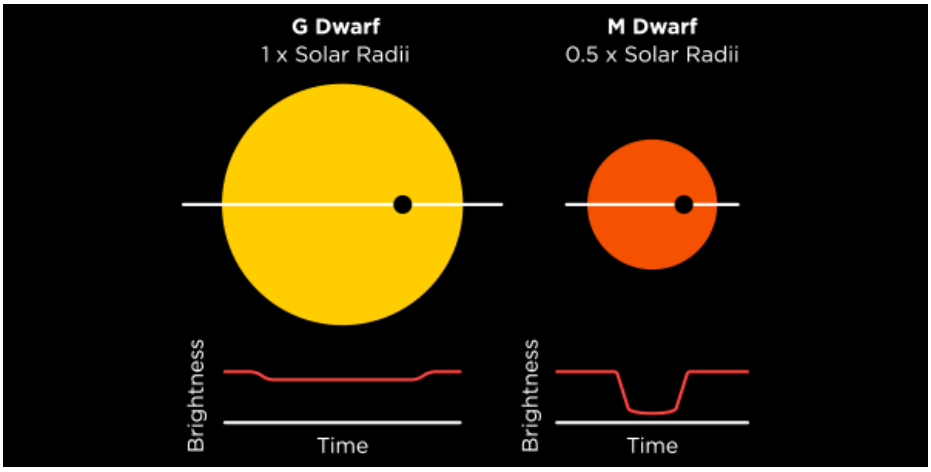

FIGURE 2.1: *The amount of star light being blocked during a transit will give an indication of the planet's radius provided the radius of the star is known (Planet Hunters, Accessed: January) 2018.*

exoplanet. Another advantage of the transit method is the ability to obtain information on the transiting planet's atmosphere. An exoplanet's spectral emission pattern can be studied to determine the composition of its atmosphere. The Sun emits a blackbody spectrum of light. Elements in the Sun's atmosphere absorb particular wavelengths of this light, leaving behind a distinct "fingerprint" of atomic absorption and emission spectral lines that indicate exactly what elements are in the atmosphere (Comins & Kaufmann 2012). Similarly, particles in the Earth's atmosphere absorb and emit wavelengths of the Sun's light, giving Earth its own spectral signature. By studying the emission and absorption features of the light received from the Sun from both ground based and space based telescopes the compositions of both the Sun and the Earth's atmospheres can be determined. This same technique can also be used to determine the composition of the atmospheres of planets outside our Solar system. When these planets transit their star, the spectrum received from the star will combine with the planet's own spectral fingerprint (Burrows 2014). Then if the planet passes behind the star, the planet's fingerprint will be completely blocked, leaving only the stars. By comparing the two spectra the elements that exist in the atmosphere of the planet can be determined (Kaltenegger, Traub & Jucks 2016).

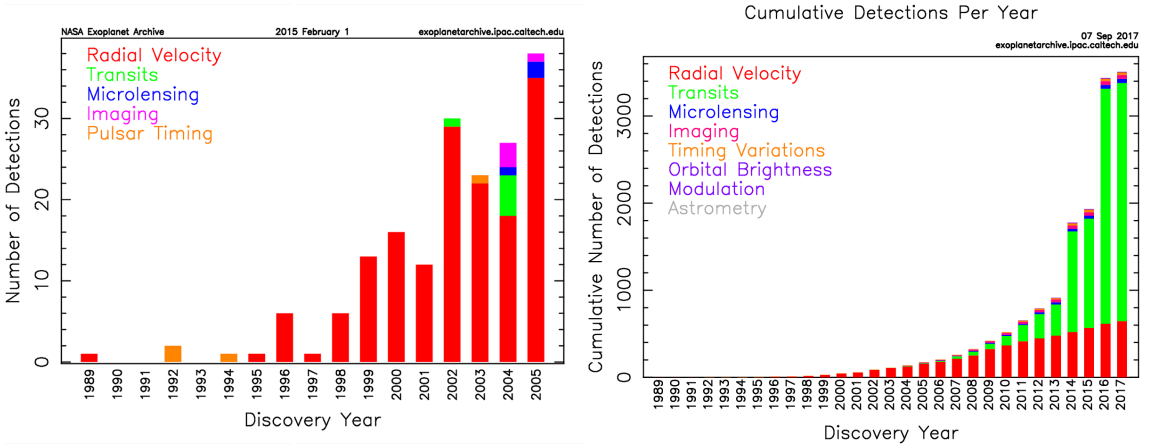

FIGURE 2.2: *Left Panel: The growth of exoplanet detections and their methods up to 2005. Radial velocity detection method dominated until the Kepler satellite launched in 2009. Right Panel: From Kepler launch, transits quickly became the leading detection method. (NASA Exoplanet Archive 2018)*

The success of the transit method of detection is primarily due to the launch of the *Kepler* space telescope, a NASA telescope charged with the mission to find terrestrial Earth-like planets located within the HZ of Sun-like stars (Barensten 2017). After *Kepler* launched in 2009, transits quickly overtook the RV technique of discovering exoplanets that had dominated exoplanet detection until then with only small contributions from the other techniques (see Figure 2.2).

2.1.2 The Search for Earth-like Planets

Among the many diverse planets detected by *Kepler* were some Earth-like planets as far out from their host star as the HZ of that star. The HZ is defined as the region around a star where water can exist in a liquid state on the surface of a planet with sufficient atmospheric pressure (Kasting, Whitmire, & Reynolds 1993). This is particularly important as the presence of liquid water is one of the necessary factors to support life as we know it. A planet can fall either into what we call the conservative habitable zone (CHZ) or the optimistic habitable zone (OHZ) (Kane et al. 2016). The CHZ runs from the runaway greenhouse limit where a chemical breakdown of water molecules by photons from the star will allow the now free hydrogen atoms

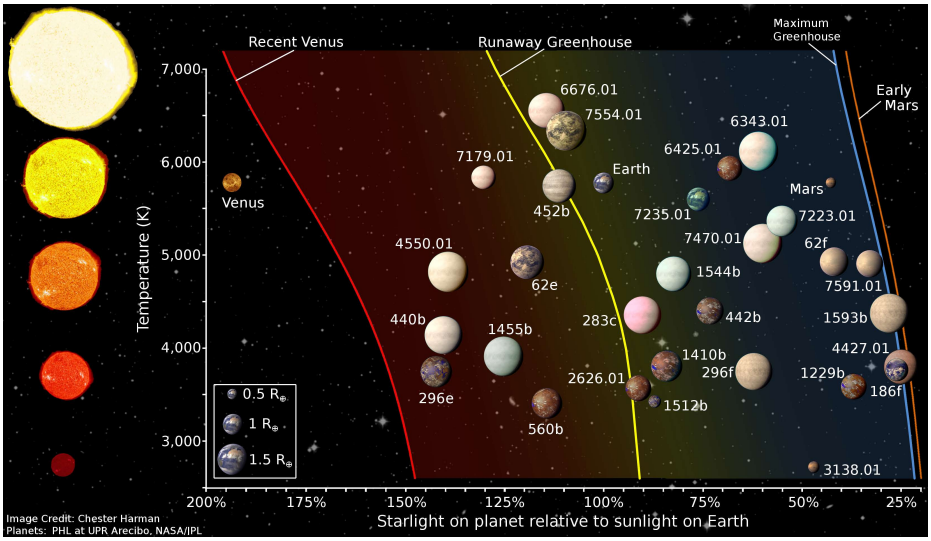

FIGURE 2.3: *Depiction of both the optimistic and conservative habitable zone boundaries. The planets portrayed here are representations of actual planets with* $< 2R\oplus$ *found in the HZ of their star. Note the x-axis is the amount of flux received from the star with Earth positioned at 100% (Harman 2015). Planets at the same distance around stars with a greater effective temperature will receive more flux from their host star, thus the habitable zone for hotter stars lies further away from the star than for cooler stars.*

to escape into space, thus completely drying out the planet at 0.99 AU in our Solar system (Kopparapu et al. 2014), to the maximum greenhouse effect at 1.7AU in our Solar system. Here the temperature on the planet drops to a point where CO_2 will condense permanently, which will in turn increase the planet's albedo or reflectivity, thus cooling the planet's surface to a point where all water is frozen (Kaltenegger & Sasselov 2011). The OHZ consists of the outer edge or the "early Mars" limit at 1.8 AU, based on the observation that Mars appears to have been habitable $\sim$ 3.8 Giga years ago. The inner edge, or the "recent Venus" limit, meanwhile lies at 0.75 AU in our Solar system, based on the empirical observation that the surface of Venus has been dry for at least a billion years (Kane, Kopparapu & Domagal-Goldman 2014). These distances will differ in other planetary systems in accordance with multiple factors including, but not limited to, the size of the star, the type of star, and the maturity of the star (see Figure 2.3). The width of the HZ will also change depending on if an orbiting body is solitary or has a companion, an attribute that will be explored later in this paper.

In a recent paper (Kane et al. 2016) I helped catalog all the HZ planets found by *Kepler* and found that within each HZ (both the OHZ and CHZ) there is a wide variety of planet sizes and particularly there is a surprising number of giant planets found in the HZ of their star; 76 Kepler candidates over $3R_{\oplus}$ were found in the OHZ. Typically giant planets are not looked for in terms of habitability, however these giant planets raise the possibility of the existence of large terrestrial exomoons that could themselves be candidates for holding life given the right conditions. The occurrence rates of these moons is directly linked to the occurrence rate of giant planets in that region. In Hill et al. (2018) (included in Appendix A) the frequency of giant planets within the OHZ was calculated using the inverse-detection-efficiency method. The frequency of giant planets $3.0 - 25R_{\oplus}$ in the OHZ was found to be $6.5 \pm 1.9\%$ for G stars, $11.5 \pm 3.1\%$ for K stars and $6 \pm 6\%$ for M stars. Comparing this with previously estimated occurrence rates of terrestrial planets in the HZ of G, K and M stars found in the literature, it was found that if each giant planet has only one large terrestrial moon then these moons are less likely to exist in the HZ than terrestrial planets. However, if each giant planet holds more than one moon, then the occurrence rates of moons in the HZ could be comparable to that of terrestrial planets, and could potentially be even more common (Hill et al. 2018).

2.2 Moons & Exomoons

2.2.1 Formation

A moon is generally defined as a body that orbits around a planet or asteroid and whose orbital barycenter is located inside the surface of the host planet or asteroid (International Astronomical Union 2006). Currently there are 175 known satellites orbiting the eight planets within the Solar system, most of which are in orbit around the two largest planets in our system with Jupiter hosting 69 known moons and Saturn hosting 62 known moons (Sheppard 2017). Moons have

been found to form in many different ways, leading to a wide variety in the compositions of these celestial bodies. In fact it is the compositions of the moons in the Solar system that have given insight into their likely methods of formation (Canup & Ward 2002, Heller, Marleau & Pudritz 2015). Most moons are thought to be formed from accretion of gas and dust circulating around planets in the early Solar system. Collisions between dust, rocks and gas due to their gravitational attraction causes the debris to gradually build, eventually growing to form a satellite (Elser et al. 2011). Other satellites may have been captured by the gravitational pull of a planet. If a celestial body passes within a planet's area of gravitational influence, or Hill radius, the planet can change the passing body's trajectory to then orbit the planet. This capture can occur before the formation of the planet during the proto-planet phase, an idea explored in the nebula drag theory (Pollack, Burns & Tauber 1979, Holt et al. 2017), or it can occur after the formation of the planet in a process called dynamical capture. Captured moons could have very different orbits and compositions to the host planet and most moons in the solar system with irregular orbits, such as those with high eccentricities, large inclinations, or even retrograde orbits, are expected to have been captured by their host planets (Nesvorny et al. 2003, Holt et al. 2017).

The widely accepted theory of the formation of Earth's Moon is known as the Giant-Collision formation theory. During formation the large proto-planet of Earth was orbiting in close proximity to another proto-planet approximately the size of Mars. The two proto-planet's mutual gravitational attraction caused them to collide, emitting a large debris disk into orbit around the Earth and from this material the Moon was formed (Hartmann & Davis 1975, Cameron & Ward 1976). This theory explains the similarities in the compositions of the Earth and Moon due to the initial close proximity of the proto-planets. The theoretical impact of the two large bodies also helps explain the above average size of Earth's Moon, which is significantly larger than is possible for any moon formed in situ with the Earth (Elser et al. 2011). The variety of possible formation methods of moons is promising as this can lead to a range in the

composition and size of moons, as is the number of moons in the Solar system, particularly the large number orbiting the Jovian planets which indicate a high probability of moons orbiting giant exoplanets.

2.2.2 Habitability Potential

The Solar system displays a breadth of variety in its moons, with wide ranges in terms of each moon's size, mass, and composition. Within each moon lies a diversity of geological phenomena and many of these Solar system satellites are examples of potentially life holding worlds. Five moons within the Solar system even show strong evidence of oceans beneath their surfaces: Ganymede, Europa and Callisto of Jupiter, as well as Enceladus and Titan of Saturn. Enceladus' geysers have been of enormous interest recently, some believing within the plumes lies the best potential for humanity to find evidence of life outside of Earth (Porco et al. 2006, Hsu et al. 2015). Ganymede, the largest moon in our Solar system, has its own magnetic field (Kivelson et al. 1996), an attribute deemed necessary to maintain the habitability of a moon as the magnetic field provides protection of the moons atmosphere from its host planet (Williams, Kasting & Wade 1997). And Io's volcanism (Morabito et al. 1979) is evidence of an internal heating mechanism that could contribute to the habitability of moons orbiting giant planets. Thus while the moons within our own HZ have shown no signs of life, namely Earth's Moon and the Martian moons of Phobos and Deimos, there is still habitability potential for the moons of giant exoplanets residing in their HZ.

Exomoons may be found to be even more habitable than Earth, an idea proposed by Dr Rene Heller, who has explored exomoon habitability in great detail [e.g. Heller 2012, Heller & Barnes 2012, 2013, Heller & Pudritz 2015, Zollinger, Armstrong & Heller 2017]. Exomoons have the potential to be "super-habitable" because they offer a diversity of energy sources to a potential biosphere, not just a reliance on the energy delivered by a star. The biosphere of a super-habitable

exomoon could receive energy from the reflected light and emitted heat of its nearby giant planet or even from the giant planet's gravitational field through tidal forces. These tidal forces can cause a moons crust to flex back and forth, creating friction that heats the moon from within. Thus exomoons should then expect to have a more stable, longer period in which the energy received could maintain a livable temperate surface condition for life to form and thrive in. Scharf (2006) proposed that this tidal heating mechanism can effectively increase the outer range of the HZ for a moon as the extra mechanical heating can compensate for the lack of stellar radiative heating provided to the moon. For the same reason, this could push out the interior edge of the HZ, causing any moon with surface water to undergo the runaway green house effect earlier than a lone body otherwise would, though the outwards movement of the inner edge has been found to be significantly less than that of the outer edge and so the effective habitable zone would still be widened for any exomoon. This variation could also enable giant exoplanets with eccentric orbits that lie, at times, outside the HZ to maintain habitable conditions on any connected exomoons, such as BD +14 4559 b in Figure 2.4 (Hinkel & Kane 2013).

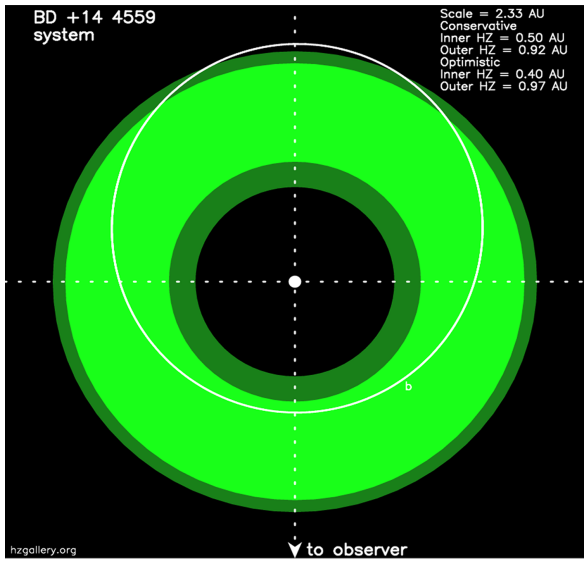

FIGURE 2.4: *The orbit of BD +14 4559 b lies just outside the habitable zone during a period of its orbit. Any satellite supported by this planet however could undergo tidal heating forces that enable it to have a surface that remains at habitable temperatures (Hinkel & Kane 2013).*

Exomoons found around giant planets in the HZ of their star have the potential advantage of being surrounded by a strong shield to protect their atmosphere from stellar winds. This added protection is provided by the giant planet's magnetosphere, which can stretch beyond the stable orbit of the moon (Heller & Zuluaga 2013). The planet's magnetosphere shields both itself and any moons within its boundary from stellar winds (see Figure 2.5). Provided the moon is large enough to hold its own magnetosphere and protect its atmosphere from being stripped away by the host planet itself, this added protection will increase the likelihood that a large exomoon will hold on to its atmosphere and thus contribute to the habitability of the moon.

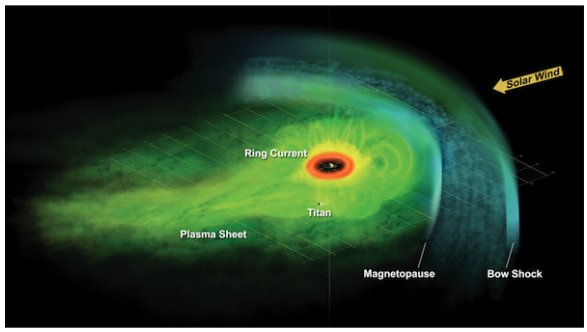

FIGURE 2.5: *Saturn's magnetosphere with Titan visibly within the magnetic boundary, or magnetopause. The magnetosphere of Saturn is so large that it envelops many of its moons, protecting them from stellar winds. Magnetospheres around giant planets can help protect the atmosphere of a moon from being stripped away and thus can contribute to the habitability of a satellite supported by the planet, provided the moon is large enough to stop its atmosphere from being stripped away by the planet itself (Phys.org 2013).*

2.2.3 Parameters Needed for Future Detection

Potential exomoons detected around a host planet will be found inside an envelope that is determined by the planets Hill radius and its Roche limit. The Hill radius is defined as the maximum distance that a body orbiting another larger body will remain in the gravitational influence of the larger mass body (Astakhov et al. 2003). Beyond the Hill radius the bodies are no longer gravitationally bound. Barnes & O'Brien (2002), Kipping, Fossey & Campanella (2009) and Hinkel & Kane (2013) found that 1/3 Hill radii was a conservative distance from

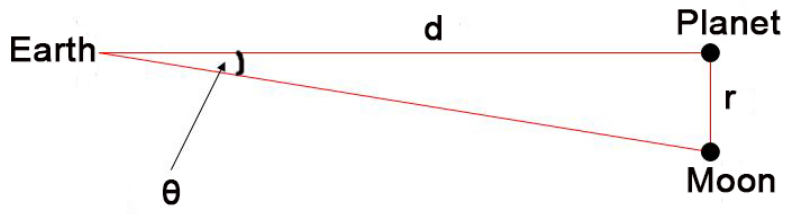

FIGURE 2.6: *The greater the angular separation of two objects the higher their likelihood of resolution as two bodies. As* $\theta = \frac{r}{d}$ *the greater the distance between the bodies, r, and the smaller the distance of the system from Earth, d, the greater the angular separation.*

the host planet that would ensure that the moon remained stable in its gravitationally bound orbit. On the inner edge the Roche limit is the closest distance a body may orbit another larger body before the gravitational pull of the larger body will start to break down/tear apart the smaller body (Hinkel & Kane 2013). This envelope between the Hill radius and Roche limit in which a potential exomoon can exist will help determine the resolution needed for future imaging missions. The greater the angular separation of a planet and its moon the higher their likelihood of resolution as two bodies (see Figure 2.6).

Both the Hill radius and Roche limit are determined by the mass of the host planet. This mass also effects the tidal heating properties a planet has on an orbiting exomoon and the possible angular separation of any such exomoon. Thus our project uses only the data from planets that have RV information and with it a mass lower limit of $M \sin i$.

The mass of the host planet not only determines the Hill radius, Roche limit and angular separation calculations above but will also determine the mass of any moon that forms in situ with the planet. Though, as moons can also be captured, this does not place a real limit to the mass of any satellite found around a giant planet. In fact Barnes & O'Brien (2002) found that "no meaningful mass limits can be placed on moons orbiting Jovian planets more than 0.6 AU from their parent stars". As the giant planets looked at in this project are in the HZ they will

reside beyond this limit and so no upper mass limit will apply to any potential exomoon in these systems.

Chapter 3

Method

3.1 Habitable Zone Giant Planet Data Analysis

The list of those exoplanets with RV information was extracted from the NASA Exoplanet Archive (2018) along with all their currently known parameters. A large portion of these planets were missing essential data including, but not limited to, their effective temperature, stellar radii, eccentricity, luminosity, and radial velocity semi-amplitude, and so a significant length of time was spent cleaning the data set. By using databases PASTEL (Ochsenbein, Bauer & Marcout 2000), HYPATIA (Hinkel & Burger 2014), and CELESTA (Chandler, McDonald & Kane 2015) to supplement the NASA Exoplanet Archive (2018), as well as the individual discovery papers of each planet, the missing parameters were either found or computed. For any stars still missing effective temperature information, the candidate was removed from the list (21 planets were dropped). For stars missing semi-major axis data, the values were calculated using:

$$P^2 = \frac{4\pi^2}{G(M_* + M_p)} a^3 \tag{3.1}$$

Where P is the Period of the planets orbit, G is the gravitational constant, M_* is the mass of the star, M_p the mass of the planet and a is the semi-major axis.

The stellar surface gravity *(log g)* information was then extracted from the NASA Exoplanet Archive (2018) to be used in determining the missing stellar radius information. Equation (3.2) was then used to estimate the radii of each star (obtained from Kane & Gelino 2012):

$$log(g) = log\frac{M_*}{M_\odot} - 2log\frac{R_*}{R_\odot} + log(g_\odot) \tag{3.2}$$

Here M_* is the mass of the star R_* is the radius of the star.

The stellar radius information was used to calculate the luminosity of each star with a RV planet using Equation (3.3), checking the calculations with known values.

$$L = 4\pi R_*^2 \sigma T^4 \tag{3.3}$$

Here σ is the Stefan-Boltzmann constant and T is the effective temperature of the star.

3.2 Calculating the Habitable Zone Boundaries

The mass radius relationship from Chen & Kipping (2016) was used to determine that $0.02M_J$ corresponds to $\geq 3R_\oplus$. The limit of $3R_\oplus$ was used as the giant planet cutoff to account for uncertainties in the stellar and planetary parameters and prevent the inclusion of potentially terrestrial planets in the list, as well as planets too small to host detectable exomoons.

$$R_p = M_p^{0.59} \tag{3.4}$$

R_p is the radius of planet in Earth radii and M_p is planet mass in Earth masses.

Using the code and equations from Kopparapu et al. (2013 & 2014), the four habitable zone flux boundaries (both the OHZ and CHZ boundaries) of all planets on the list (there were 1087 planets on the list at this stage) were calculated using a code written in Python. These calculations were then confirmed by checking against Ravi's online calculator (Kopparapu 2015). Each planet was checked to see if their semi major axis (a) lay within these zones. This would indicate that if their orbits were circular, they would stay in the HZ. 121 giant planets $\geq 0.02 M_J$ were found to have circular orbits remaining in the OHZ and 88 giant planets had circular orbits remaining in the CHZ.

Using Equations (3.5) and (3.6) the point of closest approach of the planet to the star (periastron) and furthest point of the orbit (apastron) was calculated. Using this data the eccentric orbits of each planet was analysed and the list was further refined to determine those planets whose eccentric orbits stayed in the HZ of their star. 61 giant planets $\geq 0.02 M_J$ were found to have eccentric orbits remaining in the OHZ and 26 giant planets had eccentric orbits remaining in the CHZ.

$$R_a = a(1 + e) \tag{3.5}$$

$$R_p = a(1 - e) \tag{3.6}$$

Where R_a = distance at apastron and R_p =distance at periastron, a is the semi-major axis and e is a planets eccentricity.

Due to the extra heating forces on a exomoon both the planets with eccentric orbits that lie entirely within the HZ and those whose orbits are only partially in the habitable zone are included in the list. As the heating forces effectively increase the outer edge of the HZ, the

moons that orbit slightly outside the HZ may still maintain a temperate surface temperature and thus should not be ruled out. For transparency each planet has been assigned a Group number which indicates the position of the planets orbit in relation to the HZ of the system. Group 1 is planets whose eccentric orbit lies in the CHZ, Group 2 is planets whose eccentric orbit lies in the OHZ, Group 3 is planets whose circular orbit lies in the CHZ, Group 4 is planets whose circular orbit lies in the OHZ.

3.3 Exomoon Calculations

For each potential exomoon holding candidate the Hill radius, Roche limit, maximum angular separation of the planet star system and the expected angular separation of any potential moons was calculated for use in future imaging missions. As part of this thesis project a Python code will be built to automate the calculation of the Hill radius, Roche limit and potential angular separations of each potential planet/moon pair. The Hill radius is calculated using:

$$r_H = a_{*p}\chi(1 - e_{*p})\left(\frac{M_p}{M_*}\right)^{\frac{1}{3}} \tag{3.7}$$

For those planets without eccentricity data, an eccentricity of $e = 0$ for the planet-star system is assumed and so Equation (3.7) becomes:

$$r_H = a_{*p}\chi\left(\frac{M_p}{M_*}\right)^{\frac{1}{3}} \tag{3.8}$$

Here r_H is the Hill radius, a_{*p} is the semi-major axis between the star and planet system, M_p is the mass of the planet and M_* the mass of the host star. The factor χ is added to take into account the fact that the Hill radius is just an estimate. Other effects may impact the

gravitational stability of the system, so following Barnes & O'Brien (2002), Kipping (2009) and Hinkel & Kane (2013), I have chosen to use a conservative estimate of $\chi \leq 1/3$ as any stable satellite around a giant planet is likely to reside within 1/3 of the planets Hill radius (Barnes & O'Brien 2002).

The maximum angular separation of the exomoon for its host planet is then calculated by:

$$\alpha" = \frac{\frac{1}{3}r_H}{d} \tag{3.9}$$

Where d is the distance of the planet - moon system from Earth.

The Roche limit, or closest orbital distance, is calculated using the equation obtained from Kane (2017). The equation is for what is called the fluid body Roche limit, where the body is treated as a collection of rocks/debris. In reality the bodies should be treated as somewhere between fluid and solid body but this project takes the conservative approach and uses the fluid body equation. This puts the Roche limit further away from the planet and so will give the moon a smaller envelope to reside in.

$$R_R \simeq 2.44 R_p \left(\frac{\rho_p}{\rho_m}\right)^{\frac{1}{3}} \tag{3.10}$$

Where R_p is the radius of the primary, ρ_p is the density of the primary, and ρ_m is the density of the satellite. As the size and mass of the potential satellites are unknown, 3 set density values have been used in the calculations: $\rho_m = 3,\ 4,\ 5\ g/cm^3$. These set values have been chosen to account for the various methods of formation available for moons. Moons that have formed in situ with giant planets would likely have relatively low densities as well as any satellites that may have formed outside the snow line and migrated inwards. These exomoons would likely have

lower densities and higher hydrogen content. Whereas more dense moons could have formed through collisions or capture of moons, asteroids or planets.

3.4 Confirming Orbital Solutions with RadVel

Each planets radial velocity curve was run through *RadVel* (Fulton et al. 2018) to confirm the orbital solution, starting with the most promising candidates whose eccentric orbits always stay within the CHZ, then those whose eccentric orbits always stay within the OHZ, then those whose circular orbits stay within the CHZ and finally those whose circular orbits stay within the OHZ.

RadVel enables users to model Keplerian orbits in RV time series. RadVel fits RVs using maximum a posteriori (MAP) and employs "modern Markov Chain Monte Carlo (MCMC) sampling techniques and robust convergence criteria to ensure accurately estimated orbital parameters and their associated uncertainties" (Fulton et al. 2018). RadVel allows users to either fix parameters or allow them to float free, as well as impose priors and perform Bayesian model comparison. The five orbital parameters this project used are the orbital period (P), the time of periastron (Tp), orbital eccentricity (e), the argument of periastron of the star's orbit (ω), and the velocity semi-amplitude (K). Jitter (σ) was also input for inclusion in uncertainty measurements to account for any noise from astrophysical and instrumental sources.

Once the MCMC chains are well mixed and the orbital parameters which maximize the posterior probability are found, RadVel then supplies an output of the final parameter values from the MAP fit, and provides radial velocity time series plots and MCMC corner plots showing all joint posterior distributions derived from the MCMC sampling.

3.5 Target Selection

After determining which planets show indications of linear trends an observing strategy was created, outlining which targets are best reserved for either the *MINERVA Australis*, *Keck HIRES* or *Lick Automated Planet Finder (APF)* telescopes. Each giant planet was assigned to the telescope that is best qualified to carry out follow-up observations. The magnitude, radial velocity semi-amplitude and position of the star were all considered during this selection process. Future projects will use these telescopes to make observations of what is deemed the highest priority on the refined list provided in this thesis.

Chapter 4

Results

4.1 Results

The parameters used in this project's calculations are provided in Table 4.1. The parameters were extracted and compiled from the NASA Exoplanet Archive (2018) as well as the PASTEL (Ochsenbein, Bauer & Marcout 2000), HYPATIA (Hinkel & Burger 2014), and CELESTA (Chandler, McDonald & Kane 2015) catalogs. The calculations of the planet HZ flux boundaries and their corresponding HZ physical boundaries are presented in Table 4.2. Calculations of Hill radii, Roche limit (with moon densities of 3, 4, and 5 g/cm^3), and angular separation of the potential planet/moon systems at $\frac{1}{3}$ Hill radii are presented in Table 4.3. These estimates can be used in deciding the ideal candidates for future imaging missions. Each giant planet's radial velocity curve was analysed in the *RadVel* program (Fulton et al. 2018) to confirm the orbital solution and look for linear trends to determine if there were indications for additional companions; potentially either additional planets in orbit or satellites. Table 4.4 provides the results of our *RadVel* data analysis, indicating those planets with indications linear trends. Of 128 giant planets in the HZ of their star, 55 planets showed indications of linear trends $\geq 3\sigma$. The

telescope observing strategies for the MINERVA Australis, KECK Hires and LICK Automated Planet Finder (APF) telescopes are outlined Tables 4.5 and 4.6. For those planets where more than one telescope is capable of observation, the telescope for whom that target will be assigned as priority is listed first, priority here determined by expected telescope time available. The targets that are not observable with these telescopes or whom are missing required data are left blank.

To aid with priority selection for follow up observations, the planets are listed in order of planet mass within each table. Those planets with a larger mass will have a larger radial velocity signature, as well as the ability to potentially support a larger moon or satellite, so are the highest priority for future observations.

In each table the second column is the Group column. Each Group indicates the position of the planets orbit in relation to the HZ of the system. Group 1 is the highest priority Group which includes planets whose eccentric orbits always stay within the CHZ. Group 2 is the next highest priority and includes those planets whose eccentric orbits always stay within the OHZ. Accounting for uncertainties in eccentricity, Groups 3 and 4 include the planets with circular orbits: Group 3 includes planets whose circular orbits stay within the CHZ and Group 4 includes those whose circular orbits stay within the OHZ. Note that some planets are in multiple groups e.g. Group 1 is a subset of each of the other groups as it has the most constricted criteria.

Within the Tables there is missing data where parameters were unable to be found from any sources available. For each missing parameter and their subsequent calculations the space has been left blank, including any uncertainty calculations that did not have the required elements to allow completion.

Below the Tables are the Figures presenting the results of the calculations (Figures 4.1 - 4.5) as well as some of the radial velocity fits from the *RadVel* curve analysis and an example of the

Markov-Chain Monte Carlo (MCMC) posterior distributions (Figures 4.7 - 4.13). Each *RadVel* curve fit provides two windows at the top containing the fit and residuals sequentially, followed by a window for each known planets individual fit.

4.2 Tables

4.2.1 Table Glossary

A GLOSSARY OF TABLE ABBREVIATIONS:

S-M Axis = Semi-major axis

Teff = Effective Temperature

Mag = Magnitude

Venus = Recent Venus limit

Run GH = Runaway Greenhouse limit

Max GH = Maximum Greenhouse limit

Mars = Early Mars limit

Venus HZ = Recent Venus HZ boundary

Run GH HZ = Runaway Greenhouse HZ boundary

Max GH HZ = Maximum Greenhouse HZ boundary

Mars HZ = Early Mars HZ boundary

4.2.2. *Tables: Parameters*

Table 1. Habitable Zone Giant Planets $\geq 3R_{\oplus}$: Parameters

Planet	Group	Period	S-M Axis	Eccentricity	Planet Mass	Distance	Teff	Stellar Mass	Luminosity	Mag
		Days	au		M_J	PC	K	$M_{\oplus}$	$L_{\odot}$	V
GJ 163 c	4	25.6 ± 0	0.125 ± 0	0.099 ± 0.086	0.021 ± 0.003	14.97 ± 0.45	3500 ± 100	0.4 ± 0.02	0.02 ± 0.023	11.81
LHS 1140 b	2,3,4	24.7 ± 0	0.088 ± 0.004	0.29±	0.021 ± 0.006	12.47 ± 0.42	3131 ± 100	0.15 ± 0.02	0.003 ± 0.031	14.18
HD 40307 g	2,3,4	197.8 ± 7.4	0.6 ± 0.034	0.29 ± 0.3	0.022 ± 0.008	12.83 ± 0.09	4956 ± 50	0.77 ± 0.05	0.23 ± 0.06	7.17
GJ 3293 d	1,2,3,4	48.1 ± 0.1	0.194 ± 0	0.12 ± 0.11	0.024 ± 0.003	15.77 ± 0.07	3466 ± 49	0.42±	0.022 ± 0.079	11.962
HD 69830 d	4	197 ± 3	0.63±	0.07 ± 0.07	0.057±	12.58 ± 0.12	5385 ± 20	0.86 ± 0.03	0.603 ± 0.02	6
GJ 687 b	1,2,3,4	38.1 ± 0	0.164 ± 0	0.04 ± 0.076	0.058 ± 0.007	4.53 ± 0.02	3413 ± 28	0.41 ± 0.04	0.021 ± 0.005	9.15
HD 10180 g	2,3,4	604.7 ± 10.4	1.427 ± 0.028	0.263 ± 0.152	0.073 ± 0.014	39.02 ± 1.1	5911 ± 19	1.06 ± 0.05	1.348 ± 0.115	7.321
GJ 3293 b	2,4	30.6 ± 0	0.143 ± 0	0.06 ± 0.04	0.074 ± 0.003	15.77 ± 0.07	3466 ± 49	0.42±	0.022 ± 0.079	11.962
Kepler-62 f	1,2,3,4	267.3 ± 0	0.718 ± 0.007	0.094 ± 0.002	0.11±	368±	4925 ± 70	0.69 ± 0.02	0.21 ± 0.042	13.725
Kepler-22 b	2,4	289.9 ± 0	0.849 ± 0.018	0±	0.113±	190±	5518 ± 44	0.97 ± 0.06	0.791 ± 0.022	11.664
Kepler-62 e	2,4	122.4 ± 0	0.427 ± 0.004	0.13 ± 0.112	0.113±	368±	4925 ± 70	0.69 ± 0.02	0.21 ± 0.042	13.725
K2-3 d	4	44.6 ± 0	0.208 ± 0.01	0.045 ± 0.045	0.117 ± 0.0034	42 ± 2	3896 ± 189	0.6 ± 0.09	0.065 ± 0.604	12.17
55 Cnc f	3,4	262 ± 0.5	0.788 ± 0.001	0.305 ± 0.075	0.141 ± 0.012	12.53 ± 0.13	5196 ± 24	0.91 ± 0.01	0.582 ± 0.011	5.96
BD-06 1339 c	2,3,4	125.9 ± 0.4	0.435 ± 0.007	0.31 ± 0.11	0.17 ± 0.03	20.1 ± 0.67	4324 ± 100	0.7±	0.095 ± 0.046	9.7
HD 218566 b	2,3,4	225.7 ± 0.4	0.687 ± 0.001	0.3 ± 0.1	0.21 ± 0.02	29.94 ± 1.07	4820±	0.85 ± 0.03	0.353 ± 0.04	8.628
Kepler-34 b	4	288.8 ± 0.1	1.09 ± 0.001	0.182 ± 0.018	0.22 ± 0.011	1499 ± 33	5913 ± 130	1.05 ± 0	1.489 ± 0.038	14.875
HD 137388 A b	2,3,4	330 ± 3	0.89 ± 0.02	0.36 ± 0.12	0.223 ± 0.029	38.45 ± 2.79	5240 ± 53	0.86±	0.46 ± 0.018	8.696
HD 7199 b	3,4	615 ± 7	1.36 ± 0.02	0.19 ± 0.16	0.29 ± 0.023	35.88 ± 0.89	5386 ± 45	0.89±	0.7 ± 0.023	8.027
HIP 57050 b	2,3,4	41.4 ± 0	0.164 ± 0	0.314 ± 0.086	0.298 ± 0.025	11.03 ± 0.37	3200±	0.34 ± 0.03	0.015±	11.92
GJ 649 b	3,4	598.3 ± 4.2	1.135 ± 0.035	0.3 ± 0.08	0.328 ± 0.032	10.32 ± 0.16	3700 ± 60	0.54 ± 0.05	1±	9.69
HD 564 b	1,2,3,4	492.3 ± 2.3	1.2 ± 0.02	0.096 ± 0.067	0.33 ± 0.03	53.6±	5902 ± 61	0.96 ± 0.05	1.109 ± 0.156	8.29
Kepler-16 b	1,2,3,4	228.8 ± 0	0.705 ± 0.001	0.007 ± 0.001	0.333 ± 0.016	61±	4450 ± 150	0.69 ± 0	0.148 ± 0.02	11.762
HD 181720 b	2,3,4	956 ± 14	1.78±	0.26 ± 0.06	0.37±	55.93 ± 4.12	5781 ± 18	0.92±	1.941 ± 0.024	7.849
HD 164509 b	4	282.4 ± 3.8	0.875 ± 0.008	0.26 ± 0.14	0.48 ± 0.09	51.81 ± 2.88	5922 ± 44	1.13 ± 0.02	1.151 ± 0.05	8.103
PH2 b	4	282.5 ± 0	0.828 ± 0.009	0.41 ± 0.185	0.49 ± 0.104	–	5629 ± 42	0.94 ± 0.02	0.791 ± 0.047	12.62
HD 99109 b	1,2,3,4	439.3 ± 5.6	1.105 ± 0.065	0.09 ± 0.16	0.502 ± 0.07	60.46 ± 4.82	5272±	0.93±	0.659 ± 0.046	9.1

Table 1 continued on next page

Table 1 *(continued)*

Planet	Group	Period	S-M Axis	Eccentricity	Planet Mass	Distance	Teff	Stellar Mass	Luminosity	Mag
		Days	au		M_J	PC	K	$M_\oplus$	$L_\odot$	V
HD 44219 b	4	472.3 ± 5.7	1.19 ± 0.02	0.61 ± 0.08	0.58 ± 0.05	50.4 ± 2	5752 ± 16	1±	1.82 ± 0.201	7.69
HD 43197 b	3,4	327.8 ± 1.2	0.92 ± 0.015	0.83 ± 0.03	0.6 ± 0.08	56.3 ± 3.9	5508 ± 46	0.96±	0.729 ± 0.044	8.98
HD 63765 b	2,3,4	358 ± 1	0.94 ± 0.016	0.24 ± 0.043	0.64 ± 0.05	32.62 ± 0.74	5432 ± 19	0.87 ± 0.03	0.745 ± 0.059	8.104
HD 45364 c	2,3,4	342.9 ± 0.3	0.897±	0.097 ± 0.012	0.658±	32.58 ± 0.86	5428 ± 16	0.82 ± 0.05	0.821 ± 0.064	8.062
HD 170469 b	3,4	1145 ± 18	2.1±	0.11 ± 0.08	0.67±	64.98 ± 4.71	5810 ± 44	1.14 ± 0.03	1.6 ± 0.146	8.21
HD 37124 b	4	154.4 ± 0.1	0.534 ± 0	0.054 ± 0.028	0.675 ± 0.017	33.24 ± 1.27	5424 ± 67	0.85±	0.464 ± 0.059	7.7
GJ 876 c	2,3,4	30.1 ± 0	0.13 ± 0	0.256 ± 0.001	0.714 ± 0.004	4.7 ± 0.05	3350±	0.33 ± 0.03	0.013±	10.191
HD 156411 b	4	842.2 ± 14.5	1.88 ± 0.035	0.22 ± 0.08	0.74 ± 0.045	55.1 ± 2.53	5900 ± 15	1.25±	5.383 ± 0.476	6.673
HD 197037 b	4	1035.7 ± 13	2.07 ± 0.05	0.22 ± 0.07	0.79 ± 0.05	32.83 ± 0.65	6098 ± 57	1.11±	1.504 ± 0.177	6.813
HD 34445 b	3,4	1049 ± 11	2.07 ± 0.02	0.27 ± 0.07	0.79 ± 0.07	45.01 ± 2.13	5836 ± 44	1.07 ± 0.02	2.009 ± 0.044	7.328
Kepler-68 d	2,3,4	625 ± 16	1.396 ± 0.033	0.18 ± 0.05	0.84 ± 0.05	135 ± 10	5793 ± 74	1.08 ± 0.05	1.563 ± 0.039	9.99
HD 17674 b	1,2,3,4	623.8 ± 1.6	1.42 ± 0.045	0.13±	0.87 ± 0.065	44.5 ± 0.8	5904 ± 22	0.98 ± 0.1	1.516 ± 0.281	7.56
HD 128356 b	3,4	298.2 ± 1.6	0.87 ± 0.03	0.57 ± 0.08	0.89 ± 0.07	26.03 ± 0.52	4875 ± 100	0.65 ± 0.05	0.36 ± 0.012	8.29
HD 10647 b	4	989.2 ± 8.1	2.015 ± 0.011	0.15 ± 0.08	0.94 ± 0.08	17.35 ± 0.19	6218 ± 20	1.11 ± 0.02	1.409 ± 0.08	5.52
HD 114729 b	1,2,3,4	1114 ± 15	2.11 ± 0.12	0.167 ± 0.055	0.95 ± 0.1	35 ± 1.19	5821±	1±	2.216 ± 0.145	6.68
HD 219415 b	3,4	2093.3 ± 32.7	3.2±	0.4 ± 0.09	1±	169.78±	4820 ± 20	1 ± 0.1	4.169 ± 0.15	8.94
HD 160691 b	1,2,3,4	643.3 ± 0.9	1.497±	0.128 ± 0.017	1.08±	15.28 ± 0.19	5807 ± 30	1.08 ± 0.05	1.6 ± 0.141	5.15
Kepler-97 c	1,2,3,4	789±	1.638±	0±	1.08±	–	5779 ± 74	0.94 ± 0.06	0.96 ± 0.227	12.872
HD 114783 b	3,4	493.7 ± 1.8	1.16 ± 0.019	0.144 ± 0.032	1.1 ± 0.06	20.4 ± 0.4	5135 ± 44	0.85 ± 0.03	0.44 ± 0.048	7.55
HD 73534 b	2,3,4	1770 ± 40	3.067 ± 0.068	0.074 ± 0.071	1.103 ± 0.087	81 ± 4.9	5041 ± 44	1.23 ± 0.06	3.327 ± 0.057	8.23
HD 9174 b	1,2,3,4	1179 ± 34	2.2 ± 0.09	0.12 ± 0.05	1.11 ± 0.14	78.93 ± 3.86	5577 ± 100	1.03 ± 0.05	2.41 ± 0.033	8.4
HD 100777 b	3,4	383.7 ± 1.2	1.03 ± 0.03	0.36 ± 0.02	1.16 ± 0.03	52.8 ± 3.19	5582 ± 24	1.01 ± 0.1	1.05±	8.418
HD 28254 b	3,4	1116 ± 26	2.15 ± 0.045	0.81 ± 0.035	1.16 ± 0.08	54.7 ± 1.55	5664 ± 35	1.06±	2.188 ± 0.215	7.684
HD 147513 b	2,3,4	528.4 ± 6.3	1.32±	0.26 ± 0.05	1.21±	12.87 ± 0.14	5883±	1.11±	0.977±	5.39
HD 216435 b	1,2,3,4	1311 ± 49	2.56 ± 0.17	0.07 ± 0.078	1.26 ± 0.13	33.29 ± 0.81	5999 ± 60	1.3±	2.798 ± 0.296	6.03
HD 65216 b	1,2,3,4	572.4 ± 2.1	1.3 ± 0.03	0 ± 0.02	1.26 ± 0.04	35.59 ± 0.88	5666±	0.92±	0.71±	7.964
HD 108874 b	2,3,4	395.8 ± 0.6	1.038 ± 0.014	0.082 ± 0.021	1.29 ± 0.06	68.5 ± 5.8	5551 ± 44	0.95 ± 0.04	1.074 ± 0.107	7.06
HD 210277 b	3,4	442.2 ± 0.5	1.138 ± 0.066	0.476 ± 0.017	1.29 ± 0.11	21.29 ± 0.36	5555±	1.01±	0.756 ± 0.053	6.53
HD 19994 b	2,4	466.2 ± 1.7	1.305 ± 0.016	0.063 ± 0.062	1.37 ± 0.12	22.38 ± 0.38	6188 ± 44	1.36 ± 0.04	2.602 ± 0.245	5.06

Table 1 continued on next page

Table 1 *(continued)*

Planet	Group	Period	S-M Axis	Eccentricity	Planet Mass	Distance	Teff	Stellar Mass	Luminosity	Mag
		Days	au		M_J	PC	K	$M_\oplus$	$L_\odot$	V
HD 30562 b	3,4	1159.2 ± 2.8	2.315 ± 0.004	0.778 ± 0.013	1.373 ± 0.047	26.5 ± 0.63	5994 ± 46	1.23 ± 0.03	2.708 ± 0.226	5.78
HD 133131 A b	3,4	649 ± 3	1.44 ± 0.005	0.33 ± 0.03	1.42 ± 0.04	47±	5799 ± 19	0.95±	1±	8.4
HD 20782 b	3,4	597.1 ± 0	1.397 ± 0.009	0.956 ± 0.004	1.43 ± 0.03	35.5 ± 0.8	5798 ± 44	1.02 ± 0.02	1.203 ± 0.125	7.4
HD 48265 b	2,4	780.3 ± 4.6	1.81 ± 0.07	0.08 ± 0.05	1.47 ± 0.12	85.4 ± 4.23	5650 ± 100	1.28 ± 0.05	3.837 ± 0.022	8.05
BD+14 4559 b	2,3,4	268.9 ± 1	0.777±	0.29 ± 0.03	1.47±	50.03 ± 4.06	5008 ± 20	0.86 ± 0.15	0.479 ± 0.223	9.63
HD 188015 b	1,2,3,4	461.2 ± 1.7	1.203 ± 0.07	0.137 ± 0.026	1.5 ± 0.13	52.63 ± 2.64	5746±	1.09±	1.047 ± 0.073	8.234
HD 23127 b	3,4	1214 ± 9	2.4 ± 0.3	0.44 ± 0.07	1.5 ± 0.2	89.13 ± 6.07	5626 ± 69	1.13 ± 0.1	2.062 ± 0.235	8.55
HD 4113 b	3,4	526.6 ± 0.3	1.28±	0.903 ± 0.005	1.56 ± 0.04	44.05 ± 1.93	5688 ± 26	0.99±	1.219±	7.881
HIP 109384 b	3,4	499.5 ± 0.3	1.134 ± 0.029	0.549 ± 0.003	1.56 ± 0.08	56.2 ± 2.7	5180 ± 45	0.78 ± 0.06	1±	9.63
WASP-47 c	2,3,4	580.7 ± 9.6	1.41 ± 0.3	0.36 ± 0.12	1.57 ± 0.795	200 ± 30	5576 ± 68	1.11 ± 0.69	1.166 ± 0.582	11.9
HD 221585 b	1,2,3,4	1173 ± 16	2.306 ± 0.081	0.123 ± 0.069	1.61 ± 0.14	53.59 ± 1.99	5620 ± 27	1.19 ± 0.12	2.642 ± 0.03	7.465
HD 142415 b	3,4	386.3 ± 1.6	1.05±	0.5±	1.62±	34.57 ± 1.01	6045±	1.03±	1.148±	7.327
16 Cyg B b	3,4	798.5 ± 1	1.681 ± 0.097	0.681 ± 0.017	1.68 ± 0.15	21.41 ± 0.23	5674±	0.99±	1.166 ± 0.079	6.25
HD 82943 b	2,3,4	441.5 ± 0.4	1.183 ± 0.001	0.162 ± 0.036	1.681 ± 0.028	27.46 ± 0.64	6016±	1.2±	1.419 ± 0.096	6.53
HD 45350 b	4	963.6 ± 3.4	1.92 ± 0.07	0.778 ± 0.009	1.79 ± 0.14	48.95 ± 2.36	5616±	1.02±	1.247 ± 0.085	7.885
HD 216437 b	4	1256 ± 35	2.32±	0.29 ± 0.12	1.82±	26.52 ± 0.41	5714 ± 108	1.15 ± 0.1	1.799 ± 0.254	6.05
HD 4203 b	3,4	437.1 ± 0.3	1.174 ± 0.022	0.52 ± 0.02	1.82 ± 0.05	77.82 ± 7.77	5702±	1.13±	1.276 ± 0.086	8.687
HD 190647 b	2,3,4	1038.1 ± 4.9	2.07 ± 0.06	0.18 ± 0.02	1.9 ± 0.06	54.23 ± 3.25	5628 ± 20	1.1 ± 0.1	1.982±	7.775
HD 20868 b	3,4	380.9 ± 0.1	0.947 ± 0.012	0.75 ± 0.002	1.99 ± 0.05	48.9 ± 3.5	4795 ± 124	0.78 ± 0.03	0.296 ± 0.055	9.92
kap CrB b	4	1261.9 ± 26.4	2.8 ± 0.075	0.044±	2±	30.5 ± 0.2	4788 ± 17	1.47 ± 0.04	12.134 ± 0.007	4.82
HD 159868 b	1,2,3,4	1178.4 ± 8.8	2.25 ± 0.03	0.01 ± 0.03	2.1 ± 0.11	52.72 ± 2.99	5558 ± 15	1.09 ± 0.03	2.934 ± 0.219	7.242
NGC 26..978 b	1,2,3,4	511.2 ± 2	1.39±	0.16 ± 0.07	2.18 ± 0.17	628.9 ± 185.9	4200 ± 21	1.37 ± 0.02	1±	9.71
HD 154857 b	4	408.6 ± 0.5	1.291 ± 0.008	0.46 ± 0.02	2.24 ± 0.05	68.54 ± 4.29	5605±	1.72 ± 0.03	2.74 ± 0.188	7.238
HD 73526 c	4	379.1 ± 0.5	1.03 ± 0.02	0.28 ± 0.05	2.25 ± 0.13	94.61 ± 9.12	5493 ± 14	1.01 ± 0.05	1.735 ± 0.132	8.971
GJ 876 b	1,2,3,4	61.1 ± 0	0.208 ± 0	0.032 ± 0.001	2.276 ± 0.005	4.7 ± 0.05	3350±	0.33 ± 0.03	0.013±	10.191
HD 145934 b	1,2,3,4	2730 ± 100	4.6 ± 0.14	0.053 ± 0.058	2.28 ± 0.26	−	4899 ± 44	1.75 ± 0.1	14.942 ± 2.995	8.5
HD 163607 c	2,3,4	1314 ± 8	2.42 ± 0.01	0.12 ± 0.06	2.29 ± 0.16	69.44 ± 3.09	5543 ± 44	1.09 ± 0.02	2.301 ± 0.038	7.979
HD 4732 c	2,3,4	2732 ± 81	4.6 ± 0.23	0.23 ± 0.07	2.37 ± 0.38	56.5 ± 3.17	4959 ± 25	1.74 ± 0.17	15.488 ± 2.673	5.89
HD 23079 b	1,2,3,4	730.6 ± 5.7	1.596 ± 0.093	0.102 ± 0.031	2.45 ± 0.21	34.6 ± 0.67	5927 ± 44	1.01±	1.5 ± 0.145	7.12

Table 1 continued on next page

Table 1 *(continued)*

Planet	Group	Period	S-M Axis	Eccentricity	Planet Mass	Distance	Teff	Stellar Mass	Luminosity	Mag
		Days	au		M_J	PC	K	$M_\oplus$	$L_\odot$	V
GJ 317 b	2,3,4	692 ± 2	1.15 ± 0.05	0.11 ± 0.05	2.5 ± 0.55	15.1 ± 0.22	3510 ± 50	0.42 ± 0.05	1±	11.97
47 UMa b	2,3,4	1078 ± 2	2.1 ± 0.02	0.032 ± 0.014	2.53 ± 0.065	14.08 ± 0.13	5892 ± 70	1.03 ± 0.05	1.634 ± 0.078	5.05
HD 196885 b	3,4	1333 ± 15	2.37 ± 0.02	0.48 ± 0.06	2.58 ± 0.16	32.99 ± 0.89	6254 ± 44	1.28 ± 0.05	2.399 ± 0.03	6.398
HD 164604 b	2,3,4	606.4 ± 9	1.3 ± 0.05	0.24 ± 0.14	2.7 ± 1.3	37.98 ± 2.67	4618 ± 80	0.8±	1±	9.7
HD 153950 b	4	499.4 ± 3.6	1.28 ± 0.01	0.34 ± 0.021	2.73 ± 0.05	51.87 ± 3.41	6076 ± 13	1.12 ± 0.03	2.218 ± 0.034	7.39
HD 165155 b	1,2,3,4	434.5 ± 2.1	1.13 ± 0.04	0.2 ± 0.03	2.89 ± 0.23	64.98 ± 7.26	5426 ± 100	1.02 ± 0.05	0.7 ± 0.05	9.36
HD 125612 b	3,4	559.4 ± 1.3	1.37±	0.46 ± 0.01	3±	52.83 ± 3.93	5900 ± 18	1.09 ± 0.03	1.089±	8.317
HD 221287 b	2,3,4	456.1 ± 6.8	1.25 ± 0.04	0.08 ± 0.11	3.09 ± 0.79	52.88 ± 2.3	6304 ± 45	1.25 ± 0.1	1.66±	7.807
HD 1605 c	1,2,3,4	2111 ± 37	3.52 ± 0.05	0.098 ± 0.027	3.48 ± 0.12	84.6 ± 6.63	4757 ± 50	1.31 ± 0.11	6.607 ± 0.05	7.52
HD 92788 b	4	325 ± 0.5	0.96±	0.35 ± 0.01	3.58±	32.32 ± 1.04	5821±	1.1±	1.047±	7.3
HD 183263 b	2,3,4	626.5 ± 1.1	1.51 ± 0.087	0.357 ± 0.009	3.67 ± 0.3	52.83 ± 2.97	5936±	1.17 ± 0.1	1.395 ± 0.095	7.861
KELT-6 c	1,2,3,4	1276 ± 74	2.39 ± 0.11	0.21 ± 0.038	3.71 ± 0.21	222 ± 8	6272 ± 61	1.13 ± 0.06	3.246 ± 0.724	10.418
HD 169830 c	4	2102 ± 264	3.6±	0.33 ± 0.02	4.04±	36.32 ± 1.2	6299±	1.4±	4.592±	5.902
ups And d	3,4	1276.5 ± 0.6	2.513 ± 0.001	0.299 ± 0.007	4.132 ± 0.029	13.47 ± 0.13	6027 ± 26	1.3±	2.878 ± 0.05	4.1
Kepler-454 c	1,2,3,4	523.9 ± 0.7	1.286 ± 0.017	0.021 ± 0.008	4.46 ± 0.12	–	5701 ± 34	1.03 ± 0.04	1.084 ± 0.046	11.57
HD 213240 b	3,4	951 ± 42	2.03±	0.45 ± 0.04	4.5±	40.75 ± 1.35	5886 ± 52	1.14 ± 0.06	2.103 ± 0.213	6.814
HD 111998 b	1,2,3,4	825.9 ± 6.2	1.82 ± 0.07	0.03 ± 0.04	4.51 ± 0.5	32.73 ± 0.32	6557 ± 96	1.18 ± 0.12	3.483 ± 0.543	6.11
HD 16175 b	3,4	995.4 ± 2.8	2.148 ± 0.076	0.637 ± 0.02	4.77 ± 0.37	59.84 ± 3.49	6022 ± 34	1.34 ± 0.14	3.221 ± 0.034	7.282
HD 13908 c	2,3,4	931 ± 17	2.03 ± 0.04	0.12 ± 0.02	5.13 ± 0.25	66.89 ± 3.82	6255 ± 66	1.29 ± 0.04	3.999 ± 0.623	7.508
HD 28185 b	1,2,3,4	385.9 ± 0.6	1.032 ± 0.019	0.092 ± 0.019	5.59 ± 0.33	39.6 ± 1.7	5546 ± 75	0.98 ± 0.05	0.864 ± 0.12	7.81
HD 224538 b	3,4	1189.1 ± 5.1	2.28 ± 0.08	0.464 ± 0.022	5.97 ± 0.42	77.76 ± 4.41	6097 ± 100	1.34 ± 0.05	2.951 ± 0.025	8.06
HIP 67851 c	4	2131.8 ± 88.3	3.82 ± 0.23	0.17 ± 0.06	5.98 ± 0.76	65.96 ± 1.7	4890 ± 100	1.63 ± 0.22	17.539 ± 0.066	6.17
HD 70573 b	4	851.8 ± 11.6	1.76 ± 0.05	0.4 ± 0.1	6.1 ± 0.4	45.7±	5737 ± 70	1 ± 0.1	1±	11.424
Kepler-424 c	2,4	223.3 ± 2.1	0.73 ± 0.075	0±	6.97 ± 0.62	–	5460 ± 81	1.01 ± 0.05	0.708 ± 0.065	14.256
HD 86264 b	3,4	1475 ± 55	2.86 ± 0.07	0.7 ± 0.2	7 ± 1.6	72.57 ± 4.34	6300 ± 44	1.4 ± 0.04	3.187 ± 0.306	7.407
Kepler-419 c	4	675.5 ± 0.1	1.68 ± 0.03	0.184 ± 0.002	7.3 ± 0.4	–	6430 ± 79	1.39 ± 0.08	4.638 ± 0.604	13.005
HD 23596 b	2,3,4	1561 ± 12	2.772 ± 0.062	0.266 ± 0.014	7.71 ± 0.39	52 ± 2.3	5904 ± 44	1.16 ± 0.06	4.229 ± 0.397	7.244
HD 222582 b	3,4	572.4 ± 0.6	1.347 ± 0.078	0.725 ± 0.012	7.75 ± 0.65	41.95 ± 1.96	5727±	0.99±	1.252 ± 0.086	7.68
HD 33564 b	3,4	388 ± 3	1.1±	0.34 ± 0.02	9.1±	20.98 ± 0.23	6250±	1.25 ± 0.04	1±	5.08

Table 1 continued on next page

Table 1 *(continued)*

Planet	Group	Period	S-M Axis	Eccentricity	Planet Mass	Distance	Teff	Stellar Mass	Luminosity	Mag
		Days	au		M_J	PC	K	$M_\oplus$	$L_\odot$	V
HD 141937 b	3,4	653.2 ± 1.2	1.488 ± 0.01	0.41 ± 0.01	9.316 ± 0.329	33.46 ± 1.21	5879 ± 70	1.03 ± 0.02	1.052 ± 0.073	7.25
30 Ari B b	4	335.1 ± 2.5	0.995 ± 0.012	0.289 ± 0.092	9.88 ± 0.94	39.43 ± 1.72	6300 ± 60	1.16 ± 0.04	1.803 ± 0.165	7.458
HD 38801 b	2,4	696.3 ± 2.7	1.7 ± 0.037	0±	10.7 ± 0.5	99.4 ± 17.73	5222 ± 44	1.36 ± 0.09	4.56 ± 0.045	8.269
HD 217786 b	4	1319 ± 4	2.38 ± 0.04	0.4 ± 0.05	13 ± 0.8	54.8 ± 2	5966 ± 65	1.02 ± 0.03	1.888 ± 0.254	7.8
HAT-P-13 c	4	446.3 ± 0.2	1.226 ± 0.025	0.662 ± 0.005	14.28 ± 0.28	214 ± 12	5653 ± 90	1.22 ± 0.08	2.218 ± 0.061	10.622
HD 214823 b	3,4	1877 ± 15	3.18 ± 0.12	0.154 ± 0.014	19.2 ± 1.4	97.47 ± 8.42	6215 ± 30	1.22 ± 0.13	4.345 ± 0.058	8.068
Kepler-47 c	3,4	303.1 ± 0	0.991 ± 0.016	0.411±	28±	1500±	5636 ± 100	1.05 ± 0.06	0.839 ± 0.035	15.178

4.2.3. *Tables: Habitable Zone Calculations*

Table 2. Habitable Zone Giant Planets $\geq 3R_\oplus$: Habitable Zone Calculations

Planet Name	Group	Periastron	Apastron	Venus	Run GH	Max GH	Mars	Venus HZ	Run GH HZ	Max GH HZ	Mars HZ
		au	au	$Flux_\oplus$	$Flux_\oplus$	$Flux_\oplus$	$Flux_\oplus$	au	au	au	au
GJ 163 c	4	0.113	0.138	1.49	0.932	0.247	0.222	0.115	0.145	0.282	0.297
LHS 1140 b	2,3,4	0.062	0.113	1.48	0.924	0.236	0.212	0.045	0.057	0.112	0.119
HD 40307 g	2,3,4	0.426	0.774	1.62	1.01	0.308	0.277	0.376	0.477	0.863	0.91
GJ 3293 d	1,2,3,4	0.171	0.217	1.49	0.931	0.246	0.221	0.121	0.154	0.299	0.315
HD 69830 d	4	0.586	0.674	1.7	1.06	0.332	0.298	0.595	0.754	1.347	1.422
GJ 687 b	1,2,3,4	0.157	0.17	1.49	0.93	0.244	0.22	0.12	0.151	0.295	0.311
HD 10180 g	2,3,4	1.052	1.802	1.8	1.12	0.364	0.327	0.865	1.097	1.924	2.03
GJ 3293 b	2,4	0.135	0.152	1.49	0.931	0.246	0.221	0.121	0.154	0.299	0.315
Kepler-62 f	1,2,3,4	0.65	0.786	1.62	1.01	0.306	0.275	0.36	0.456	0.828	0.874
Kepler-22 b	2,4	0.849	0.849	1.72	1.07	0.34	0.306	0.678	0.86	1.525	1.607
Kepler-62 e	2,4	0.371	0.483	1.62	1.01	0.306	0.275	0.36	0.456	0.828	0.874
K2-3 d	4	0.198	0.217	1.51	0.943	0.26	0.234	0.207	0.262	0.499	0.526
55 Cnc f	3,4	0.548	1.028	1.66	1.04	0.321	0.289	0.592	0.748	1.347	1.419
BD-06 1339 c	2,3,4	0.3	0.57	1.55	0.964	0.277	0.249	0.248	0.314	0.586	0.618

Table 2 continued on next page

Table 2 *(continued)*

Planet Name	Group	Periastron	Apastron	Venus	Run GH	Max GH	Mars	Venus HZ	Run GH HZ	Max GH HZ	Mars HZ
		au	au	$Flux_{\oplus}$	$Flux_{\oplus}$	$Flux_{\oplus}$	$Flux_{\oplus}$	au	au	au	au
HD 218566 b	2,3,4	0.481	0.893	1.6	0.999	0.301	0.27	0.47	0.595	1.083	1.144
Kepler-34 b	4	0.891	1.288	1.8	1.12	0.364	0.327	0.91	1.153	2.023	2.134
HD 137388 A b	2,3,4	0.57	1.21	1.67	1.04	0.324	0.291	0.525	0.665	1.192	1.258
HD 7199 b	3,4	1.102	1.618	1.7	1.06	0.332	0.298	0.642	0.813	1.452	1.532
HIP 57050 b	2,3,4	0.112	0.215	1.485	0.9256	0.238	0.215	0.101	0.128	0.252	0.265
GJ 649 b	3,4	0.795	1.476	1.5	0.937	0.253	0.228	0.816	1.033	1.988	2.094
HD 564 b	1,2,3,4	1.085	1.315	1.8	1.12	0.363	0.327	0.785	0.995	1.748	1.842
Kepler-16 b	1,2,3,4	0.7	0.71	1.56	0.971	0.283	0.254	0.309	0.391	0.724	0.765
HD 181720 b	2,3,4	1.317	2.243	1.78	1.11	0.356	0.32	1.044	1.322	2.335	2.463
HD 164509 b	4	0.648	1.103	1.81	1.13	0.365	0.328	0.797	1.009	1.776	1.873
PH2 b	4	0.489	1.167	1.74	1.09	0.347	0.312	0.674	0.852	1.51	1.592
HD 99109 b	1,2,3,4	1.006	1.204	1.68	1.04	0.325	0.292	0.626	0.796	1.423	1.502
HD 44219 b	4	0.464	1.916	1.77	1.1	0.354	0.318	1.014	1.286	2.267	2.392
HD 43197 b	3,4	0.156	1.684	1.72	1.07	0.34	0.305	0.651	0.826	1.465	1.547
HD 63765 b	2,3,4	0.714	1.166	1.7	1.06	0.335	0.301	0.662	0.838	1.491	1.573
HD 45364 c	2,3,4	0.81	0.985	1.7	1.06	0.335	0.301	0.695	0.88	1.566	1.652
HD 170469 b	3,4	1.869	2.331	1.78	1.11	0.358	0.322	0.948	1.2	2.114	2.229
HD 37124 b	4	0.505	0.562	1.7	1.06	0.334	0.301	0.523	0.662	1.179	1.242
GJ 876 c	2,3,4	0.096	0.163	1.49	0.929	0.243	0.218	0.093	0.118	0.231	0.244
HD 156411 b	4	1.466	2.294	1.8	1.12	0.363	0.327	1.729	2.192	3.851	4.057
HD 197037 b	4	1.615	2.525	1.85	1.15	0.376	0.338	0.902	1.144	2	2.109
HD 34445 b	3,4	1.511	2.629	1.79	1.11	0.359	0.323	1.059	1.345	2.366	2.494
Kepler-68 d	2,3,4	1.145	1.647	1.78	1.11	0.357	0.321	0.937	1.187	2.093	2.207
HD 17674 b	1,2,3,4	1.235	1.605	1.8	1.12	0.364	0.327	0.918	1.164	2.041	2.153
HD 128356 b	3,4	0.374	1.366	1.61	1	0.304	0.273	0.473	0.6	1.088	1.148
HD 10647 b	4	1.713	2.317	1.87	1.17	0.383	0.344	0.868	1.098	1.918	2.024
HD 114729 b	1,2,3,4	1.758	2.462	1.78	1.11	0.358	0.322	1.116	1.413	2.488	2.623
HD 219415 b	3,4	1.92	4.48	1.6	0.999	0.301	0.27	1.614	2.043	3.721	3.929
HD 160691 b	1,2,3,4	1.305	1.689	1.78	1.11	0.358	0.322	0.948	1.201	2.114	2.229

Table 2 continued on next page

Table 2 *(continued)*

Planet Name	Group	Periastron	Apastron	Venus	Run GH	Max GH	Mars	Venus HZ	Run GH HZ	Max GH HZ	Mars HZ
		au	au	$Flux_{\oplus}$	$Flux_{\oplus}$	$Flux_{\oplus}$	$Flux_{\oplus}$	au	au	au	au
Kepler-97 c	1,2,3,4	1.638	1.638	1.78	1.11	0.356	0.32	0.734	0.93	1.642	1.732
HD 114783 b	3,4	0.993	1.327	1.65	1.03	0.318	0.286	0.516	0.653	1.176	1.24
HD 73534 b	2,3,4	2.84	3.294	1.64	1.02	0.312	0.281	1.424	1.806	3.265	3.441
HD 9174 b	1,2,3,4	1.936	2.464	1.73	1.08	0.344	0.309	1.18	1.494	2.647	2.793
HD 100777 b	3,4	0.659	1.401	1.73	1.08	0.344	0.309	0.779	0.986	1.747	1.843
HD 28254 b	3,4	0.409	3.892	1.75	1.09	0.349	0.314	1.118	1.417	2.504	2.64
HD 147513 b	2,3,4	0.977	1.663	1.8	1.12	0.362	0.326	0.737	0.934	1.643	1.731
HD 216435 b	1,2,3,4	2.381	2.739	1.82	1.14	0.37	0.332	1.24	1.567	2.75	2.903
HD 65216 b	1,2,3,4	1.3	1.3	1.75	1.09	0.349	0.314	0.637	0.807	1.426	1.503
HD 108874 b	2,3,4	0.953	1.123	1.73	1.08	0.342	0.307	0.788	0.997	1.772	1.871
HD 210277 b	3,4	0.596	1.68	1.73	1.08	0.342	0.308	0.661	0.837	1.487	1.567
HD 19994 b	2,4	1.223	1.387	1.87	1.16	0.381	0.343	1.18	1.498	2.614	2.754
HD 30562 b	3,4	0.514	4.116	1.82	1.14	0.369	0.332	1.22	1.541	2.709	2.856
HD 133131 A b	3,4	0.965	1.915	1.78	1.11	0.357	0.321	0.75	0.949	1.674	1.765
HD 20782 b	3,4	0.061	2.733	1.78	1.11	0.357	0.321	0.822	1.041	1.836	1.936
HD 48265 b	2,4	1.665	1.955	1.75	1.09	0.348	0.313	1.481	1.876	3.321	3.501
BD+14 4559 b	2,3,4	0.552	1.002	1.63	1.02	0.311	0.279	0.542	0.685	1.241	1.31
HD 188015 b	1,2,3,4	1.038	1.368	1.77	1.1	0.354	0.318	0.769	0.976	1.72	1.815
HD 23127 b	3,4	1.344	3.456	1.74	1.09	0.346	0.311	1.089	1.375	2.441	2.575
HD 4113 b	3,4	0.124	2.436	1.76	1.1	0.35	0.315	0.832	1.053	1.866	1.967
HIP 109384 b	3,4	0.511	1.757	1.66	1.03	0.32	0.288	0.776	0.985	1.768	1.863
WASP-47 c	2,3,4	0.902	1.918	1.73	1.08	0.343	0.309	0.821	1.039	1.844	1.942
HD 221585 b	1,2,3,4	2.022	2.59	1.74	1.09	0.346	0.311	1.232	1.557	2.764	2.915
HD 142415 b	3,4	0.525	1.575	1.83	1.14	0.372	0.335	0.792	1.004	1.757	1.851
16 Cyg B b	3,4	0.536	2.826	1.75	1.09	0.35	0.314	0.816	1.034	1.826	1.927
HD 82943 b	2,3,4	0.991	1.375	1.83	1.14	0.37	0.333	0.881	1.116	1.959	2.065
HD 45350 b	4	0.426	3.414	1.74	1.09	0.346	0.311	0.847	1.07	1.899	2.003
HD 216437 b	4	1.647	2.993	1.76	1.1	0.352	0.316	1.011	1.279	2.261	2.386
HD 4203 b	3,4	0.563	1.784	1.76	1.1	0.351	0.316	0.852	1.077	1.907	2.01

Table 2 continued on next page

Table 2 *(continued)*

Planet Name	Group	Periastron	Apastron	Venus	Run GH	Max GH	Mars	Venus HZ	Run GH HZ	Max GH HZ	Mars HZ
		au	au	$Flux_{\oplus}$	$Flux_{\oplus}$	$Flux_{\oplus}$	$Flux_{\oplus}$	au	au	au	au
HD 190647 b	2,3,4	1.697	2.443	1.74	1.09	0.347	0.312	1.067	1.348	2.39	2.52
HD 20868 b	3,4	0.237	1.657	1.6	0.997	0.299	0.269	0.43	0.545	0.995	1.049
kap CrB b	4	2.677	2.923	1.6	0.997	0.299	0.269	2.754	3.489	6.37	6.716
HD 159868 b	1,2,3,4	2.228	2.273	1.73	1.08	0.343	0.308	1.302	1.648	2.925	3.087
NGC 26..978 b	1,2,3,4	1.168	1.613	1.53	0.957	0.272	0.244	0.808	1.022	1.917	2.024
HD 154857 b	4	0.697	1.885	1.74	1.08	0.345	0.31	1.255	1.593	2.818	2.973
HD 73526 c	4	0.742	1.318	1.72	1.07	0.338	0.304	1.004	1.274	2.266	2.389
GJ 876 b	1,2,3,4	0.202	0.215	1.49	0.929	0.243	0.218	0.093	0.118	0.231	0.244
HD 145934 b	1,2,3,4	4.356	4.844	1.61	1.01	0.305	0.274	3.046	3.846	6.999	7.385
HD 163607 c	2,3,4	2.13	2.71	1.73	1.08	0.341	0.307	1.153	1.46	2.598	2.738
HD 4732 c	2,3,4	3.542	5.658	1.62	1.01	0.308	0.277	3.092	3.916	7.091	7.478
HD 23079 b	1,2,3,4	1.433	1.759	1.81	1.13	0.365	0.328	0.91	1.152	2.027	2.139
GJ 317 b	2,3,4	1.024	1.277	1.5	0.932	0.247	0.222	0.816	1.036	2.012	2.122
47 UMa b	2,3,4	2.033	2.167	1.8	1.12	0.363	0.326	0.953	1.208	2.122	2.239
HD 196885 b	3,4	1.232	3.508	1.88	1.17	0.385	0.346	1.13	1.432	2.496	2.633
HD 164604 b	2,3,4	0.988	1.612	1.58	0.983	0.291	0.261	0.796	1.009	1.854	1.957
HD 153950 b	4	0.845	1.715	1.84	1.15	0.374	0.336	1.098	1.389	2.435	2.569
HD 165155 b	1,2,3,4	0.904	1.356	1.7	1.06	0.334	0.301	0.642	0.813	1.448	1.525
HD 125612 b	3,4	0.74	2	1.8	1.12	0.363	0.327	0.778	0.986	1.732	1.825
HD 221287 b	2,3,4	1.15	1.35	1.89	1.18	0.388	0.349	0.937	1.186	2.068	2.181
HD 1605 c	1,2,3,4	3.175	3.865	1.59	0.994	0.297	0.267	2.038	2.578	4.717	4.974
HD 92788 b	4	0.624	1.296	1.78	1.11	0.358	0.322	0.767	0.971	1.71	1.803
HD 183263 b	2,3,4	0.971	2.049	1.81	1.13	0.366	0.329	0.878	1.111	1.952	2.059
KELT-6 c	1,2,3,4	1.888	2.892	1.89	1.17	0.386	0.347	1.311	1.666	2.9	3.059
HD 169830 c	4	2.412	4.788	1.89	1.18	0.388	0.349	1.559	1.973	3.44	3.627
ups And d	3,4	1.763	3.264	1.83	1.14	0.371	0.334	1.254	1.589	2.785	2.935
Kepler-454 c	1,2,3,4	1.258	1.314	1.76	1.1	0.351	0.316	0.785	0.993	1.757	1.852
HD 213240 b	3,4	1.117	2.944	1.8	1.12	0.362	0.326	1.081	1.37	2.41	2.54
HD 111998 b	1,2,3,4	1.765	1.875	1.95	1.22	0.403	0.363	1.336	1.69	2.94	3.098

Table 2 continued on next page

Table 2 *(continued)*

Planet Name	Group	Periastron	Apastron	Venus	Run GH	Max GH	Mars	Venus HZ	Run GH HZ	Max GH HZ	Mars HZ
		au	au	$Flux_{\oplus}$	$Flux_{\oplus}$	$Flux_{\oplus}$	$Flux_{\oplus}$	au	au	au	au
HD 16175 b	3,4	0.78	3.516	1.83	1.14	0.371	0.333	1.327	1.681	2.947	3.11
HD 13908 c	2,3,4	1.786	2.274	1.88	1.17	0.385	0.346	1.459	1.849	3.223	3.4
HD 28185 b	1,2,3,4	0.937	1.127	1.73	1.08	0.342	0.307	0.707	0.894	1.589	1.677
HD 224538 b	3,4	1.222	3.338	1.85	1.15	0.376	0.338	1.263	1.602	2.802	2.955
HIP 67851 c	4	3.171	4.469	1.61	1.01	0.304	0.274	3.301	4.167	7.596	8.001
HD 70573 b	4	1.056	2.464	1.77	1.1	0.354	0.318	0.752	0.953	1.681	1.773
Kepler-424 c	2,4	0.73	0.73	1.71	1.07	0.337	0.302	0.643	0.813	1.449	1.531
HD 86264 b	3,4	0.858	4.862	1.89	1.18	0.388	0.349	1.299	1.643	2.866	3.022
Kepler-419 c	4	1.371	1.989	1.92	1.2	0.396	0.356	1.554	1.966	3.422	3.61
HD 23596 b	2,3,4	2.035	3.509	1.8	1.12	0.364	0.327	1.533	1.943	3.408	3.596
HD 222582 b	3,4	0.37	2.324	1.77	1.1	0.353	0.317	0.841	1.067	1.883	1.987
HD 33564 b	3,4	0.726	1.474	1.88	1.17	0.385	0.346	0.729	0.925	1.612	1.7
HD 141937 b	3,4	0.878	2.098	1.8	1.12	0.362	0.326	0.764	0.969	1.705	1.796
30 Ari B b	4	0.707	1.283	1.89	1.18	0.388	0.349	0.977	1.236	2.155	2.273
HD 38801 b	2,4	1.7	1.7	1.67	1.04	0.322	0.29	1.653	2.094	3.763	3.966
HD 217786 b	4	1.428	3.332	1.82	1.13	0.367	0.33	1.019	1.293	2.268	2.392
HAT-P-13 c	4	0.415	2.037	1.75	1.09	0.348	0.313	1.126	1.427	2.525	2.662
HD 214823 b	3,4	2.69	3.67	1.87	1.17	0.383	0.344	1.524	1.927	3.368	3.554
Kepler-47 c	3,4	0.584	1.398	1.75	1.09	0.347	0.312	0.693	0.878	1.555	1.64

4.2.4. *Tables: Exomoon calculations*

Table 3. Habitable Zone Giant Planets $\geq 3R_{\oplus}$: Potential Satellite Calculations

Planet Name	Group	Roche ($\rho = 3g/cm$)	Roche ($\rho = 4g/cm$)	Roche ($\rho = 5g/cm$)	Hill Radius	Angular Seperation
		x10^{-6} au	x10^{-6} au	x10^{-6} au	au	x10^{-6}″
GJ 163 c	4	241.1 ± 11.3	219.1 ± 10.2	203.4 ± 9.5	0.003 ± 0	65 ± 12
GJ 3293 d	1,2,3,4	250.2 ± 10.5	227.3 ± 9.5	211.1 ± 8.8	0.004±	95±

Table 3 continued on next page

Table 3 *(continued)*

Planet Name	Group	Roche ($\rho = 3g/cm$)	Roche ($\rho = 4g/cm$)	Roche ($\rho = 5g/cm$)	Hill Radius	Angular Seperation
		x10^{-6} au	x10^{-6} au	x10^{-6} au	au	x10^{-6}″
HD 40307 g	2,3,4	244.5 ± 29.2	222.1 ± 26.6	206.2 ± 24.7	0.009 ± 0.006	232 ± 146
LHS 1140 b	2,3,4	239.3 ± 22.9	217.4 ± 20.8	201.9 ± 19.3	0.002 ± 0	59 ± 13
HD 69830 d	4	334.3 ± 0	303.7 ± 0	281.9 ± 0	0.016±	429±
GJ 687 b	1,2,3,4	336.2 ± 13.5	305.5 ± 12.3	283.6 ± 11.4	0.006 ± 0.001	411 ± 64
GJ 3293 b	2,4	364.8 ± 4.9	331.4 ± 4.5	307.6 ± 4.2	0.005±	109±
HD 10180 g	2,3,4	363.3 ± 23.2	330.1 ± 21	306.5 ± 19.5	0.029 ± 0.009	252 ± 84
Kepler-22 b	2,4	419.9 ± 0	381.5 ± 0	354.2 ± 0	0.028±	50±
Kepler-62 e	2,4	419.9 ± 0	381.5 ± 0	354.2 ± 0	0.014±	13±
Kepler-62 f	1,2,3,4	416.2 ± 0	378.1 ± 0	351 ± 0	0.024±	22±
K2-3 d	4	424.8 ± 4.1	386 ± 3.7	358.3 ± 3.5	0.008 ± 0.001	62 ± 13
55 Cnc f	3,4	452.1 ± 12.8	410.7 ± 11.7	381.3 ± 10.8	0.02 ± 0.003	534 ± 81
BD-06 1339 c	2,3,4	481.2 ± 28.3	437.2 ± 25.7	405.8 ± 23.9	0.013±	212±
HD 218566 b	2,3,4	516.3 ± 16.4	469.1 ± 14.9	435.4 ± 13.8	0.021 ± 0.004	229 ± 51
Kepler-34 b	4	524.3 ± 8.7	476.4 ± 7.9	442.2 ± 7.4	0.036 ± 0.001	8±
HD 137388 A b	2,3,4	526.7 ± 22.8	478.6 ± 20.7	444.3 ± 19.3	0.025±	215±
HD 7199 b	3,4	574.9 ± 15.2	522.4 ± 13.8	484.9 ± 12.8	0.052±	481±
HIP 57050 b	2,3,4	580.2 ± 16.2	527.1 ± 14.7	489.3 ± 13.7	0.007 ± 0.001	221 ± 48
GJ 649 b	3,4	599 ± 19.5	544.2 ± 17.7	505.2 ± 16.4	0.046 ± 0.01	1484 ± 332
HD 564 b	1,2,3,4	600.2 ± 18.2	545.3 ± 16.5	506.2 ± 15.3	0.052 ± 0.007	323 ± 45
Kepler-16 b	1,2,3,4	602 ± 9.6	547 ± 8.8	507.8 ± 8.1	0.037 ± 0.001	205±
HD 181720 b	2,3,4	623.6 ± 0	566.5 ± 0	525.9 ± 0	0.066±	396±
HD 164509 b	4	680.1 ± 42.5	617.9 ± 38.6	573.6 ± 35.8	0.033 ± 0.009	214 ± 69
PH2 b	4	684.8 ± 48.4	622.1 ± 44	577.6 ± 40.9	0.027 ± 0.011	±
HD 99109 b	1,2,3,4	690.3 ± 32.1	627.2 ± 29.2	582.2 ± 27.1	0.056±	308±
HD 44219 b	4	724.4 ± 20.8	658.1 ± 18.9	610.9 ± 17.6	0.026±	175±
HD 43197 b	3,4	732.6 ± 32.6	665.6 ± 29.6	617.9 ± 27.5	0.009±	54±
HD 63765 b	2,3,4	748.5 ± 19.5	680.1 ± 17.7	631.3 ± 16.4	0.044 ± 0.005	451 ± 60
HD 45364 c	2,3,4	755.4 ± 0	686.4 ± 0	637.2 ± 0	0.051±	526±
HD 170469 b	3,4	760 ± 0	690.5 ± 0	641 ± 0	0.107±	548±

Table 3 continued on next page

Table 3 *(continued)*

Planet Name	Group	Roche ($\rho = 3g/cm$)	Roche ($\rho = 4g/cm$)	Roche ($\rho = 5g/cm$)	Hill Radius	Angular Seperation
		x10^{-6} au	x10^{-6} au	x10^{-6} au	au	x10^{-6}″
HD 37124 b	4	761.9 ± 6.4	692.3 ± 5.8	642.6 ± 5.4	0.032±	320±
GJ 876 c	2,3,4	776.4 ± 1.4	705.4 ± 1.3	654.8 ± 1.2	0.009 ± 0	604 ± 27
HD 156411 b	4	785.6 ± 15.9	713.8 ± 14.5	662.6 ± 13.4	0.084±	508±
HD 197037 b	4	802.9 ± 16.9	729.5 ± 15.4	677.2 ± 14.3	0.098±	999±
HD 34445 b	3,4	802.9 ± 23.7	729.5 ± 21.5	677.2 ± 20	0.093 ± 0.013	690 ± 130
Kepler-68 d	2,3,4	819.6 ± 16.3	744.6 ± 14.8	691.2 ± 13.7	0.072 ± 0.009	177 ± 34
HD 17674 b	1,2,3,4	829.2 ± 20.7	753.4 ± 18.8	699.4 ± 17.4	0.081 ± 0.007	607 ± 66
HD 128356 b	3,4	835.5 ± 21.9	759.1 ± 19.9	704.7 ± 18.5	0.028 ± 0.008	363 ± 106
HD 10647 b	4	850.8 ± 24.1	773 ± 21.9	717.6 ± 20.4	0.111 ± 0.015	2125 ± 308
HD 114729 b	1,2,3,4	853.9 ± 30	775.8 ± 27.2	720.2 ± 25.3	0.118±	1123±
HD 219415 b	3,4	868.6 ± 0	789.2 ± 0	732.6 ± 0	0.131±	257±
HD 160691 b	1,2,3,4	891.1 ± 0	809.7 ± 0	751.6 ± 0	0.089±	1944±
Kepler-97 c	1,2,3,4	891.1 ± 0	809.7 ± 0	751.6 ± 0	0.117±	±
HD 114783 b	3,4	896.6 ± 16.3	814.6 ± 14.8	756.2 ± 13.7	0.074 ± 0.006	1207 ± 125
HD 73534 b	2,3,4	897.4 ± 23.6	815.4 ± 21.4	756.9 ± 19.9	0.187 ± 0.026	769 ± 155
HD 9174 b	1,2,3,4	899.3 ± 37.8	817.1 ± 34.4	758.5 ± 31.9	0.135 ± 0.021	572 ± 117
HD 100777 b	3,4	912.6 ± 7.9	829.2 ± 7.1	769.7 ± 6.6	0.047 ± 0.005	298 ± 48
HD 28254 b	3,4	912.6 ± 21	829.2 ± 19.1	769.7 ± 17.7	0.029±	175±
HD 147513 b	2,3,4	925.6 ± 0	840.9 ± 0	780.6 ± 0	0.069±	1777±
HD 216435 b	1,2,3,4	938.1 ± 32.3	852.4 ± 29.3	791.3 ± 27.2	0.161±	1610±
HD 65216 b	1,2,3,4	938.1 ± 9.9	852.4 ± 9	791.3 ± 8.4	0.099±	923±
HD 108874 b	2,3,4	945.5 ± 14.7	859.1 ± 13.3	797.5 ± 12.4	0.072 ± 0.005	351 ± 53
HD 210277 b	3,4	945.5 ± 26.9	859.1 ± 24.4	797.5 ± 22.7	0.044±	691±
HD 19994 b	2,4	964.7 ± 28.2	876.5 ± 25.6	813.6 ± 23.8	0.084 ± 0.01	1246 ± 168
HD 30562 b	3,4	965.4 ± 11	877.1 ± 10	814.2 ± 9.3	0.036 ± 0.003	458 ± 47
HD 133131 A b	3,4	976.3 ± 9.2	887 ± 8.3	823.4 ± 7.7	0.075±	534±
HD 20782 b	3,4	978.6 ± 6.8	889.1 ± 6.2	825.3 ± 5.8	0.005 ± 0.001	44 ± 6
HD 48265 b	2,4	987.6 ± 26.9	897.3 ± 24.4	833 ± 22.7	0.119 ± 0.016	465 ± 85
BD+14 4559 b	2,3,4	987.6 ± 0	897.3 ± 0	833 ± 0	0.045±	300±

Table 3 continued on next page

Table 3 *(continued)*

Planet Name	Group	Roche ($\rho = 3g/cm$)	Roche ($\rho = 4g/cm$)	Roche ($\rho = 5g/cm$)	Hill Radius	Angular Seperation
		x10^{-6} au	x10^{-6} au	x10^{-6} au	au	x10^{-6}″
HD 188015 b	1,2,3,4	994.3 ± 28.7	903.4 ± 26.1	838.6 ± 24.2	0.079±	499±
HD 23127 b	3,4	994.3 ± 44.2	903.4 ± 40.1	838.6 ± 37.3	0.101 ± 0.033	377 ± 148
HD 4113 b	3,4	1007.4 ± 8.6	915.2 ± 7.8	849.6 ± 7.3	0.01±	75±
HIP 109384 b	3,4	1007.4 ± 17.2	915.2 ± 15.6	849.6 ± 14.5	0.044 ± 0.003	261 ± 32
WASP-47 c	2,3,4	1009.5 ± 170.4	917.2 ± 154.8	851.4 ± 143.7	0.069 ± 0.054	115 ± 107
HD 221585 b	1,2,3,4	1018 ± 29.5	924.9 ± 26.8	858.6 ± 24.9	0.153 ± 0.027	950 ± 203
HD 142415 b	3,4	1020.1 ± 0	926.8 ± 0	860.4 ± 0	0.042±	402 ± 12
16 Cyg B b	3,4	1032.6 ± 30.7	938.1 ± 27.9	870.9 ± 25.9	0.044±	680±
HD 82943 b	2,3,4	1032.8 ± 5.7	938.3 ± 5.2	871.1 ± 4.8	0.076±	919±
HD 45350 b	4	1054.6 ± 27.5	958.2 ± 25	889.5 ± 23.2	0.035±	239±
HD 216437 b	4	1060.5 ± 0	963.5 ± 0	894.4 ± 0	0.131±	1647±
HD 4203 b	3,4	1060.5 ± 9.7	963.5 ± 8.8	894.4 ± 8.2	0.045±	193±
HD 190647 b	2,3,4	1075.8 ± 11.3	977.4 ± 10.3	907.4 ± 9.6	0.139 ± 0.013	855 ± 132
HD 20868 b	3,4	1092.5 ± 9.2	992.6 ± 8.3	921.5 ± 7.7	0.022 ± 0.001	151 ± 17
kap CrB b	4	1094.3 ± 0	994.3 ± 0	923 ± 0	0.202±	2213±
HD 159868 b	1,2,3,4	1112.3 ± 19.4	1010.6 ± 17.6	938.1 ± 16.4	0.189 ± 0.013	1196 ± 152
NGC 2682 Sand 978 b	1,2,3,4	1126.2 ± 29.3	1023.2 ± 26.6	949.9 ± 24.7	0.093±	49±
HD 154857 b	4	1136.5 ± 8.5	1032.6 ± 7.7	958.5 ± 7.1	0.052 ± 0.003	253 ± 30
HD 73526 c	4	1138.2 ± 21.9	1034.1 ± 19.9	960 ± 18.5	0.066 ± 0.008	233 ± 51
GJ 876 b	1,2,3,4	1142.5 ± 0.8	1038 ± 0.8	963.6 ± 0.7	0.026 ± 0.001	1857 ± 79
HD 145934 b	1,2,3,4	1143.2 ± 43.5	1038.7 ± 39.5	964.2 ± 36.7	0.325 ± 0.048	±
HD 163607 c	2,3,4	1144.9 ± 26.7	1040.2 ± 24.2	965.6 ± 22.5	0.186 ± 0.019	894 ± 131
HD 4732 c	2,3,4	1158 ± 61.9	1052.2 ± 56.2	976.7 ± 52.2	0.268 ± 0.061	1581 ± 448
HD 23079 b	1,2,3,4	1170.9 ± 33.5	1063.9 ± 30.4	987.6 ± 28.2	0.131±	1266±
GJ 317 b	2,3,4	1178.8 ± 86.4	1071 ± 78.5	994.3 ± 72.9	0.127 ± 0.027	2795 ± 635
47 UMa b	2,3,4	1183.5 ± 10.1	1075.3 ± 9.2	998.2 ± 8.5	0.187 ± 0.009	4432 ± 257
HD 196885 b	3,4	1191.3 ± 24.6	1082.4 ± 22.4	1004.8 ± 20.8	0.106 ± 0.017	1074 ± 198
HD 164604 b	2,3,4	1209.5 ± 194.1	1098.9 ± 176.4	1020.1 ± 163.7	0.101±	888±
HD 153950 b	4	1213.9 ± 7.4	1102.9 ± 6.7	1023.9 ± 6.3	0.078 ± 0.004	499 ± 60

Table 3 continued on next page

Table 3 *(continued)*

Planet Name	Group	Roche ($\rho = 3g/cm$)	Roche ($\rho = 4g/cm$)	Roche ($\rho = 5g/cm$)	Hill Radius	Angular Seperation
		x10^{-6} au	x10^{-6} au	x10^{-6} au	au	x10^{-6}″
HD 165155 b	1,2,3,4	1237.2 ± 32.8	1124.1 ± 29.8	1043.5 ± 27.7	0.087 ± 0.01	448 ± 102
HD 125612 b	3,4	1252.7 ± 0	1138.2 ± 0	1056.6 ± 0	0.071±	447±
HD 221287 b	2,3,4	1265.1 ± 107.8	1149.4 ± 98	1067 ± 90.9	0.106 ± 0.028	669 ± 205
HD 1605 c	1,2,3,4	1316.2 ± 15.1	1195.9 ± 13.7	1110.2 ± 12.8	0.3 ± 0.025	1183 ± 192
HD 92788 b	4	1328.7 ± 0	1207.2 ± 0	1120.7 ± 0	0.063±	651±
HD 183263 b	2,3,4	1339.8 ± 36.5	1217.3 ± 33.2	1130 ± 30.8	0.097 ± 0.012	612 ± 112
KELT-6 c	1,2,3,4	1344.6 ± 25.4	1221.7 ± 23.1	1134.1 ± 21.4	0.192 ± 0.025	288 ± 48
HD 169830 c	4	1383.4 ± 0	1256.9 ± 0	1166.8 ± 0	0.234±	2151±
ups And d	3,4	1393.8 ± 3.3	1266.3 ± 3	1175.6 ± 2.8	0.177±	4378±
Kepler-454 c	1,2,3,4	1429.7 ± 12.8	1299 ± 11.7	1205.9 ± 10.8	0.14 ± 0.006	±
HD 213240 b	3,4	1434 ± 0	1302.9 ± 0	1209.5 ± 0	0.12±	984±
HD 111998 b	1,2,3,4	1435.1 ± 53	1303.8 ± 48.2	1210.4 ± 44.7	0.188 ± 0.028	1919 ± 308
HD 16175 b	3,4	1462.1 ± 37.8	1328.4 ± 34.3	1233.2 ± 31.9	0.081 ± 0.012	453 ± 95
HD 13908 c	2,3,4	1498 ± 24.3	1361 ± 22.1	1263.5 ± 20.5	0.193 ± 0.013	963 ± 121
HD 28185 b	1,2,3,4	1541.5 ± 30.3	1400.6 ± 27.6	1300.2 ± 25.6	0.114 ± 0.009	962 ± 114
HD 224538 b	3,4	1575.7 ± 37	1431.6 ± 33.6	1329 ± 31.2	0.137 ± 0.015	588 ± 99
HIP 67851 c	4	1576.6 ± 66.8	1432.4 ± 60.7	1329.7 ± 56.3	0.334 ± 0.073	1687 ± 414
HD 70573 b	4	1587 ± 34.7	1441.9 ± 31.5	1338.6 ± 29.3	0.132 ± 0.033	961±
Kepler-424 c	2,4	1659.2 ± 49.2	1507.4 ± 44.7	1399.4 ± 41.5	0.095 ± 0.014	±
HD 86264 b	3,4	1661.5 ± 126.6	1509.6 ± 115	1401.4 ± 106.8	0.1 ± 0.078	460 ± 385
Kepler-419 c	4	1684.9 ± 30.8	1530.9 ± 28	1421.1 ± 26	0.163 ± 0.009	±
HD 23596 b	2,3,4	1715.9 ± 28.9	1559 ± 26.3	1447.3 ± 24.4	0.261 ± 0.02	1674 ± 200
HD 222582 b	3,4	1718.9 ± 48.1	1561.7 ± 43.7	1449.7 ± 40.5	0.05±	399±
HD 33564 b	3,4	1813.4 ± 0	1647.6 ± 0	1529.5 ± 0	0.096±	1526±
HD 141937 b	3,4	1827.6 ± 21.5	1660.5 ± 19.5	1541.5 ± 18.1	0.125 ± 0.005	1244 ± 97
30 Ari B b	4	1863.8 ± 59.1	1693.4 ± 53.7	1572 ± 49.9	0.099 ± 0.018	834 ± 190
HD 38801 b	2,4	1914 ± 29.8	1739 ± 27.1	1614.3 ± 25.1	0.231 ± 0.014	774 ± 184
HD 217786 b	4	2042.3 ± 41.9	1855.6 ± 38.1	1722.6 ± 35.3	0.228 ± 0.03	1385 ± 231
HAT-P-13 c	4	2107.3 ± 13.8	1914.6 ± 12.5	1777.3 ± 11.6	0.064 ± 0.004	100 ± 12

Table 3 continued on next page

Table 3 *(continued)*

Planet Name	Group	Roche ($\rho = 3g/cm$)	Roche ($\rho = 4g/cm$)	Roche ($\rho = 5g/cm$)	Hill Radius	Angular Seperation
		x10^{-6} au	x10^{-6} au	x10^{-6} au	au	x10^{-6}″
HD 214823 b	3,4	2325.8 ± 56.5	2113.1 ± 51.4	1961.7 ± 47.7	0.46 ± 0.053	1574 ± 316
Kepler-47 c	3,4	2637.5 ± 0	2396.3 ± 0	2224.6 ± 0	0.119±	26±

4.2.5. *Tables: RadVel results*

Table 4. Habitable Zone Giant Planets $\geq 3R_{\oplus}$: Linear Trends

Planet Name	Group	No. Planets in System	RV Semi Amp m/s	dv/dt	$\Delta dv/dt$	Linear Trend $\geq 3\sigma$
GJ 163 c	4	3	2.75	-4.47E-07	4.76E-07	N
LHS 1140 b	2,3,4	1	5.34	–	–	N
HD 40307 g	2,3,4	5	0.95	9.99E-04	3.76E-03	N
GJ 3293 d	1,2,3,4	4	2.42	-4.29E-06	1.21E-06	Y
HD 69830 d	4	3	2.2	3.71E-04	2.83E-04	N
GJ 687 b	1,2,3,4	1	6.43	1.96E-03	2.02E-04	Y
HD 10180 g	2,3,4	6	1.754	-2.29E-03	3.72E-04	Y
GJ 3293 b	2,4	4	8.603	-4.29E-06	1.21E-06	Y
Kepler-62 f	1,2,3,4	5	–	–	–	N
Kepler-22 b	2,4	1	–	–	–	N
Kepler-62 e	2,4	5	–	–	–	N
K2-3 d	4	3	–	–	–	N
55 Cnc f	3,4	5	4.87	4.61E-03	4.01E-04	Y
BD-06 1339 c	2,3,4	2	9.1	-2.06E-03	4.31E-04	Y
HD 218566 b	2,3,4	1	8.3	4.30E-04	1.13E-03	N
Kepler-34 b	4	1	–	–	–	N
HD 137388 A b	2,3,4	1	7.94	7.05E-03	7.45E-04	Y
HD 7199 b	3,4	1	7.76	-4.99E-04	4.25E-04	N
HIP 57050 b	2,3,4	1	37.8	4.72E-03	6.61E-04	Y
GJ 649 b	3,4	1	12.4	3.20E-04	5.32E-04	N

Table 4 continued on next page

Table 4 *(continued)*

Planet Name	Group	No. Planets in System	RV Semi Amp m/s	dv/dt	$\Delta dv/dt$	Linear Trend $\geq 3\sigma$
HD 564 b	1,2,3,4	1	8.79	7.36E-04	3.22E-04	N
Kepler-16 b	1,2,3,4	1	–	–	–	N
HD 181720 b	2,3,4	1	8.4	1.14E-03	8.78E-04	N
HD 164509 b	4	1	14.2	-1.14E-02	1.42E-03	Y
PH2 b	4	1	14	7.14E-01	4.05E-01	N
HD 99109 b	1,2,3,4	1	14.1	1.50E-03	3.00E-03	N
HD 44219 b	4	1	19.4	2.00E-02	3.80E-03	Y
HD 43197 b	3,4	1	32.4	5.14E-04	8.37E-04	N
HD 63765 b	2,3,4	1	20.9	–	–	N
HD 45364 c	2,3,4	2	21.92	-8.01E-03	3.67E-03	N
HD 170469 b	3,4	1	12	1.27E-03	4.98E-04	N
HD 37124 b	4	3	28.5	1.87E-03	5.55E-04	Y
GJ 876 c	2,3,4	4	88.34	-0.0054	1.01E+00	N
HD 156411 b	4	1	14	-3.97E-03	8.03E-04	Y
HD 197037 b	4	1	15.5	-5.34E-03	7.40E-04	Y
HD 34445 b	3,4	1	12.01	2.61E-04	2.66E-04	N
Kepler-68 d	2,3,4	3	19.06	5.42E-02	1.66E-02	Y
HD 17674 b	1,2,3,4	1	21.1	2.89E-03	2.25E-03	N
HD 128356 b	3,4	1	36.9	4.37E-03	2.52E-03	N
HD 10647 b	4	1	18.1	-1.82E-04	1.33E-03	N
HD 114729 b	1,2,3,4	1	18.8	3.11E-04	1.12E-03	N
HD 219415 b	3,4	1	18.2	-1.64E-03	1.31E-03	N
HD 160691 b	1,2,3,4	4	37.78	9.33E-03	9.90E-04	Y
Kepler-97 c	1,2,3,4	2	25	–	–	N
HD 114783 b	3,4	1	31.9	5.53E-03	1.28E-03	Y
HD 73534 b	2,3,4	1	16.2	1.12E-01	7.19E-03	Y
HD 9174 b	1,2,3,4	1	20.8	-5.32E-03	5.63E-03	N
HD 100777 b	3,4	1	34.9	-5.51E-03	3.32E-03	N
HD 28254 b	3,4	1	37.3	8.09E-03	6.07E-04	Y

Table 4 continued on next page

Table 4 *(continued)*

Planet Name	Group	No. Planets in System	RV Semi Amp m/s	dv/dt	$\Delta dv/dt$	Linear Trend $\geq 3\sigma$
HD 147513 b	2,3,4	1	29.3	-2.74E-02	8.29E-03	Y
HD 216435 b	1,2,3,4	1	19.6	-3.50E-04	5.65E-04	N
HD 65216 b	1,2,3,4	2	33.7	1.41E-05	5.66E-03	N
HD 108874 b	2,3,4	2	37	8.12E-05	1.26E-03	N
HD 210277 b	3,4	1	38.94	2.03E-02	3.34E-03	N
HD 19994 b	2,4	1	29.3	1.41E-02	4.37E-04	Y
HD 30562 b	3,4	1	36.8	1.84E-03	8.79E-04	N
HD 133131 A b	3,4	2	36.52	5.30E-04	1.31E-03	N
HD 20782 b	3,4	1	116	4.96E-03	1.43E-03	Y
HD 48265 b	2,4	1	27.7	5.35E-02	2.50E-03	Y
BD+14 4559 b	2,3,4	1	55.21	-1.93E-02	1.38E-02	N
HD 188015 b	1,2,3,4	1	37.6	-2.26E-02	6.87E-03	Y
HD 23127 b	3,4	1	27.5	-3.72E-03	7.28E-04	Y
HD 4113 b	3,4	1	97.1	7.87E-02	6.07E-04	Y
HIP 109384 b	3,4	1	56.53	-7.76E-03	2.99E-03	N
WASP-47 c	2,3,4	4	29.4	-1.49E-01	2.93E-01	N
HD 221585 b	1,2,3,4	1	27.9	3.16E-02	9.06E-04	Y
HD 142415 b	3,4	1	51.3	-9.83E-03	1.60E-03	Y
16 Cyg B b	3,4	1	50.5	1.43E-03	6.77E-04	N
HD 82943 b	2,3,4	2	41.91	-8.33E-03	7.64E-03	N
HD 45350 b	4	1	58	-9.21E-04	7.45E-04	N
HD 216437 b	4	1	34.6	2.26E-03	9.10E-04	N
HD 4203 b	3,4	2	52.82	5.59E-03	7.02E-03	N
HD 190647 b	2,3,4	1	36.4	1.20E-01	4.95E-03	Y
HD 20868 b	3,4	1	100.34	-2.96E-02	4.06E-03	Y
kap CrB b	4	1	25.17	1.25E-02	1.51E-03	Y
HD 159868 b	1,2,3,4	2	38.3	1.87E-03	4.49E-03	N
NGC 2682 Sand 978 b	1,2,3,4	1	45.48	6.28E-03	3.65E-03	N
HD 154857 b	4	2	48.3	5.08E-02	6.82E-03	Y

Table 4 continued on next page

Table 4 *(continued)*

Planet Name	Group	No. Planets in System	RV Semi Amp m/s	dv/dt	$\Delta dv/dt$	Linear Trend $\geq 3\sigma$
HD 73526 c	4	2	65.1	-1.66E-02	1.83E-03	Y
GJ 876 b	1,2,3,4	4	214	-3.44E-02	3.05E-03	Y
HD 145934 b	1,2,3,4	1	22.9	-5.54E-02	2.44E-04	Y
HD 163607 c	2,3,4	2	40.4	-3.90E-04	1.35E-03	N
HD 4732 c	2,3,4	2	24.4	-3.97E-02	4.48E-03	Y
HD 23079 b	1,2,3,4	1	54.9	-3.70E-04	5.00E-03	N
GJ 317 b	2,3,4	1	75.2	2.69E-02	6.07E-03	Y
47 UMa b	2,3,4	3	48.4	-2.20E-03	3.84E-03	N
HD 196885 b	3,4	1	53.9	-9.07E-02	8.63E-04	Y
HD 164604 b	2,3,4	1	77	-4.69E-02	6.07E-03	Y
HD 153950 b	4	1	69.2	2.34E-03	2.18E-03	N
HD 165155 b	1,2,3,4	1	75.8	-6.52E-02	2.47E-03	Y
HD 125612 b	3,4	3	79.8	-2.26E-02	2.03E-02	N
HD 221287 b	2,3,4	1	71	8.30E-03	3.59E-03	N
HD 1605 c	1,2,3,4	2	46.5	-1.83E-02	7.87E-04	Y
HD 92788 b	4	1	106.2	-4.52E-03	1.04E-03	Y
HD 183263 b	2,3,4	2	84	9.63E-03	3.84E-03	N
KELT-6 c	1,2,3,4	2	65.7	-1.69E-01	5.38E-02	Y
HD 169830 c	4	2	54.3	-5.54E-01	4.13E-02	Y
ups And d	3,4	3	66.7	1.86E-04	4.25E-04	N
Kepler-454 c	1,2,3,4	2	110.44	1.04E-02	5.35E-03	N
HD 213240 b	3,4	1	91	-2.11E-03	1.53E-03	N
HD 111998 b	1,2,3,4	1	87.6	–	–	N
HD 16175 b	3,4	1	103.5	5.50E-05	2.50E-03	N
HD 13908 c	2,3,4	2	90.9	3.61E-03	3.71E-03	N
HD 28185 b	1,2,3,4	1	158.8	2.74E-02	1.93E-03	Y
HD 224538 b	3,4	1	107	-4.05E-03	1.18E-03	Y
HIP 67851 c	4	2	69	2.06E-01	4.14E-02	Y
HD 70573 b	4	1	148.5	–	–	N

Table 4 continued on next page

Table 4 *(continued)*

Planet Name	Group	No. Planets in System	RV Semi Amp m/s	dv/dt	$\Delta dv/dt$	Linear Trend $\geq 3\sigma$
Kepler-424 c	2,4	2	246	8.71E-02	3.51E-02	N
HD 86264 b	3,4	1	132	6.31E-03	3.08E-03	N
Kepler-419 c	4	2	–	–	–	N
HD 23596 b	2,3,4	1	127	6.40E-03	1.41E-03	Y
HD 222582 b	3,4	1	276.3	-1.89E-02	2.76E-03	Y
HD 33564 b	3,4	1	232	–	–	N
HD 141937 b	3,4	1	234.5	9.63E-03	3.84E-03	N
30 Ari B b	4	1	272	-2.36E-01	2.36E-02	Y
HD 38801 b	2,4	1	200	1.91E-02	5.82E-03	Y
HD 217786 b	4	1	261	1.90E-01	5.67E-03	Y
HAT-P-13 c	4	2	440	-4.06E-02	2.20E-02	N
HD 214823 b	3,4	1	281.4	5.40E-03	2.75E-03	N
Kepler-47 c	3,4	2	–	–	–	N

4.2.6. *Tables: Observing Strategy*

Table 5. Habitable Zone Giant Planets $\geq 3R_{\oplus}$: Telescope Strategy of Planets with Linear Trend

Planet Name	Group	Right Ascension degrees	Declination degrees	Magnitude Optical	RV Semi Amplitude m/s	Telescope
HD 1605 c	1,2,3,4	5.13133	30.974804	7.52	46.5 ± 1.5	APF/KECK
HD 221585 b	1,2,3,4	353.225189	63.155483	7.465	27.9 ± 1.6	APF/KECK
HD 23596 b	2,3,4	57.001556	40.530636	7.244	127 ± 2	APF/KECK
55 Cnc f	3,4	133.149216	28.330818	5.96	4.87 ± 0.43	APF/KECK
HD 196885 b	3,4	309.966156	11.249649	6.398	53.9 ± 3.7	APF/KECK
30 Ari B b	4,	39.240585	24.648064	7.458	272 ± 24	APF/KECK
HD 164509 b	4,	270.380127	0.104556	8.103	14.2 ± 2.7	APF/KECK
HD 197037 b	4,	309.887329	42.24855	6.813	15.5 ± 1	APF/KECK

Table 5 continued on next page

Table 5 *(continued)*

Planet Name	Group	Right Ascension	Declination	Magnitude	RV Semi Amplitude	Telescope
		degrees	degrees	Optical	m/s	
HD 37124 b	4,	84.260361	20.730787	7.7	28.5 ± 0.78	APF/KECK
kap CrB b	4,	237.808044	35.657383	4.82	25.17 ± 1.12	APF/KECK
HD 19994 b	2,4	48.193485	-1.196101	5.06	29.3 ± 2.1	APF/MINERVA/KECK
HD 114783 b	3,4	198.182434	-2.26504	7.55	31.9 ± 0.9	APF/MINERVA/KECK
HD 217786 b	4,	345.78418	-0.429622	7.8	261 ± 20	APF/MINERVA/KECK
HD 92788 b	4,	160.702209	-2.183756	7.3	106.2 ± 1.8	APF/MINERVA/KECK
GJ 3293 d	1,2,3,4	67.14882	-25.169301	11.962	2.42 ± 0.338	KECK
GJ 687 b	1,2,3,4	264.10791	68.339142	9.15	6.43 ± 0.769	KECK
HD 145934 b	1,2,3,4	243.29114	13.239476	8.5	22.9 ± 2.6	KECK
HD 188015 b	1,2,3,4	298.018921	28.100376	8.234	37.6 ± 1.2	KECK
KELT-6 c	1,2,3,4	195.981868	30.640051	10.418	65.7 ± 2.6	KECK
GJ 317 b	2,3,4	130.24673	-23.456289	11.97	75.2 ± 3	KECK
HD 73534 b	2,3,4	129.815842	12.960376	8.23	16.2 ± 1.1	KECK
HIP 57050 b	2,3,4	175.4333	42.75219167	11.92	37.8 ± 4.5	KECK
Kepler-68 d	2,3,4	291.032305	49.040272	9.99	19.06 ± 0.58	KECK
GJ 3293 b	2,4	67.14882	-25.169301	11.962	8.603 ± 0.32	KECK
GJ 876 b	1,2,3,4	343.319733	-14.2637	10.191	214 ± 0.42	MINERVA
HD 160691 b	1,2,3,4	266.036255	-51.834053	5.15	37.78 ± 0.4	MINERVA
HD 165155 b	1,2,3,4	271.488953	-29.917253	9.36	75.8 ± 3	MINERVA
HD 28185 b	1,2,3,4	66.609673	-10.550821	7.81	158.8 ± 4.2	MINERVA
BD-06 1339 c	2,3,4	88.251183	-5.994844	9.7	9.1 ± 2.9	MINERVA
HD 10180 g	2,3,4	24.473234	-60.511528	7.321	1.754 ± 0.38	MINERVA
HD 137388 A b	2,3,4	233.916367	-80.20459	8.696	7.94±	MINERVA
HD 147513 b	2,3,4	246.005371	-39.192982	5.39	29.3 ± 1.8	MINERVA
HD 164604 b	2,3,4	270.7789	-28.560644	9.7	77 ± 32	MINERVA
HD 190647 b	2,3,4	301.83197	-35.538631	7.775	36.4 ± 1.2	MINERVA
HD 4732 c	2,3,4	12.308117	-24.136671	5.89	24.4 ± 2.2	MINERVA
HD 38801 b	2,4	86.996567	-8.3277	8.269	200 ± 3.9	MINERVA
HD 48265 b	2,4	100.007195	-48.541954	8.05	27.7 ± 1.2	MINERVA

Table 5 continued on next page

Table 5 *(continued)*

Planet Name	Group	Right Ascension	Declination	Magnitude	RV Semi Amplitude	Telescope
		degrees	degrees	Optical	m/s	
HD 142415 b	3,4	239.419968	-60.200256	7.327	51.3±	MINERVA
HD 20782 b	3,4	50.014908	-28.854071	7.4	116 ± 4.2	MINERVA
HD 20868 b	3,4	50.177895	-33.730103	9.92	100.34 ± 0.42	MINERVA
HD 222582 b	3,4	355.464722	-5.985757	7.68	276.3 ± 7	MINERVA
HD 224538 b	3,4	359.715668	-61.586773	8.06	107 ± 2.4	MINERVA
HD 23127 b	3,4	54.848495	-60.077843	8.55	27.5 ± 1	MINERVA
HD 28254 b	3,4	66.211273	-50.622192	7.684	37.3 ± 5.1	MINERVA
HD 4113 b	3,4	10.802486	-37.982632	7.881	97.1 ± 3.8	MINERVA
HD 154857 b	4,	257.815521	-56.680798	7.238	48.3 ± 1	MINERVA
HD 156411 b	4,	259.964172	-48.54932	6.673	14 ± 0.8	MINERVA
HD 169830 c	4,	276.956177	-29.816866	5.902	54.3 ± 3.6	MINERVA
HD 44219 b	4,	95.059677	-10.725009	7.69	19.4 ± 3	MINERVA
HD 73526 c	4,	129.31868	-41.319103	8.971	65.1 ± 2.6	MINERVA
HIP 67851 c	4,	208.466919	-35.314362	6.17	69 ± 3.3	MINERVA

Table 6. Habitable Zone Giant Planets $\geq 3R_{\oplus}$: Telescope Strategy of Planets with No Linear Trend

Planet Name	Group	Right Ascension	Declination	Magnitude	RV Semi Amplitude	Telescope
		degrees	degrees	Optical	m/s	
HD 17674 b	1,2,3,4	42.767853	30.286739	7.56	21.1 ± 0.6	APF/KECK
47 UMa b	2,3,4	164.866562	40.430256	5.05	48.4 ± 0.8	APF/KECK
HD 108874 b	2,3,4	187.612015	22.879829	7.06	37 ± 0.8	APF/KECK
HD 13908 c	2,3,4	34.560665	65.59436	7.508	90.9 ± 3	APF/KECK
HD 163607 c	2,3,4	268.418732	56.391956	7.979	40.4 ± 1.3	APF/KECK
HD 183263 b	2,3,4	292.102386	8.358054	7.861	84 ± 3.7	APF/KECK
16 Cyg B b	3,4	295.466553	50.517525	6.25	50.5 ± 1.6	APF/KECK
HD 16175 b	3,4	39.257961	42.062634	7.282	103.5 ± 5	APF/KECK
HD 214823 b	3,4	340.082794	31.787594	8.068	281.4 ± 3.7	APF/KECK

Table 6 continued on next page

Table 6 *(continued)*

Planet Name	Group	Right Ascension	Declination	Magnitude	RV Semi Amplitude	Telescope
		degrees	degrees	Optical	m/s	
HD 33564 b	3,4	80.639717	79.231148	5.08	232 ± 5	APF/KECK
HD 34445 b	3,4	79.420746	7.353343	7.328	12.01 ± 0.52	APF/KECK
ups And d	3,4	24.199345	41.40546	4.1	66.7 ± 1.42	APF/KECK
HD 45350 b	4,	97.19046	38.962963	7.885	58 ± 1.7	APF/KECK
HD 111998 b	1,2,3,4	193.296494	-3.553098	6.11	87.6 ± 3.4	APF/MINERVA/KECK
Kepler-454 c	1,2,3,4	287.478529	38.228866	11.57	110.44 ± 0.96	KECK
Kepler-97 c	1,2,3,4	287.326624	48.673431	12.872	25±	KECK
NGC 2682 Sand 978 b	1,2,3,4	132.82283	11.756299	9.71	45.48 ± 3.65	KECK
BD+14 4559 b	2,3,4	318.399963	14.689387	9.63	55.21 ± 2.29	KECK
WASP-47 c	2,3,4	331.203047	-12.018885	11.9	29.4 ± 6.1	KECK
GJ 649 b	3,4	254.53688	25.74416	9.69	12.4 ± 1.1	KECK
HD 170469 b	3,4	277.295746	11.695502	8.21	12 ± 1.9	KECK
HD 219415 b	3,4	348.724278	56.730328	8.94	18.2 ± 2.2	KECK
HD 4203 b	3,4	11.171676	20.448927	8.687	52.82 ± 1.5	KECK
HIP 109384 b	3,4	332.405823	71.314331	9.63	56.53 ± 0.22	KECK
HAT-P-13 c	4,	129.882536	47.352051	10.622	440 ± 11	KECK
HD 70573 b	4,	125.708135	1.859323	11.424	148.5 ± 16.5	KECK
PH2 b	4,	289.76359	51.962601	12.62	14±	KECK
HD 114729 b	1,2,3,4	198.184402	-31.873348	6.68	18.8 ± 1.3	MINERVA
HD 159868 b	1,2,3,4	264.748016	-43.145515	7.242	38.3 ± 1.1	MINERVA
HD 216435 b	1,2,3,4	343.408051	-48.598286	6.03	19.6 ± 1.5	MINERVA
HD 23079 b	1,2,3,4	54.929562	-52.915836	7.12	54.9 ± 1.1	MINERVA
HD 564 b	1,2,3,4	2.470091	-50.267822	8.29	8.79 ± 0.45	MINERVA
HD 65216 b	1,2,3,4	118.422173	-63.647324	7.964	33.7 ± 1.1	MINERVA
HD 9174 b	1,2,3,4	22.504177	-19.604502	8.4	20.8 ± 2.2	MINERVA
GJ 876 c	2,3,4	343.319733	-14.2637	10.191	88.34 ± 0.47	MINERVA
HD 181720 b	2,3,4	290.720764	-32.919056	7.849	8.4 ± 0.4	MINERVA
HD 221287 b	2,3,4	352.834747	-58.209732	7.807	71 ± 18	MINERVA
HD 45364 c	2,3,4	96.410316	-31.480953	8.062	21.92 ± 0.43	MINERVA

Table 6 continued on next page

Table 6 *(continued)*

Planet Name	Group	Right Ascension	Declination	Magnitude	RV Semi Amplitude	Telescope
		degrees	degrees	Optical	m/s	
HD 63765 b	2,3,4	116.957161	-54.264145	8.104	20.9 ± 1.3	MINERVA
HD 82943 b	2,3,4	143.711395	-12.129546	6.53	41.91 ± 0.77	MINERVA
HD 125612 b	3,4	215.222977	-17.481522	8.317	$79.8\pm$	MINERVA
HD 128356 b	3,4	219.270355	-25.802563	8.29	36.9 ± 1.2	MINERVA
HD 133131 A b	3,4	225.897705	-27.842573	8.4	36.52 ± 0.93	MINERVA
HD 141937 b	3,4	238.07312	-18.436066	7.25	234.5 ± 6.4	MINERVA
HD 210277 b	3,4	332.374451	-7.548654	6.53	38.94 ± 0.75	MINERVA
HD 213240 b	3,4	337.751526	-49.43327	6.814	91 ± 3	MINERVA
HD 30562 b	3,4	72.151604	-5.674045	5.78	36.8 ± 1.1	MINERVA
HD 43197 b	3,4	93.39859	-29.89727	8.98	32.4 ± 10.9	MINERVA
HD 7199 b	3,4	17.696762	-66.188164	8.027	7.76 ± 0.58	MINERVA
HD 86264 b	3,4	149.240997	-15.895122	7.407	132 ± 33	MINERVA
HD 10647 b	4,	25.622149	-53.740833	5.52	18.1 ± 1.7	MINERVA
HD 153950 b	4,	256.128632	-43.309769	7.39	69.2 ± 1.2	MINERVA
HD 216437 b	4,	343.66452	-70.073708	6.05	34.6 ± 5.7	MINERVA
HD 69830 d	4,	124.599777	-12.632174	6	2.2 ± 0.19	MINERVA
HD 99109 b	1,2,3,4	171.072327	-1.529076	9.1	14.1 ± 2.2	MINERVA/KECK
HD 218566 b	2,3,4	347.294708	-2.260742	8.628	8.3 ± 0.7	MINERVA/KECK
HD 100777 b	3,4	173.964676	-4.755697	8.418	34.9 ± 0.8	MINERVA/KECK
Kepler-16 b	1,2,3,4	289.07571	51.757439	11.762	$\pm$	
Kepler-62 f	1,2,3,4	283.212747	45.349865	13.725	$\pm$	
HD 40307 g	2,3,4	88.51767	-60.023472	7.17	0.95 ± 0.32	
LHS 1140 b	2,3,4	11.24724	-15.271532	14.18	5.34 ± 1.1	
Kepler-22 b	2,4	289.217484	47.884464	11.664	$\pm$	
Kepler-424 c	2,4	298.62489	48.577454	14.256	246 ± 17	
Kepler-62 e	2,4	283.212747	45.349865	13.725	$\pm$	
Kepler-47 c	3,4	295.297916	46.920467	15.178	$\pm$	
GJ 163 c	4,	62.315273	-53.373699	11.81	2.75 ± 0.35	
K2-3 d	4,	172.334946	-1.454787	12.17	$\pm$	

Table 6 continued on next page

Table 6 *(continued)*

Planet Name	Group	Right Ascension	Declination	Magnitude	RV Semi Amplitude	Telescope
		degrees	degrees	Optical	m/s	
Kepler-34 b	4,	296.435821	44.64156	14.875	±	
Kepler-419 c	4,	295.417899	51.184765	13.005	±	

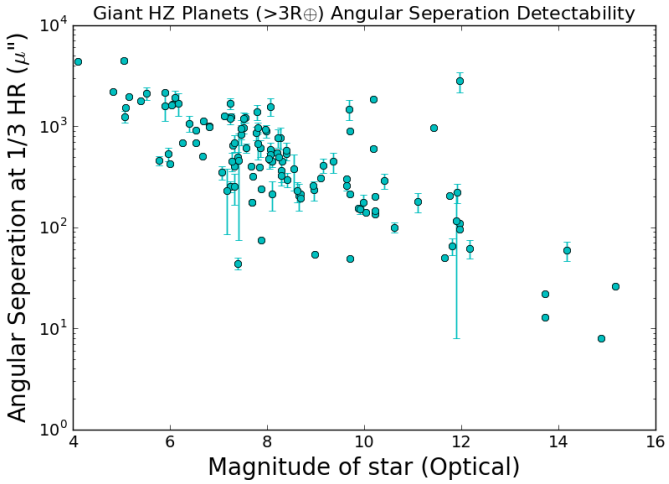

FIGURE 4.1: *The magnitude of the host star of the HZ planets is plotted against the expected angular separation of the planet/moon system to determine the expected detectability of these moons. Note the Y axis is the angular separation at* $\frac{1}{3}$ *Hill radius which is taken as the typical distance of a stable moon. Future imaging missions thus will need the capabilities to resolve a separation between 10 – 4400* μ *arc seconds to image any potential moons in this data set.*

4.3 Figures

4.3.1 Figures: Moon Calculations

The calculations provided in Table 4.3 indicate that giant planets found in the habitable zone will likely have a Hill radius between 1 x10^{-3} $\sim$ 460 x10^{-3} AU and a Roche limit between 0.1 x10^{-3} $\sim$ 2.6 x10^{-3} AU. These ranges can be seen clearly in Figures 4.5 and 4.6 respectively. With a moon at the full Hill radius, the maximum angular separation of the moon from the host planet is between 1 $\sim$ 13000 μ arc seconds (Figure 4.2). However is a moon is found at the estimated typical stable orbit of $\frac{1}{3}$ Hill radius, the angular separation between a potential moon and its host planet will be in the range of 10 $\sim$ 4400 μ arc seconds, as shown in Figure 4.1. Plots of the magnitude of the host star of the giant HZ planets and their expected radial velocity semi amplitude are also provided, with each planet identified by the telescope that has been deemed to be the most appropriate for follow up observations in Figure 4.3, then identified by Group in Figure 4.4.

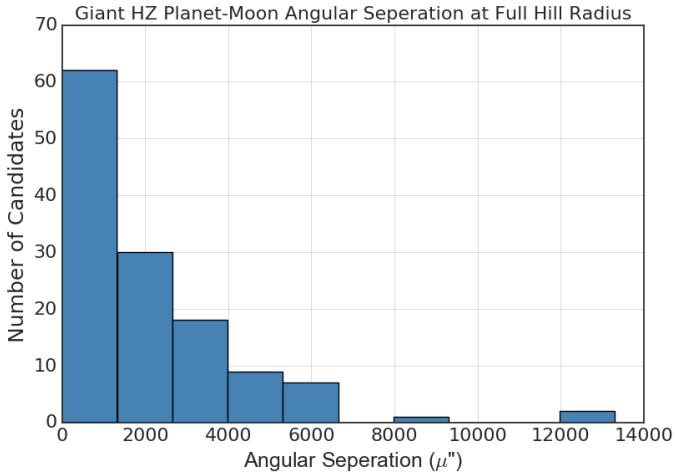

FIGURE 4.2: *The distribution of the giant habitable zone planets ($> 3R\oplus$) planet/moon angular separation, with moons positioned at the full Hill radii. Potential moons of giant planets found in the habitable zone will likely have a maximum angular separation from their host planet between $1 \sim 13000$ μ arc seconds. This information can be used for planning of imaging future missions if these planets are assumed to be representative of the entire population of stars and planets.*

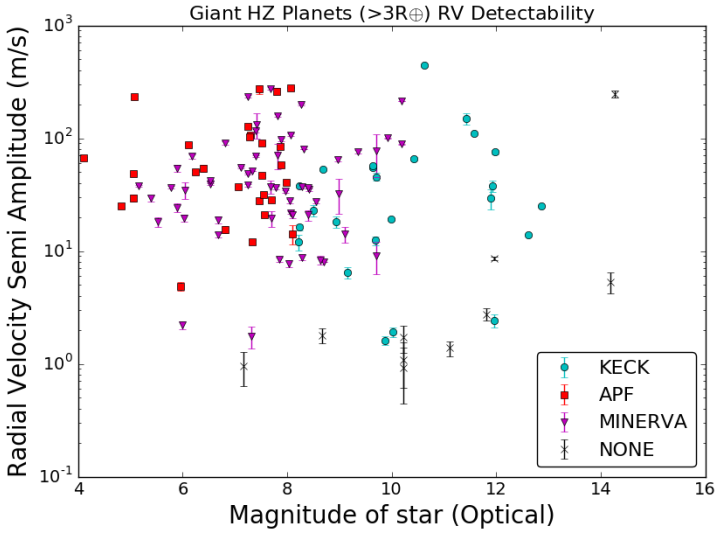

FIGURE 4.3: *The magnitude of the host star of the HZ planets and their expected radial velocity semi amplitude to determine the expected detectability of these planets. Each planet is separated by which telescope has been deemed the most appropriate for follow up observations. The large majority of the planets in our list will be detectable by either the Keck, Lick APF or MINERVA Australis telescopes. Those planets that either are missing data or are unlikely to be able to be detected by these telescopes are marked with black crosses. Future radial velocity missions to follow up on these candidates should focus on those found closest to the top left corner of the graph, where the brightest stars host candidates with large RV semi amplitudes.*

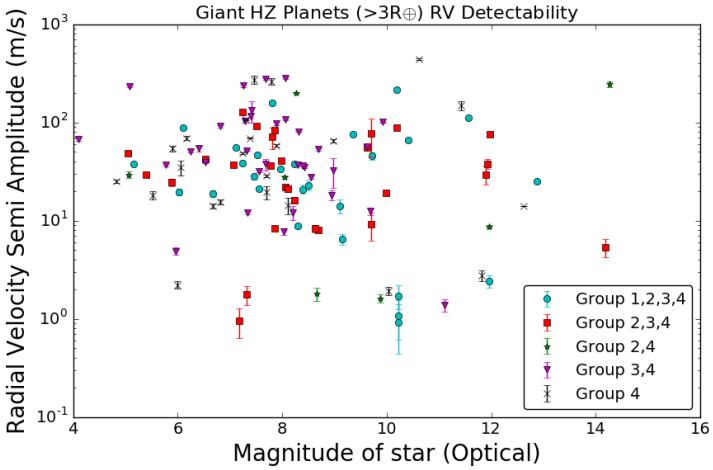

FIGURE 4.4: *The magnitude of the host star of the HZ planets and their expected radial velocity semi amplitude to determine the expected detectability of these planets. Each planet is separated by its Group which indicates the position of the planets orbit in relation to the HZ of the system. Group 1 is planets whose eccentric orbit lies in the CHZ, Group 2 is planets whose eccentric orbit lies in the OHZ, Group 3 is planets whose circular orbit lies in the CHZ, Group 4 is planets whose circular orbit lies in the OHZ. Future radial velocity missions to follow up on these candidates start with planets from Group 1 then work their way through the successive groups.*

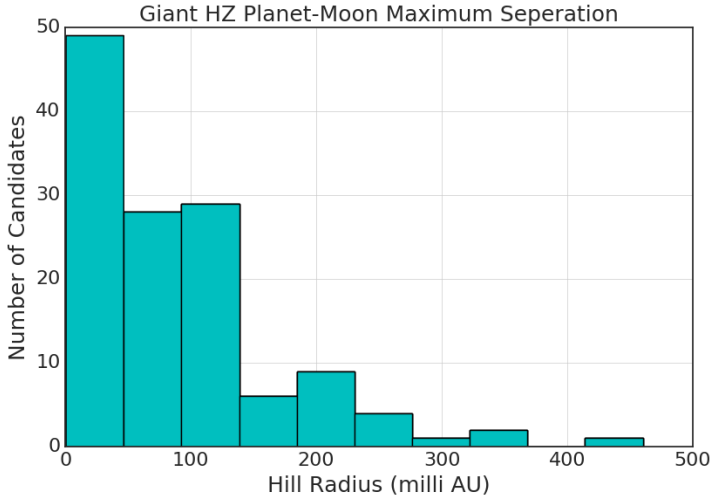

FIGURE 4.5: *The distribution of the giant habitable zone planets (> 3R⊕) Hill radii. Giant planets found in the habitable zone will likely have a maximum radius of gravitational influence between 1 $x10^{-3}$ ∼ 460 $x10^{-3}$ AU. This information can be used for planning of imaging future missions as these planets can be considered representative of the entire population of giant habitable zone planets.*

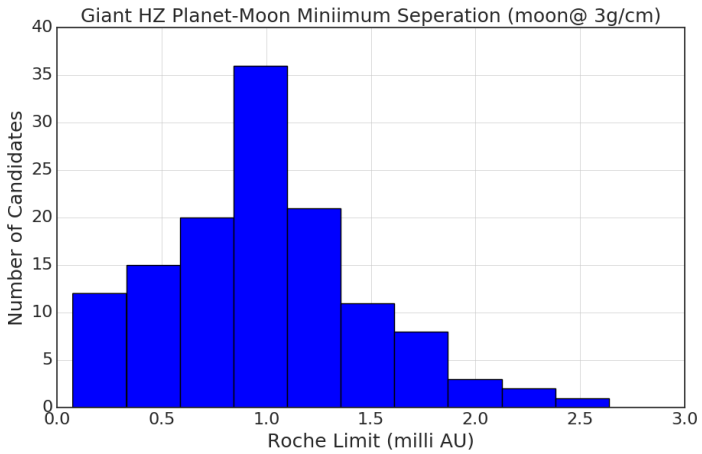

FIGURE 4.6: *Here the distribution of the giant habitable zone planets ($> 3R\oplus$) Roche limit is shown. The closest possible orbit of a moon without being destroyed by the pull of the host planet lies between 0.1 $x10^{-3}$ $\sim$ 2.6 $x10^{-3}$ AU for the giant habitable zone planets in our list. Moons are unlikely to be observed any closer to their host planet than this.*

4.3.2 Figures: RadVel Curves

Each giant planet's radial velocity curve was analysed in the *RadVel* program (Fulton et al. 2018) to confirm the orbital solution and look for linear trends to determine if there were indications for additional companions; potentially either additional planets in orbit or satellites. Figures 4.7 to 4.13 are examples of *RadVel* fits for some of the planets from Table 4.5 that have linear trends indicating the presence of another body in orbit. *RadVel* uses MCMC to estimate the parameter uncertainties and provides a corner plot for each planet radial velocity curve analysis displaying the posterior distributions as seen in Figure 4.8. Window (a) of each plot shows the MAP Keplerian orbital model with the blue line indicating the best model fit. Window (b) in the plots below shows the residuals of the best model. Then the Keplerian orbital models for each planet is provided in windows (c) onwards with one planets orbit per window. The legend, if provided, in the top right corner of panel (a) shows which spectograph the data used in the fit was obtained from.

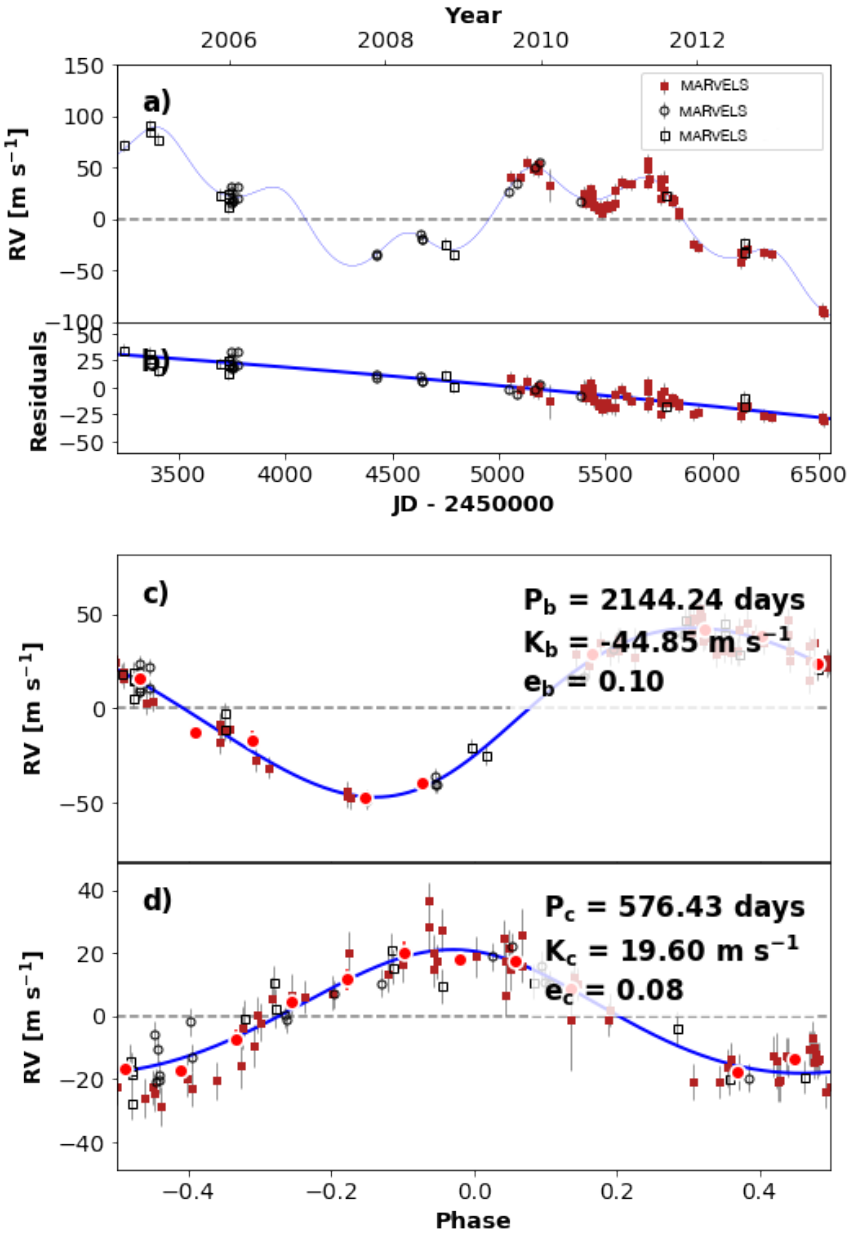

FIGURE 4.7: *HD 1605 RadVel time series plot. This shows the MAP 2-planet Keplerian orbital model. The blue line in window (a) is the 2-planet model. The data from three spectographs was used in this fit as indicated by the legend in the top right corner of window (a). HD 1605 shows a strong linear trend indicating the presence of another body in orbit. Currently two planets has been detected in orbit around HD 1605. HD 1605 c, whose Keplarian orbit is shown in window (c), is in Group 1 thus its eccentric orbit lies in the CHZ. Due to the stars position in the sky, magnitude and RV semi amplitude it is potentially observable by both APF and KECK telescopes, with priority given to the APF.*

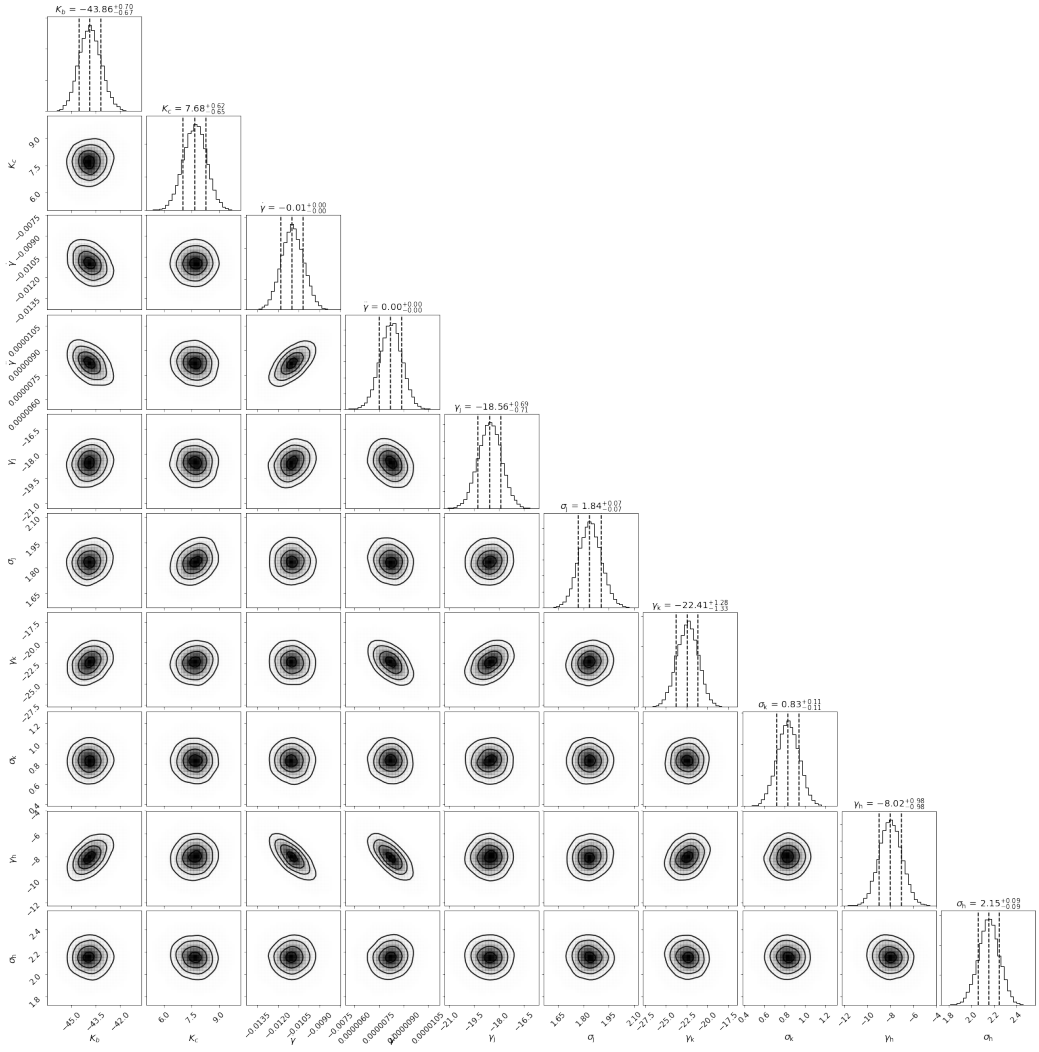

FIGURE 4.8: *HD 1605 MCMC corner plot displaying all joint posterior distributions derived from the MCMC sampling. RadVel uses MCMC to estimate the parameter uncertainties and provides a corner plot for each planet radial velocity curve analysis.*

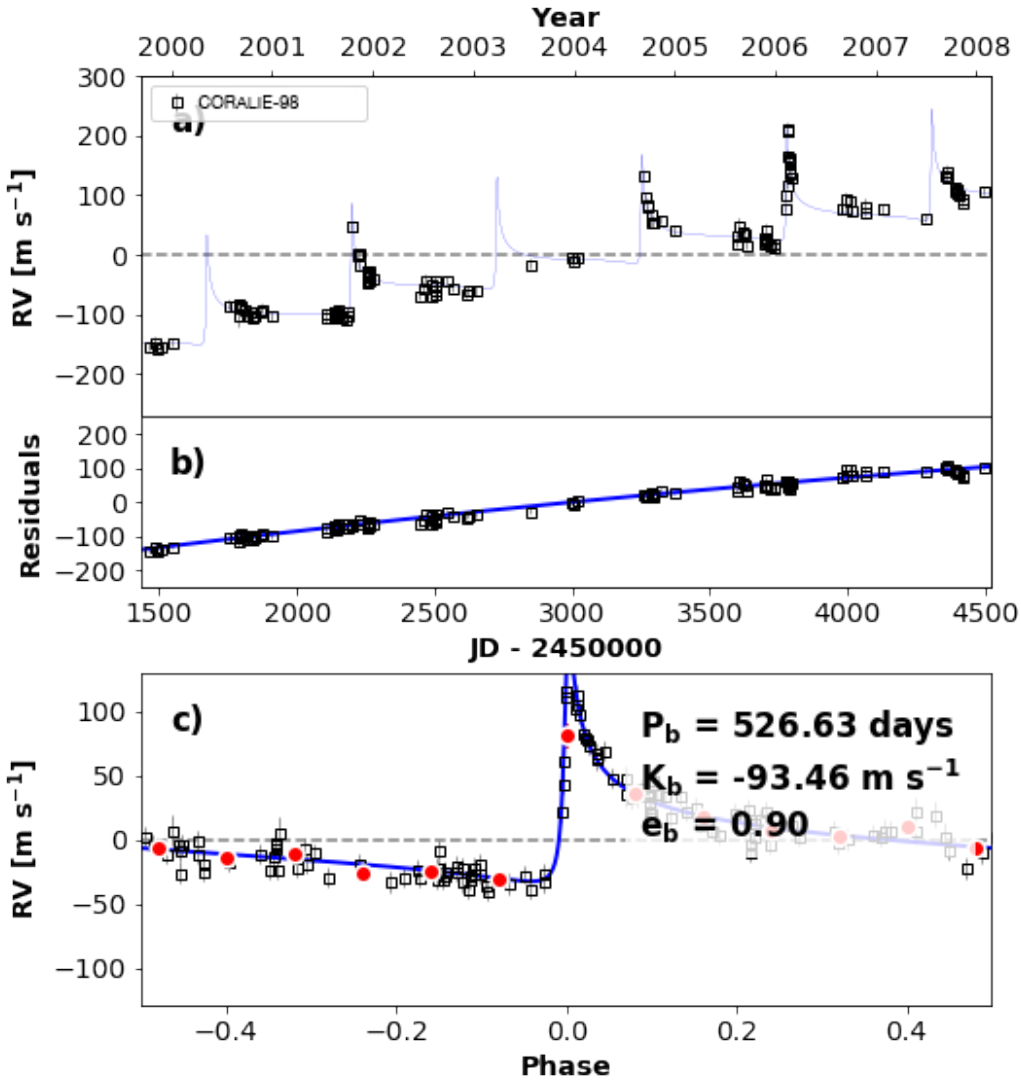

FIGURE 4.9: *HD 4113 RadVel time series plot. This shows the MAP 1-planet Keplerian orbital model. The blue line in window (a) is the 1-planet model. HD 4113 shows a very strong linear trend (≥129 σ) indicating the presence of another body in orbit. Currently only one planet has been detected in orbit around HD 4113. Due to the stars position in the sky, magnitude and RV semi amplitude it is potentially observable by MINERVA Australis. HD 4113 b, whose Keplerian orbit is shown in window (c), is in Group 3 thus its circular orbit lies in the CHZ.*

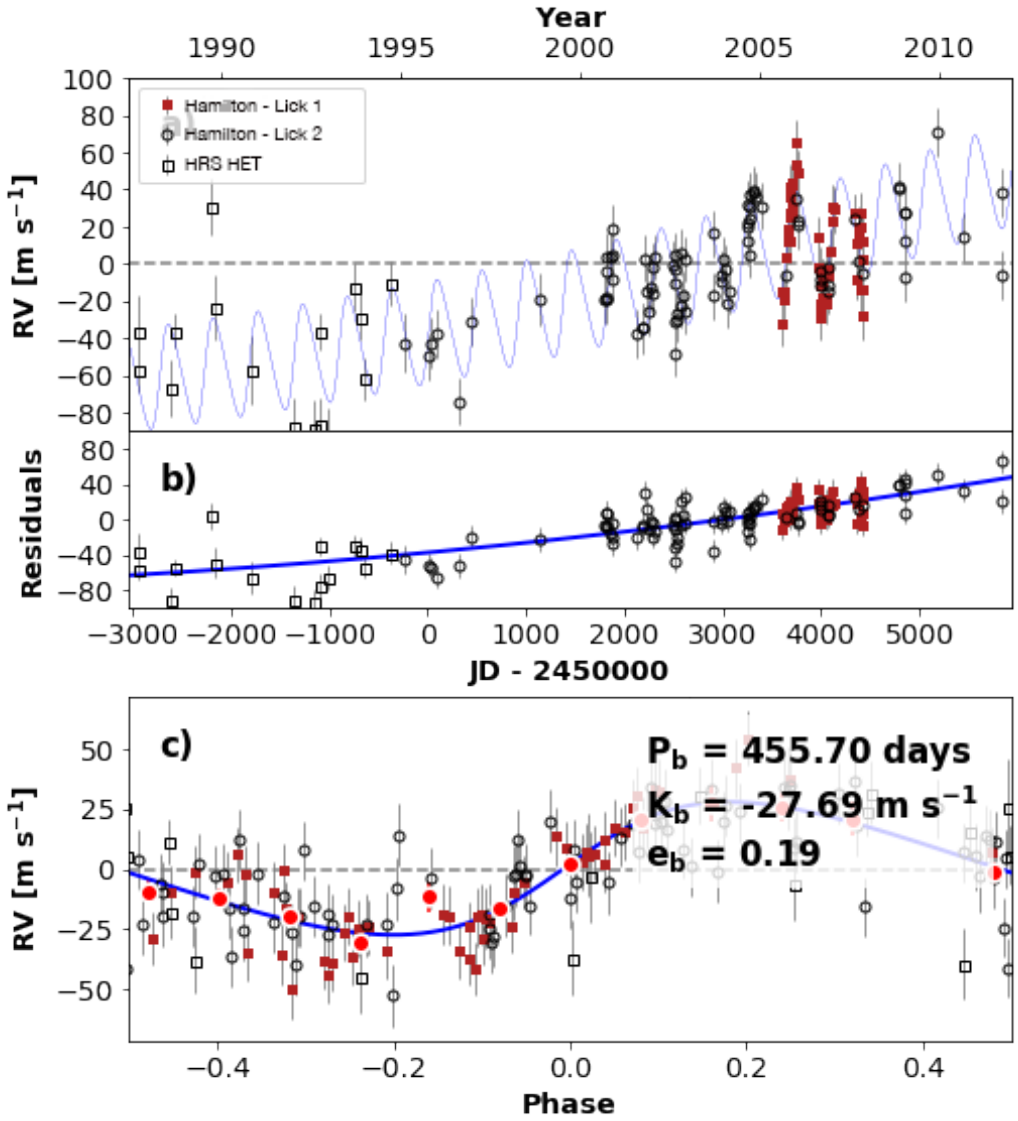

FIGURE 4.10: *HD 19994 RadVel time series plot. This shows the MAP 1-planet Keplerian orbital model. The blue line in window (a) is the 1-planet model. HD 19994 shows a strong linear trend indicating the presence of another body in orbit. Currently only one planet has been detected in orbit around HD 19994. Due to the stars position in the sky, magnitude and RV semi amplitude it is potentially observable by all three telescopes, with priority given to the APF. HD 19994 b, whose Keplarian orbit is shown in window (c), is in Group 2 thus its eccentric orbit lies in the OHZ.*

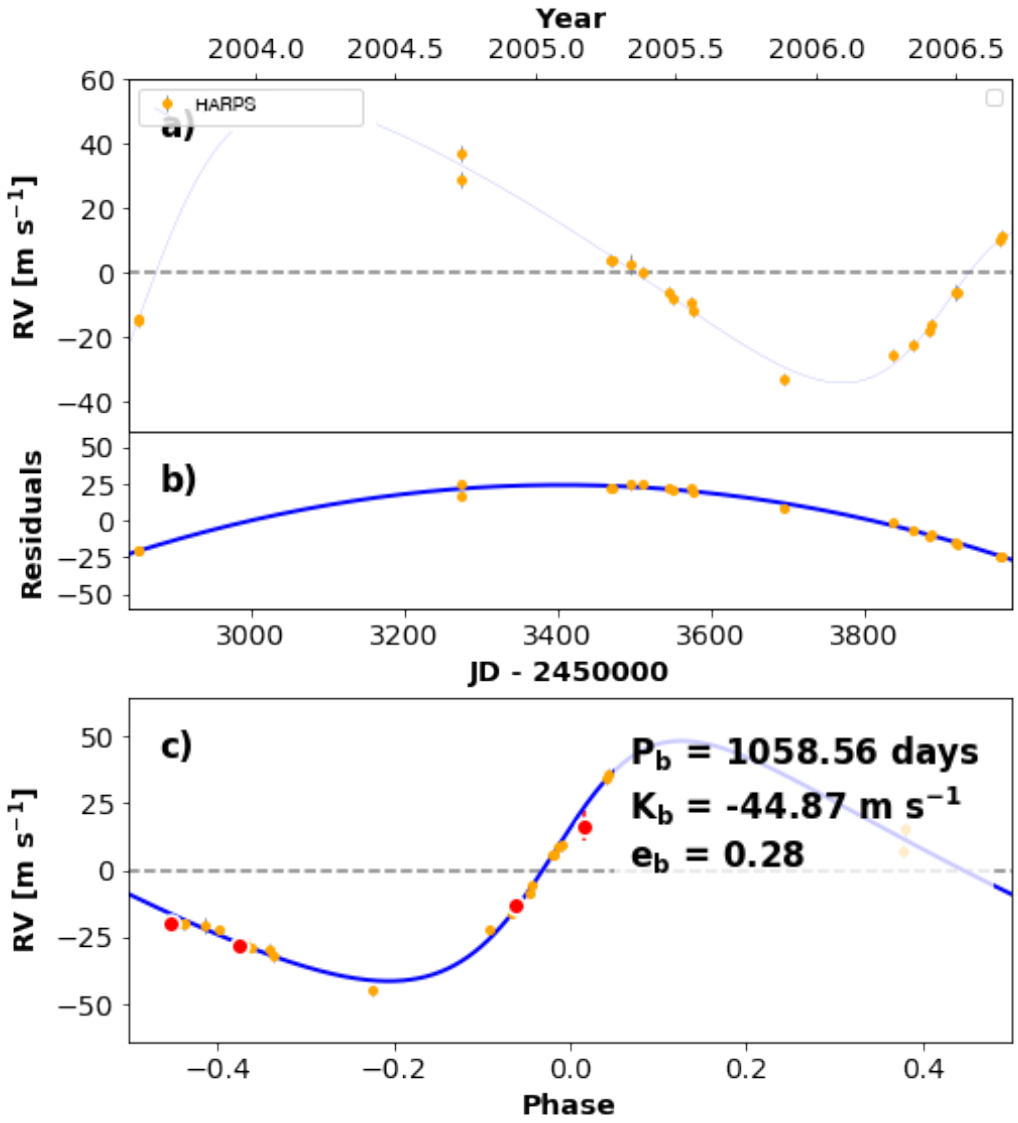

FIGURE 4.11: *HD 190647 RadVel time series plot. This shows the MAP 1-planet Keplerian orbital model. The blue line in window (a) is the 1-planet model. HD 190647 shows a linear trend indicating the presence of another body in orbit. Currently only one planet has been detected in orbit around HD 190647. HD 190647 b, whose Keplarian orbit is shown in window (c), is in Group 2 thus its eccentric orbit lies in the OHZ. Due to the stars position in the sky, magnitude and RV semi amplitude it is potentially observable by the MINERVA Australis telescope.*

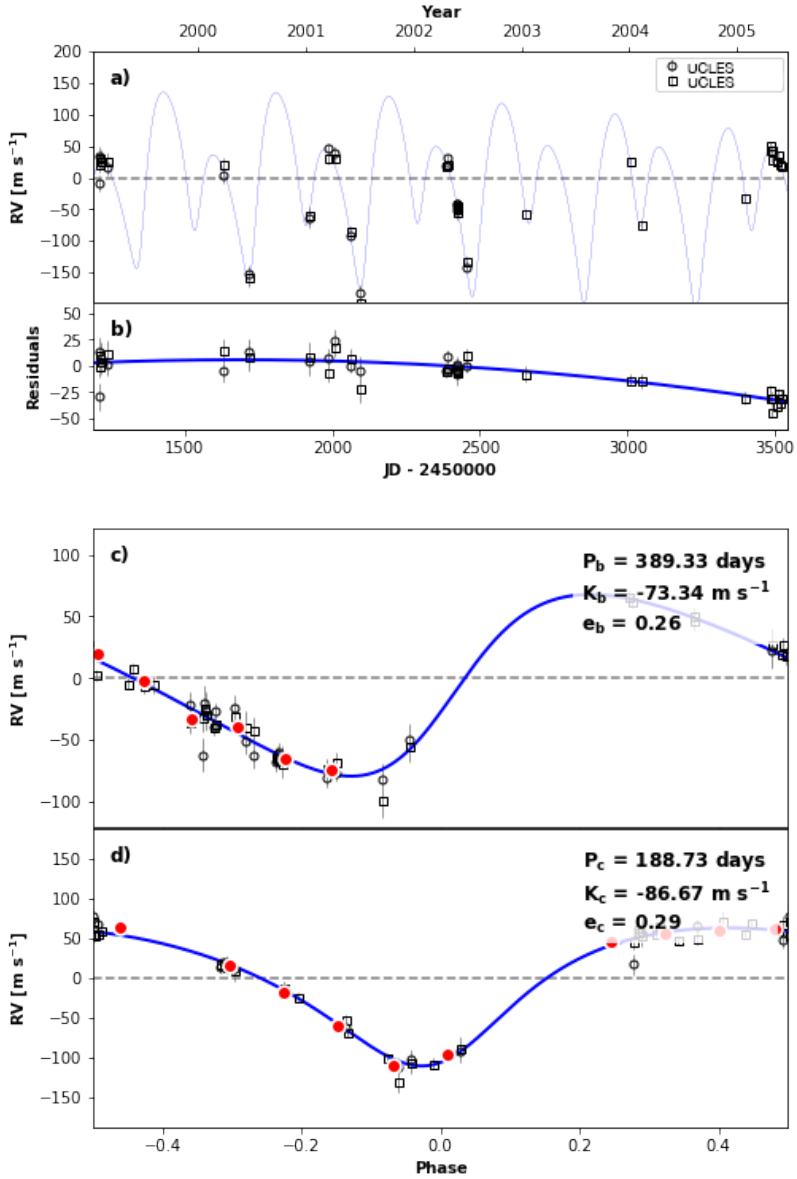

FIGURE 4.12: *HD 73526 RadVel time series plot. This shows the MAP 2-planet Keplerian orbital model. The blue line in window (a) is the 2-planet model. HD 73526 shows a linear trend indicating the presence of another body in orbit. Currently two planets has been detected in orbit around HD 73526. HD 73526 c, whose Keplarian orbit is shown in window (c), is in Group 4 thus its circular orbit lies in the OHZ. Due to the stars position in the sky, magnitude and RV semi amplitude it is potentially observable by the MINERVA Australis telescope.*

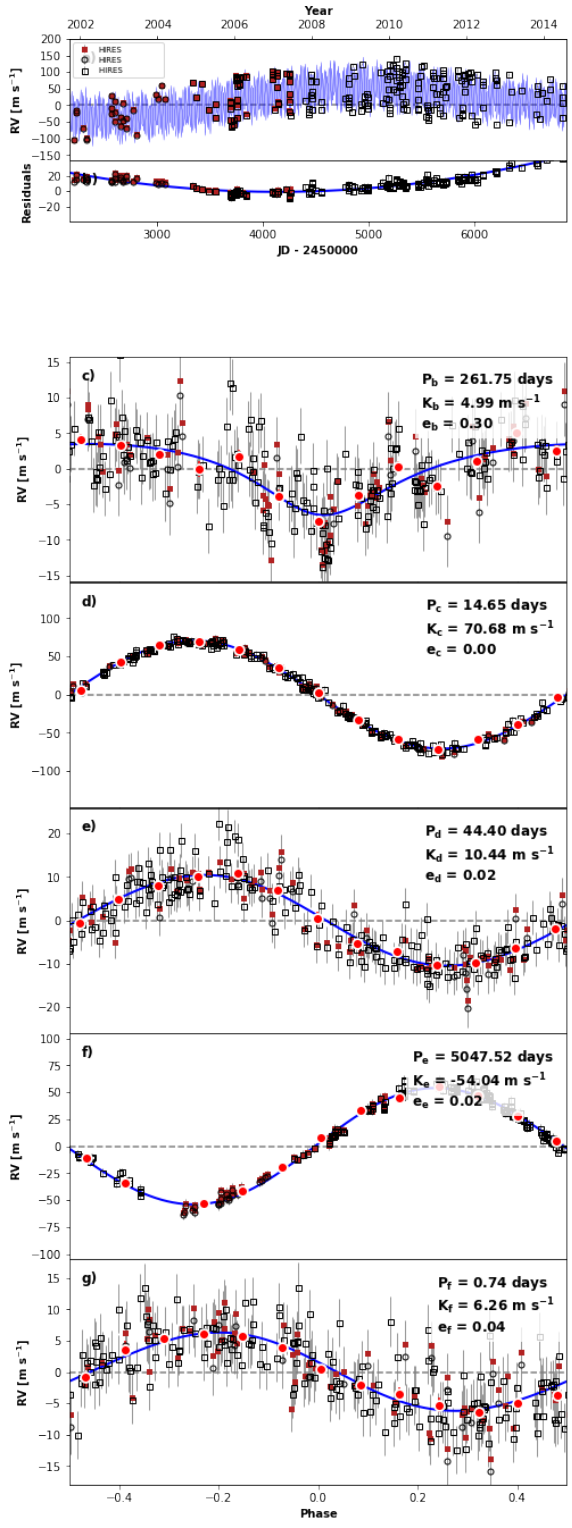

FIGURE 4.13: *55Cnc RadVel time series plot. This shows the MAP 5-planet Keplerian orbital model. The blue line in window (a) is the 5-planet model. 55 Cnc shows a linear trend indicating the presence of another body in orbit. Currently five planets has been detected in orbit around 55 Cnc. 55 Cnc f, whose Keplarian orbit is shown in window (c), is in Group 3 thus its circular orbit lies in the CHZ. Due to the stars position in the sky, magnitude and RV semi amplitude it is potentially observable by both the APF and KECK telescopes, with priority given to the APF.*

Chapter 5

Discussion

5.1 The BRHARVOS Method

This project aimed to develop a method to be followed in order to determine the best candidates likely to host HZ satellites. The method, which has been coined the 'BRHARVOS' method (pronounced 'Braa-vos'), is outlined in Section 3 and can be followed in future projects to systematically choose the best habitable zone planet candidates for follow up observations:

B: Future projects should start with calculation of the HZ Boundaries of each star and determine which planets reside in either the CHZ or the OHZ.

R: Then the Roche limit,

H: Hill radius,

A: and the Angular separation of the planet and potential exomoon should be calculated to determine those planet-moon systems with the greatest potential observability.

RV: After running the RV curves through RadVel, planets that show indications of orbital companions can be determined.

OS: Planets can then finally be assigned to telescopes best suited for their position, stellar magnitude and RV semi amplitude, completing the Observing Strategy.

A Python code was built to automate the calculation of the Hill radius, Roche limit and angular separations of each potential planet/moon pair and this will soon be made publicly available.

5.2 Moon Calculations

The calculations presented in Section 4 are intended for the design of future missions and observing strategies. Giant planets found in the habitable zone will likely have a Hill radius or maximum radius of gravitational influence between 1 x10^{-3}–460 x10^{-3} AU (Figure 4.5) while the Roche limit, or the closest possible orbit of a moon without being destroyed by the pull of the host planet lies between 0.1x10^{-3}–2.6 x10^{-3} AU (Figure 4.6). This is the envelope in which any potential exomoon orbiting the planets presented in Section 4 would reside. Taking a moons typical stable residence to be $\frac{1}{3}$ the Hill radius of the planet, the angular separation between a potential moon and its host planet will be in the range of 10 – 4400 μ arc seconds, as shown in Figure 4.1. This separation can potentially be extended if a moon is found to be at the Hill radius of the planet. The maximum angular separation of the moon from the host planet then increases to between 1 $\sim$ 13000 μ arc seconds (Figure 4.2). However, moons at this point are unlikely to be stable and so are not ideal in terms of habitability. Thus a moon orbiting a giant planet in the HZ is most likely to be observed with an angular separation between 10 – 4400 μ arc seconds and future imaging missions will need the capabilities to resolve this angular separation in order to image any potential moons in this data set.

5.3 Observing Strategy

This projects main goal was to determine which giant HZ planets showed indications of companions and provide an observing strategy for the *MINERVA Australis*, *Keck HIRES* and *Lick Automated Planet Finder (APF)* telescopes. The results from the RadVel data analysis is provided in Table 4.4, with a "Y" in the final column indicating those planets with linear trends. Of 121 giant planets in the HZ of their star, 51 planets showed indications of linear trends $\geq 3\sigma$. As these planets show indications of companions, either additional planets, exomoons or other celestial bodies, they will be considered the highest priority targets in our future observing missions (to be conducted in a subsequent project as part of my PhD). The linear trends discovered in this project, particularly those that are very large trends, are most likely to other planets in orbit around the star or possibly other nearby stars whose gravitational influence is affecting the known planet. After collecting any additional existing data for these systems and also making further observations, the next stage of this ongoing project will identify the additional companions in orbit with these HZ giant exoplanets. Identifying the likely stellar or planetary companions and then further refining the orbital parameters of the existing giant exoplanet will help in the future detection of exomoons around these planets.

As part of the observing strategy each giant planet was assigned to the telescope that is best qualified to carry out follow-up observations. The magnitude, radial velocity semi-amplitude and position of each star was considered during this selection process and compared to the specifications of each telescope. Currently *Keck HIRES* has the ability to observe an radial velocity RMS of 1-3 m/s down to 13.5 V magnitude (at 45 minutes per exposure) and *Lick APF* can obtain a radial velocity RMS of 1-3 m/s down to 8 V magnitude (Isaacson, H 2018, pers. comm., 27 April). Once *MINERVA Australis* is installed with 4 telescopes (6 are currently

planned) it is expected to have the capability of viewing a radial velocity RMS of 3 m/s down to 10 V magnitude at ∼30 minutes per exposure (Wittenmyer, R 2018, pers. comm., 26 April).

The telescope observing strategies for the *MINERVA Australis*, *Keck HIRES* and *Lick APF* telescopes were constructed for each subset of planets and are presented in Tables 4.5 and 4.6. The Tables have been sorted by which telescope each planet will be assigned to and also by their Group number, with planets in Group 1 being the highest priority targets for follow up observations. For those planets where more than one telescope is capable of observation, the telescope for whom that target will be assigned is listed first. The large majority of the planets in our list will be detectable for follow up observations by either the *Keck HIRES*, *Lick APF* or *MINERVA Australis* telescopes. Among those with indications of linear trends 27 are potentially observable by *MINERVA Australis*, 14 by *Lick APF* and 10 by *Keck HIRES*. These planets will be observed to try to resolve any possible additional planets in orbit or potential moons. Among those without indications of linear trends 30 are potentially observable by *MINERVA Australis*, 14 by *Lick APF* and 13 by *Keck HIRES*. Observations of these planets will be made to help refine the orbital parameters and masses of the planets. As these planets reside in the HZ of their star they are relatively far out and so are likely to have poor orbital constraints. As these directly effect the exomoon property calculations, any observations made will greatly help in refining the known orbital parameters.

For those planets either unobservable by the *Keck HIRES*, *Lick APF* or *MINERVA Australis* telescopes, or that were missing data required for observations, the column was left blank. Note these planets may still be observable, just not by the three telescopes that are to be used for follow up observations in the next stage of this study (to be undertaken during my PhD). If not already observable by alternative ground based telescopes these stars may be observable after the installation of some currently planned telescopes, such as the *Giant Magellan Telescope (GMT)* (Szentgyorgyi et al. 2016).

A plot of the magnitude of the host star of the giant HZ planets and their expected radial velocity semi amplitude is shown in Figure 4.3, with each planet identified by the telescope that has been deemed to be the most appropriate for follow up observations. Future missions to follow up on these candidates should focus on those found closest to the top left corner of the graph, where the brightest stars host candidates with large RV semi amplitudes.

The magnitude of the host star of the HZ planets and their expected radial velocity semi amplitude was also plotted with each planet separated by its Group in Figure 4.4. The Group number indicates the position of the planets orbit in relation to the HZ of the system. Group 1 is planets whose eccentric orbit lies in the CHZ, Group 2 is planets whose eccentric orbit lies in the OHZ, Group 3 is planets whose circular orbit lies in the CHZ, Group 4 is planets whose circular orbit lies in the OHZ. If observers wish to prioritise those planets whose orbits stay in the CHZ they should start with planets from Group 1 then work their way through the successive groups.

Exomoon hunters are on the cusp of being able to detect exomoons and the giant planets listed in Tables 4.1 to 4.6 of this project along with the calculations provided will provide an excellent starting point for target selection. So far the primary method of exomoon detection is still uncertain, with transit timing variations, transits, and imaging methods all good contenders, as well as some methods unexplored in this project (namely microlensing (Liebig & Wambsganss 2010) and spectroastrometry (Agol et al. 2015)). However, imaging may prove to be the best way to detect exomoons in the future; it was found by Sartoretti & Schneider (1999) that multiple moons around a single planet may wash out any timing variation signal. In addition the small radius combined with the low contrast between planet and moon brightness mean transits are unlikely to be a good method for detection. In contrast Hill et al. (2018) noted that tidally heated exomoons can potentially be detected in direct imaging if the contrast ratio of the satellite and the planet is favorable (Peters & Turner 2013). Thus once telescopes develop to where they

are able to resolve a separation of 10 – 4400 μ arc seconds, imaging may be our best method of detecting these potentially habitable worlds.

Chapter 6

Conclusion and Future Work

6.1 A Brief Overview

Using the BRHARVOS method it was found that giant planets in the habitable zones tend to have a maximum radius of gravitational influence between 1 x10^{-3} $\sim$ 460 x10^{-3} AU while the closest possible orbit of a moon without being destroyed by the pull of the host planet lies between 0.1 x10^{-3} $\sim$ 2.6 x10^{-3} AU. If imaging of an exomoon orbiting a giant planet in the habitable zone is desired, instruments must have the capability to resolve a separation between 10 $\sim$ 4400 μ arc seconds in order to image any moon found at the estimated stable orbital distance of $\frac{1}{3}$ Hill radius. Following the RadVel analysis of each planets RV curve, it was found that among those planets with indications of linear trends, 27 are potentially observable by *MINERVA Australis*, 14 by *Lick APF* and 10 by *Keck HIRES*. Among those without indications of linear trends, 30 are potentially observable by *MINERVA Australis*, 14 by *Lick APF* and 13 by *Keck HIRES*.

6.2 Future Work

Using the calculations and refined list of giant planets found in Section 4, an observation plan to observe these planets is in development as part of my next project (PhD work). Planets with indications of linear trends will be observed to try to resolve any possible additional planets in orbit or potential moons. Following the order of priority, targets in Group 1 will be observed first and then subsequent groups will follow. Priority will also be given to planets with larger masses due to their ability to potentially host larger exomoons. Then observations will be made of the planets with no indications of linear trends in order to help refine the orbital parameters and masses of the planets.

The length of the observations will vary with each target. As the giant planets from this project reside in the HZ of their star, their orbital periods can be relatively long. In order to refine the orbital parameters an observation would ideally survey a full orbit. However, constant surveillance of the full orbit of a HZ planet could take many hundreds of days and so is a poor use of the limited telescope time available. Thus a minimum observation time of each target will be calculated to ensure the observation of just one of the turn around points of a planet. This is done by assuming the worst case scenario where a beginning observation has just missed the turn around point of a planets orbit. From this point to the estimated turn around will give the minimum time needed to observe. From here observing time of the target may indeed be shorter if the planet was closer to its turn around point than assumed. For those planets with linear trends, the orbital period for any possible additional planet is not constrained. Thus the time needed for observation of the turn around point of the planets orbit is unclear.

6.3 Concluding Remarks

The inclusion of exomoons orbiting giant planets in the HZ of their star is a significant addition to the search for habitable worlds. Given the expected occurrence rates of giant planets in the HZ, and assuming more than one terrestrial moon per giant planet, there may be as many exomoons in the HZ as there are terrestrial planets, potentially doubling the number of possibly habitable worlds out in the universe. Due to the nature of these exomoons they may be considered to have an even greater potential to hold life than that of Earth-like terrestrial planets. These potential life-supporting characteristics include the thermal and reflected radiation from the host planet and the tidal effects on an exomoon that help increase the outer range of the HZ, creating a wider temperate zone in which a stable satellite may exist. The extra protection of the giant host planets magnetosphere also increases the likelihood that a large exomoon will hold on to its atmosphere, another essential ingredient to life as we know it. The rich diversity of size, density and geological phenomena in our own Solar system's satellites also provide clues as to the potential of these satellites and are themselves examples of potentially life holding worlds. Thus the detection and characterisation of exomoons is of utmost importance in the search for habitable worlds. Once imaging capabilities have improved, the detection of potentially habitable moons around these giant hosts will be much more accessible. Until then the properties of the giant host planets must continue to be refined, starting with radial velocity follow-up observations of giant HZ candidates.

Appendix A

Exploring Kepler Giant Planets in the Habitable Zone

The following pages contain the paper *Exploring Kepler Giant Planets in the Habitable Zone* (Hill et al. 2018) which was written concurrently with this honours thesis. It includes supporting research and is provided here for reference. This paper has been accepted for publication in The Astrophysical Journal.

Draft version May 22, 2018
Typeset using LaTeX **twocolumn** style in AASTeX61

EXPLORING KEPLER GIANT PLANETS IN THE HABITABLE ZONE

Michelle L. Hill,[1,2,3] Stephen R. Kane,[4,1] Eduardo Seperuelo Duarte,[5] Ravi K. Kopparapu,[6,7,8]
Dawn M. Gelino,[9] and Robert A. Wittenmyer[1]

[1] *University of Southern Queensland, Computational Engineering and Science Research Centre, Toowoomba, Queensland 4350, Australia*
[2] *University of New England, Department of Physics, Armidale, NSW 2351, Australia*
[3] *San Francisco State University, Department of Physics & Astronomy, 1600 Holloway Avenue, San Francisco, CA 94132, USA*
[4] *University of California, Riverside, Department of Earth Sciences, CA 92521, USA*
[5] *Instituto Federal do Rio de Janeiro, Grupo de Física e Astronomia, R. Cel. Delio Menezes Porto, 1045, CEP 26530-060, Nilópolis - RJ, Brazil*
[6] *NASA Goddard Space Flight Center, 8800 Greenbelt Road, Mail Stop 699.0 Building 34, Greenbelt, MD 20771*
[7] *NASA Astrobiology Institutes Virtual Planetary Laboratory, P.O. Box 351580, Seattle, WA 98195, USA*
[8] *Sellers Exoplanet Environments Collaboration, NASA Goddard Space Flight Center.*
[9] *NASA Exoplanet Science Institute, Caltech, MS 100-22, 770 South Wilson Avenue, Pasadena, CA 91125, USA*

Submitted to ApJ

ABSTRACT

The *Kepler* mission found hundreds of planet candidates within the Habitable Zones (HZ) of their host star, including over 70 candidates with radii larger than 3 Earth radii ($R_\oplus$) within the optimistic HZ (OHZ) (Kane et al. 2016). These giant planets are potential hosts to large terrestrial satellites (or exomoons) which would also exist in the HZ. We calculate the occurrence rates of giant planets ($R_p = 3.0$–$25\ R_\oplus$) in the OHZ and find a frequency of $(6.5 \pm 1.9)\%$ for G stars, $(11.5 \pm 3.1)\%$ for K stars, and $(6 \pm 6)\%$ for M stars. We compare this with previously estimated occurrence rates of terrestrial planets in the HZ of G, K and M stars and find that if each giant planet has one large terrestrial moon then these moons are less likely to exist in the HZ than terrestrial planets. However, if each giant planet holds more than one moon, then the occurrence rates of moons in the HZ would be comparable to that of terrestrial planets, and could potentially exceed them. We estimate the mass of each planet candidate using the mass-radius relationship developed by Chen & Kipping (2016). We calculate the Hill radius of each planet to determine the area of influence of the planet in which any attached moon may reside, then calculate the estimated angular separation of the moon and planet for future imaging missions. Finally, we estimate the radial velocity semi-amplitudes of each planet for use in follow up observations.

Keywords: astrobiology – astronomical databases: miscellaneous – planetary systems – techniques: photometric, radial velocity, imaging

michellelouhill@gmail.com

1. INTRODUCTION

The search for exoplanets has progressed greatly in the last 3 decades and the number of confirmed planets continues to grow steadily. These planets orbiting stars outside our solar system have already provided clues to many of the questions regarding the origin and prevalence of life. They have provided further understanding of the formation and evolution of the planets within our solar system, and influenced an escalation in the area of research into what constitutes a habitable planet that could support life. With the launch of NASA's *Kepler* telescope thousands of planets were found, in particular planets as far out from their host star as the Habitable Zone (HZ) of that star were found, the HZ being defined as the region around a star where water can exist in a liquid state on the surface of a planet with sufficient atmospheric pressure (Kasting et al. 1993). The HZ can further divided into two regions called the conservative HZ (CHZ) and the optimistic HZ (OHZ) (Kane et al. 2016). The CHZ inner edge consists of the runaway greenhouse limit, where a chemical breakdown of water molecules by photons from the sun will allow the now free hydrogen atoms to escape into space, drying out the planet at 0.99 AU in our solar system (Kopparapu et al. 2014). The CHZ outer edge consists of the maximum greenhouse effect, at 1.7 AU in our solar system, where the temperature on the planet drops to a point where CO_2 will condense permanently, which will in turn increase the planet's albedo, thus cooling the planet's surface to a point where all water is frozen (Kaltenegger & Sasselov 2011). The OHZ in our solar system lies between 0.75–1.8 AU, where the inner edge is the "recent Venus" limit, based on the empirical observation that the surface of Venus has been dry for at least a billion years, and the outer edge is the "early Mars" limit, based on the observation that Mars appears to have been habitable ∼3.8 Gyrs ago (Kopparapu et al. 2013). The positions of the HZ boundaries vary in other planetary systems in accordance with multiple factors including the effective temperature, stellar flux and luminosity of a host star.

A primary goal of the *Kepler* mission was to determine the occurrence rate of terrestrial-size planets within the HZ of their host stars. Kane et al. (2016) cataloged all Kepler candidates that were found in their HZ, providing a list of HZ exoplanet candidates using the Kepler data release 24, Q1–Q17 data vetting process, combined with the revised stellar parameters from DR25 stellar properties table. Planets were then split into 4 groups depending on their position around their host star and their radius. Categories 1 and 2 held planets that were $< 2\ R_\oplus$ in the CHZ and OHZ respectively and Categories 3 and 4 held planets of any radius in the CHZ and OHZ respectively. In Category 4, where candidates of any size radius are found to be in the OHZ, 76 planets of size 3 $R_\oplus$ and above were found.

Often overshadowed by the discoveries of numerous transiting Earth-size planets in recent years (e.g. Gillon et al. 2017; Dittmann et al. 2017), Jupiter-like planets are nonetheless a critical feature of a planetary system if we are to understand the occurrence of truly Solar-system like architectures. The frequency of close-in planets, with orbits $a \leq 0.5$ AU, has been investigated in great detail thanks to the thousands of *Kepler* planets (Howard et al. 2012; Fressin et al. 2013; Burke et al. 2015). In the icy realm of Jupiter analogs, giant planets in orbits beyond the ice line ∼3 AU, radial velocity (RV) legacy surveys remain the critical source of insight. These surveys, with time baselines exceeding 15 years, have the sensitivity to reliably detect or exclude Jupiter analogs (Wittenmyer et al. 2006; Cumming et al. 2008; Wittenmyer et al. 2011; Rowan et al. 2016). For example, an analysis of the 18-year Anglo-Australian Planet search by Wittenmyer et al. (2016) yielded a Jupiter-analog occurrence rate of $6.2^{+2.8}_{-1.6}$% for giant planets in orbits from 3 to 7 AU. Similar studies from the Keck Planet search (Cumming et al. 2008) and the ESO planet search programs (Zechmeister et al. 2013) have arrived at statistically identical results: in general, Jupiter-like planets in Jupiter-like orbits are present around less than 10% of solar-type stars. While these giant planets are not favored in the search for Earth-like planets, the discovery of a number of these large planets in the habitable zone of their star (Diaz et al. 2016) do indicate a potential for large rocky moons also residing in the HZ.

A moon is generally defined as a celestial body that orbits around a planet or asteroid and whose orbital barycenter is located inside the surface of the host planet or asteroid. There are currently 175 known satellites orbiting the 8 planets within the solar system, most of which are in orbit around the two largest planets in our system with Jupiter hosting 69 known moons and Saturn hosting 62 known moons[1]. The diverse compositions of the satellites in the solar system give insight into their formation (Canup & Ward 2002; Heller et al. 2015). Most moons are thought to be formed from accretion within the discs of gas and dust circulating around planets in the early solar system. Through gravitational collisions between the dust, rocks and gas the debris gradually builds, bonding together to form a satellite

[1] http://www.dtm.ciw.edu/users/sheppard/satellites/

(Elser et al. 2011). Other satellites may have been captured by the gravitational pull of a planet if the satellite passes within the planets area of gravitational influence, or Hill radius. This capture can occur either prior to formation during the proto-planet phase, as proposed in the nebula drag theory (Holt et al. 2017; Pollack et al. 1979), or after formation of the planet, also known as dynamical capture. Moons obtained via dynamical capture could have vastly different compositions to the host planet and can explain irregular satellites such as those with high eccentricities, large inclinations, or even retrograde orbits (Holt et al. 2017; Nesvorny et al. 2003). The Giant-Collision formation theory, widely accepted as the theory of the formation of Earths Moon, proposes that during formation the large proto-planet of Earth was struck by another proto-planet approximately the size of Mars that was orbiting in close proximity. The collision caused a large debris disk to orbit the Earth and from this the material the Moon was formed (Hartmann et al. 1975; Cameron & Ward 1976). The close proximity of each proto-planet explains the similarities in the compositions of the Earth and Moon while the impact of large bodies helps explain the above average size of Earths Moon (Elser et al. 2011). The large number of moons in the solar system, particularly the large number orbiting the Jovian planets, indicate a high probability of moons orbiting giant exoplanets.

Exomoons have been explored many times in the past (e.g. Williams et al. 1997; Kipping et al. 2009; Heller 2012). Exomoon habitability particularly has been explored in great detail by Dr Rene Heller, (e.g. Heller 2012; Heller & Barnes 2013; Heller & Pudritz 2015; Zollinger et al. 2017) who proposed that an exomoon may even provide a better environment to sustain life than Earth. Exomoons have the potential to be what he calls "super-habitable" because they offer a diversity of energy sources to a potential biosphere, not just a reliance on the energy delivered by a star, like earth. The biosphere of a super-habitable exomoon could receive energy from the reflected light and emitted heat of its nearby giant planet or even from the giant planet's gravitational field through tidal forces. Thus exomoons should then expect to have a more stable, longer period in which the energy received could maintain a livable temperate surface condition for life to form and thrive in.

Another leader in the search for exomoons has been the "Hunt for Exomoons with Kepler" (HEK) team; (e.g. Kipping et al. 2012, 2013a,b, 2014, 2015). Here Kipping and others investigated the potential capability and the results of *Kepler*, focusing on the use of transit timing variations (TTV's) and and transit duration variations (TDV's) to detect exomoon signatures. Though several attempts to search for companions to exoplanets through high-precision space-based photometry yielded null results, the latest HEK paper (Teachey et al. 2017) indicates the potential signature of a planetary companion, exomoon Candidate Kepler-1625b I. This exomoon is yet to be confirmed and as such caution must be exercised as the data is based on only 3 planetary transits. Still, this is the closest any exomoon hunter has come to finding the first exomoon. As we await the results of the follow up observations on this single candidate, it is clear future instruments will need greater sensitivity for the detection of exomoons to prosper. While the HEK papers focused on using the TTV/TDV methodology's to detect exomoons around all of the *Kepler* planets, our paper complements this study by determining the estimated angular separation of only those Kepler planet candidates $3R_\oplus$ and above that are found in the optimistic HZ of their star. We choose the lower limit of $3R_\oplus$ as we are interested only in those planets deemed to be gas giants that have the potential to host large satellites. While there is a general consensus that the boundary between terrestrial and gaseous planets likely lies close to $1.6R_\oplus$, we use $3R_\oplus$ as our cutoff to account for uncertainties in the stellar and planetary parameters and prevent the inclusion of potentially terrestrial planets in our list, as well as planets too small to host detectable exomoons. We use these giant planets to determine the future mission capabilities required for imaging of potential HZ exomoons. We also include RV semi-amplitude calculations for follow up observations of the HZ giant planets.

In Section 2 of this paper we explore the potential of these HZ moons, citing the vast diversity of moons within our solar system. We predict the frequency of HZ giant planets using the inverse-detection-efficiency method in Section 3. In Section 4 we present the calculations and results for the estimated planet mass, Hill radius of the planet, angular separation of the planet from the host star and of any potential exomoon from its host planet, and the RV semi-amplitude of the planet on its host star. Finally, in Section 5 we discuss the calculations and their implications for exomoons and outline proposals for observational prospects of the planets and potential moons, providing discussion of caveats and concluding remarks.

2. SCIENCE MOTIVATION

Within our solar system we observe a large variability of moons in terms of size, mass, and composition. Five icy moons of Jupiter and Saturn show strong evidence of oceans beneath their surfaces: Ganymede, Europa and

Callisto at Jupiter, and Enceladus and Titan at Saturn. From the detection of water geysers and deep oceans below the icy crust of Enceladus (Porco et al. 2006; Hsu et al. 2015) to the volcanism on Io (Morabito et al. 1979), our own solar system moons display a diversity of geological phenomena and are examples of potentially life holding worlds. Indeed Ganymede, the largest moon in our solar system, has its own magnetic field (Kivelson et al. 1996), an attribute that would increase the potential habitability of a moon due to the extra protection of the moons atmosphere from its host planet (Williams et al. 1997). And while the moons within our own HZ have shown no signs of life, namely Earth's moon and the Martian moons of Phobos and Deimos, there is still great habitability potential for the moons of giant exoplanets residing in their HZ.

The occurrence rate of moons in the HZ is intrinsically connected to the occurrence rate of giant planets in that region. We thus consider the frequency of giant planets within the OHZ. We choose to use the wider OHZ due to warming effects any exomoon will undergo as it orbits its host planet. The giant planet will increase the effective temperature of the moon due to contributions of thermal and reflected radiation from the giant planet (Hinkel & Kane 2013). Tidal effects will also play a significant role, as seen with Io. Scharf (2006) proposed that this heating mechanism can effectively increase the outer range of the HZ for a moon as the extra mechanical heating can compensate for the lack of radiative heating provided to the moon. For the same reason this could reduce the interior edge of the HZ causing any moon with surface water to undergo the runaway green house effect earlier than a lone body otherwise would, though the outwards movement of the inner edge has been found to be significantly less than that of the outer edge and so the effective habitable zone would still be widened for any exomoon. This variation could also possibly enable giant exoplanets with eccentric orbits that lie, at times, outside the OHZ to maintain habitable conditions on any connected exomoons (Hinkel & Kane 2013).

3. FREQUENCY OF HABITABLE ZONE GIANT PLANETS

The occurrence rates of terrestrial planets in the HZ has been explored many times in the literature (e.g. Howard et al. 2012; Dressing & Charbonneau 2013, 2015; Kopparapu 2013; Petigura et al. 2013). The planet occurrence rate is defined as the number of planets per star (NPPS) given a range of planetary radius and orbital period. It is simply represented by the expression

$$NPPS = \frac{N_p}{N_*} \tag{1}$$

where N_p is the real number of planets and N_* is the number of stars in the *Kepler* survey. However, N_p is unknown due to some limitations of the mission. The first limitation is produced by the duty cycle which is the fraction of time in which a target was effectively observed (Burke et al. 2015). The requirement adopted by the Kepler mission to reliably detect a planet is to observe at least three consecutive transits (Koch et al. 2010). This requirement is difficult to achieve for low duty cycles and for planets with long orbital periods. The second limitation is the photometric efficiency, the capability of the photometer to detect a transit signal for a given noise (Signal-to-Noise ratio; SNR). For a given star it is strongly dependent on the planet size since the transit depth depends on the square of the radius ratio between the planet and the star. Thus, smaller planets are more difficult to detect than the bigger ones. Finally, the transit method is limited to orbits nearly edge-on relative to the telescope line of sight. Assuming a randomly oriented circular orbit, the probability of observing a star with radius R_* being transited by a planet with semi-major axis a is given by R_*/a.

Those survey features contribute to the underestimation of the number of detectable planets orbiting the stars of the survey. Thus, to obtain N_p, the observed number of planets N_{obs} is corrected by taking the detection efficiencies described above into account. In Section 3.1, the method used to accomplish this goal is described.

3.1. *The Method*

The method used in this work to compute the occurrence rate, which is commonly used in the literature ((Howard et al. 2012), (Dressing & Charbonneau 2015)), is called the inverse-detection-efficiency method (Foreman-Mackey et al. 2016). It consists of calculating the occurrence rates in a diagram of radius and period binned by a grid of cells. The diagram is binned following the recommendations of the NASA ExoPAG Study Analysis Group 13, i.e, the i-th,j-th bin is defined as the interval $[1.5^{i-2}, 1.5^{i-1})R_\oplus$ and $10\text{x}[2^{j-1}, 2^j)day$. The candidates are plotted, according to their physical parameters, and the real number of planets is then computed in each cell ($N_p^{i,j}$) by summing the observed planets ($N_{obs}^{i,j}$) in the i,j bin weighted by their inverse detection probability, as

$$N_p^{i,j} = \sum_{n=1}^{N_{obs}^{i,j}} \frac{1}{p_n} \tag{2}$$

where p_n is the detection probability of planet n. Finally, the occurrence rate is calculated by Equation (3)

as a function of orbital period and planetary radius,

$$NPPS^{i,j} = \frac{N_p^{i,j}}{N_*} \quad (3)$$

3.2. *Validating Methodology*

We confirm that we are able to recover accurate occurrence rates by using the method described above to first compute the occurrence rates of planets orbiting M dwarfs and comparing the results with known values found by (Dressing & Charbonneau 2015) (here after DC15). DC15 used a stellar sample of 2543 stars with effective temperatures in the range of 2661–3999 K, stellar radii between 0.10 and 0.64 $R_\oplus$, metallicity spanning from -2.5 to 0.56 and Kepler magnitudes between 10.07 and 16.3 (Burke et al. 2015). The sample contained 156 candidates with orbital periods extending from 0.45 to 236 days and planet radii from 0.46 to 11$R_\oplus$.

The real number of planets was computed in each cell using equation (2) with p_n being the average detection probability of planet n. Then equation (3) was used to calculate the occurrence rates considering the real number of planets and the total number of stars used in the sample. We then recalculated the occurrences using the candidates from DC15 but with their disposition scores and planetary radius updated by the NASA Exoplanet Archive (Akeson et al. 2013). The disposition score is a value between 0 and 1 that indicates the confidence in the KOI disposition, a higher value indicates more confidence in its disposition. The value is calculated from a Monte Carlo technique such that the score's value is equivalent to the fraction of iterations where the Robovetter yields a disposition of "Candidate" (Akeson et al. 2013). From the 156 candidates used by DC15, 28 candidates were removed from the sample because their disposition had changed in the NASA Exoplanet Archive.

We found there is a good agreement between the results obtained in this work and those obtained by DC15 in the smaller planets domain, particularly in the range of 1.5–3.0 $R_\oplus$, while the occurrence rates for larger planets tended to be smaller in this work than the DC15 results. As our method validation compared the occurrence rates results obtained by two works that utilize basically the same method, data and planetary physical parameters, the discrepancies we observed may have been produced by differences in the detection probabilities used.

3.3. *Stellar Sample*

We selected a sample of 99,417 stars with 2400 $K \leq T_{\rm eff} < 6000$ K and $\log g \geq 4.0$ from the Q1–17 Kepler Stellar Catalog in the NASA Exoplanet Archive. From those stars, 86,383 stars have detection probabilities computed in the range of 0.6–25 $R_\oplus$ and 5–700 days (Burke, private communication). The average detection probability was calculated for each G, K and M stars subsample and then used to compute the occurrence rates as a function of spectral type as described in Section 3.1. The number of stars in each spectral type category are shown in Table 1, where the properties of the stars in each category follow the prescription of the NASA ExoPAG Study Analysis Group 13. Figure 1 shows the diagram divided into cells which are superimposed by the average detection probability for G stars.

3.4. *Planet Candidates Properties*

The properties of all 4034 candidates/confirmed planets were downloaded from the Q1–17 Kepler Object of Interest on the NASA Exoplanet Archive. From this we selected 2,586 candidates that orbit the sample of stars described in the previous section and whose planetary properties lie inside the range of parameters in which the detection efficiencies were calculated. We took a conservative approach and discarded candidates with disposition scores smaller than 0.9. The properties of the resulting candidate sample range from 0.67–22.7 $R_\oplus$ and from 5.0–470 day orbits. The planetary sample was divided into subsamples according to the spectral type of their host stars, leaving us with 1207 planets orbiting G stars, 534 planets orbiting K stars and 93 planets orbiting M stars.

3.5. *Planet Occurrence Rates*

For each sample of spectral type, the occurrence rates were computed for each cell spanning a range of planet radius and orbital period following the method described in Section 3.1 and using equation 2. For those cells in which no candidate was observed, we estimated an upper limit based on the uncertainty of the occurrence rate as if there was one detection in the center of the bin. Figures 2, 3 and 4 show the occurrence rates for each cell. The uncertainties were estimated using the relation

$$\delta NPPS^{i,j} = \frac{NPPS^{i,j}}{\sqrt{N_p^{i,j}}} \quad (4)$$

3.6. *Frequency versus Planet Radius and Insolation*

Figure 5 − 10 show the occurrence rates as a function of planet radius and orbital period. Figure 5 shows the occurrence rates for planets around G stars. Number of Planets Per Star (NPPS) is plotted against the planet radius and each line represents a band of orbital periods. The data indicates that, for G stars, planets with radii

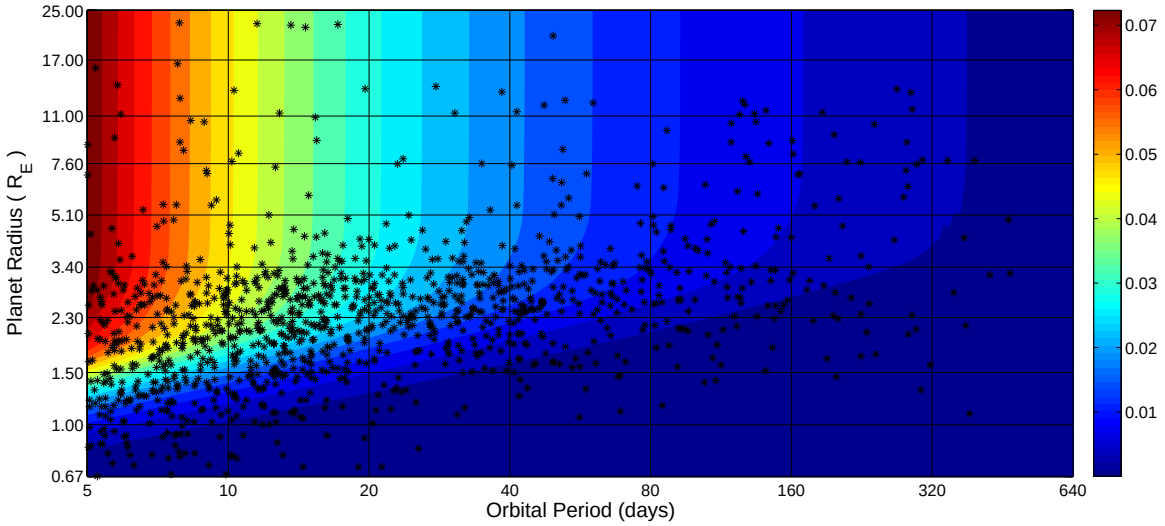

Figure 1. Average detection probability for G stars as a function of planet radius and orbital period. The star symbols represent the 1,819 *Kepler* candidates detected for these stars. Note the color bar to the right indicates the detection probability of the planets with greatest probability of detection corresponding with the top of the scale. Planets found on the top left corner of the graph will have a greater probability of detection.

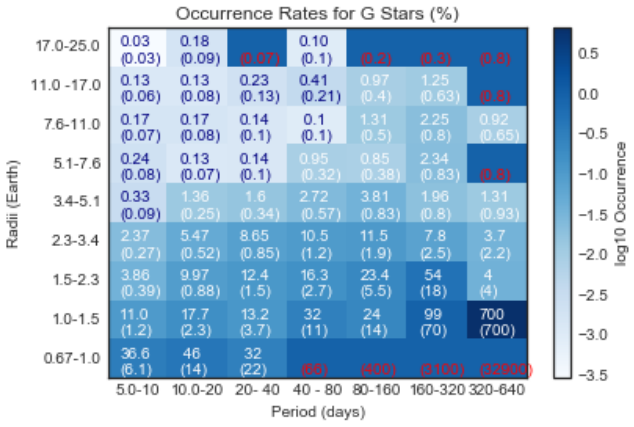

Figure 2. Binned planet occurrence rates for G stars as a function of planet radius and orbital period. Planet occurrence is given as a percentage along with uncertainty percentage (in brackets). For bins without planets we compute the uncertainty, and thus upper limit by including one detection at the center of the bin. The bins treated this way have been colored with red font for transparency.

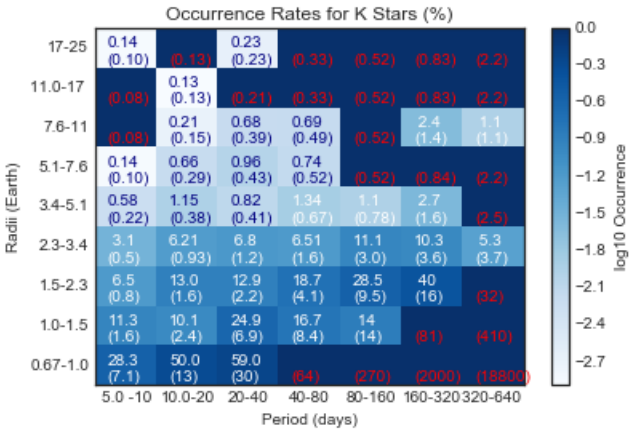

Figure 3. Binned planet occurrence rates for K stars as a function of planet radius and orbital period. Planet occurrence is given as a percentage along with uncertainty percentage (in brackets). For bins without planets we compute the uncertainty, and thus upper limit by including one detection at the center of the bin. The bins treated this way have been colored with red font for transparency.

greater than 1.5 $R_\oplus$ are most commonly found with orbital periods between 80-320 days. The occurrence for planets with orbits between 320-640 days shows a spike for planets with radii between 1.0–1.5 $R_\oplus$. In general, our results show that small planets are more abundant than giant planets in each orbital period bin which is consistent with Wittenmyer et al. (2011); Kane et al. (2016).

The trends observed for K stars follows that observed for G stars; small planets are more abundant than giant planets in each orbital period bin. While Figure 8 shows a complete lack of giant planets > 11 $R_\oplus$ with orbital periods > 40 days, this radius range represents the rarest objects detected by *Kepler*, thus there is a lack of sufficient data to complete the calculations of their oc-

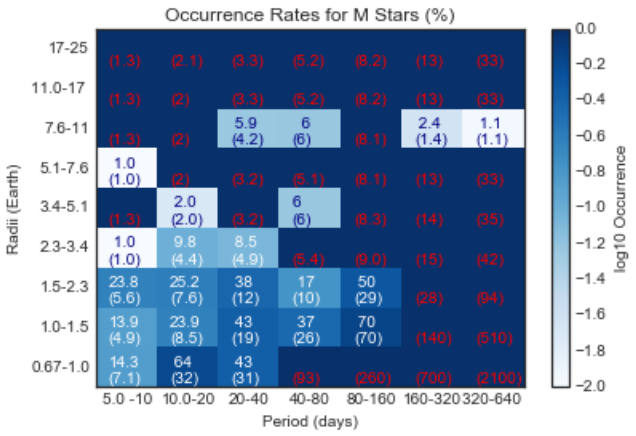

Figure 4. Binned planet occurrence rates for M stars as a function of planet radius and orbital period. Planet occurrence is given as a percentage along with uncertainty percentage (in brackets). For bins without planets we compute the uncertainty, and thus upper limit by including one detection at the center of the bin. The bins treated this way have been colored with red font for transparency.

Table 1. Planet Occurrence rates of giant planets $> 3\ R_\oplus$ in the OHZ of their star.

Spectral Type	$T_{\rm eff}$ (K)	No. stars	Planets in OHZ	NPPS (%)
G	5300–6000	59510	12	6.5 ± 1.9
K	3900–5300	24560	14	11.5 ± 3.1
M	2400–3900	2313	1	6.0 ± 6.0

currence rates. In addition, there appears to be a lack of planets with radius 5.1–7.6 $R_\oplus$ with orbits of > 80 days.

For M stars, the occurrences for different orbital periods are very similar. We observe a lack of any giant planets with $R_p > 11\ R_\oplus$ (Figure 9). Planets with $R_p = 7.6$–$11\ R_\oplus$ tend to be found with orbital periods between 20–80 days.

3.7. *Frequency of Giants in the Habitable Zone*

The OHZ for each host candidate was computed following the model described by Kopparapu et al. (2013, 2014). From the sample of candidates selected and described in Section 3.3, 12 candidates orbit within the OHZ of their respective G host stars, 14 candidates orbit in the OHZ of their K host stars and only 1 candidate orbits in the OHZ of an M star. The properties of the spectral type bins and the occurrence rates of giant planets in the OHZ is shown in Table 1.

4. PROPERTIES OF HABITABLE ZONE GIANT PLANETS

Here we present the calculations for the estimated planet mass, Hill radius of the planet, angular separation of the planet from the host star and of any potential exomoon from its host planet, both estimates of which can be used in deciding the ideal candidates for future imaging missions, and finally the RV semi-amplitude of the planet on its host star for use in follow up observations of each giant planet.

We start by estimating the mass of each of the Kepler candidates using the mass/radius relation found in Chen & Kipping (2016):

$$R_p = M_p^{0.59} \tag{5}$$

where R_p is the planet radius in Earth radii and M_p is planet mass in Earth masses.

As is noted in Chen & Kipping (2016), this relationship is only reliable up to $\sim 10R_\oplus$. As planets $10R_\oplus$ and above can vary greatly in density and thus greatly in mass, we have chosen to quantify each exoplanet with a radius of $10R_\oplus$ or greater as 3 set masses; 1 Saturn mass for the very low density planets, 1 Jupiter mass for a direct comparison with our solar system body, and 13 Jupiter mass for the higher density planets. As there is discrepancy as to the mass of a planet vs brown dwarf we have chosen to use the upper limit of 13 Jupiter masses. For any planet found to have a mass larger than this the Hill radius and RV signal will thus be greater than that calculated.

Using our mass estimate, we first consider the radius at which a moon is gravitationally bound to a planet, calculating the Hill radius using Hinkel & Kane (2013):

$$r_H = a_{sp}\chi(1 - e_{sp})\left(\frac{M_p}{M_\star}\right)^{\frac{1}{3}} \tag{6}$$

where $M_\star$ is the mass of the host star. Assuming an eccentricity of the planet–star system of $e = 0$, the above equation becomes:

$$r_H = a_{sp}\chi\left(\frac{M_p}{M_\star}\right)^{\frac{1}{3}} \tag{7}$$

The factor χ is added to take into account the fact that the Hill radius is just an estimate. Other effects may impact the gravitational stability of the system, so following (Barnes & O'Brien 2002), (Kipping 2009) and (Hinkel & Kane 2013), we have chosen to use a conservative estimate of $\chi \leq 1/3$.

The expected angular separation of the exomoon for its host planet is then calculated by:

$$\alpha'' = \frac{r_H(\chi = 1/3)}{d} \tag{8}$$

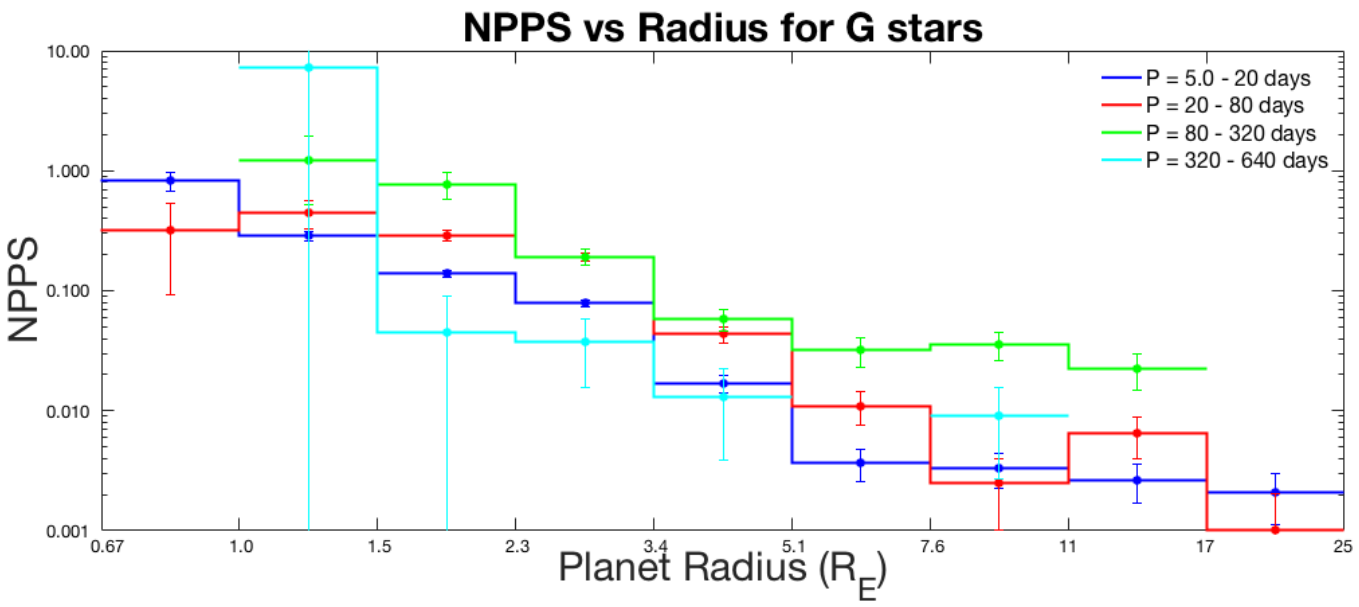

Figure 5. Number of Planets Per Star (NPPS) vs radius for G stars. Each line color represents a set range of periods. The data indicates that, for G stars, planets with radii greater than 1.5 $R_\oplus$ are most commonly found with orbital periods between 80–320 days. Also the occurrence rate of planets with orbits between 320–640 days shows a large spike for planets with radii between 1.0–1.5 $R_\oplus$.

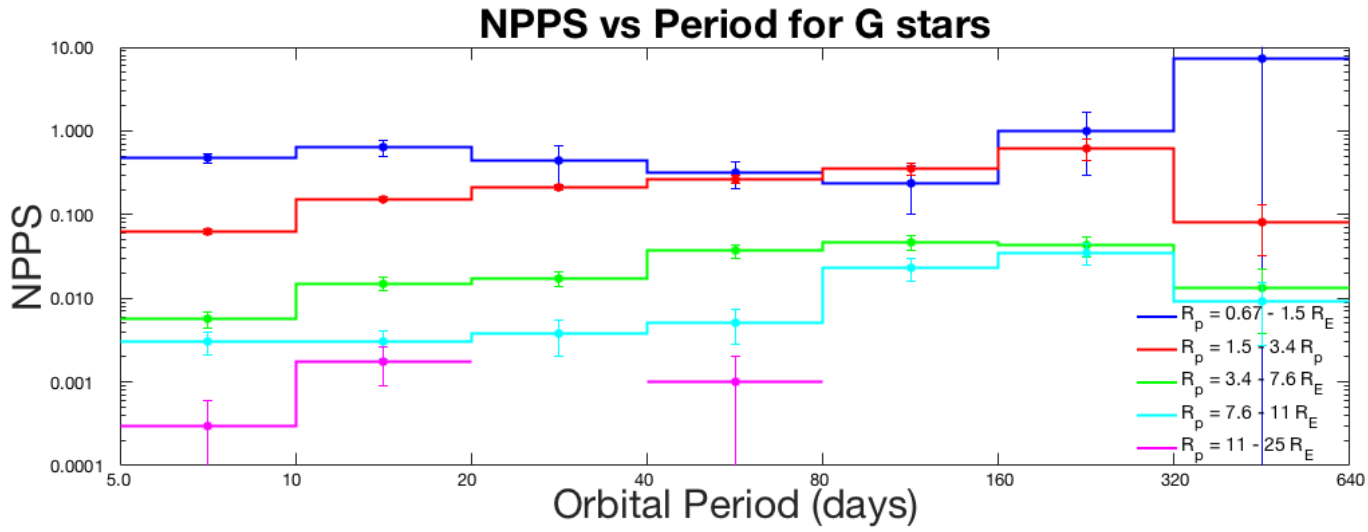

Figure 6. Number of Planets Per Star (NPPS) vs period for G stars. Each line color represents a set range of radii. The data indicates that, for G stars, small planets are more abundant than giant planets in each orbital period bin. The magenta line indicating planets with radii between 11 and 25 $R_\oplus$ represents the rarest objects detected by *Kepler*, thus there is a lack of sufficient data to complete the calculations of their occurrence rates at longer orbital periods.

Here d represents the distance of the star planet system in parsecs (PC) and Hill radius is expressed in (AU).

Finally, we calculate the RV semi-amplitude, K, of each planet given its estimated mass:

$$K = \frac{(2\pi G)}{P^{1/3}} \frac{(M_p \sin i)}{((M_\star + M_p)^{2/3}} \tag{9}$$

We further assume an orbital inclination of ∼90° and $e = 0$.

Table 2 includes each of the parameters used in our calculations which have been extracted from the HZ catalogue (Kane et al. 2016) as well as the NASA exoplanet archive. Table 3 presents our calculations of planet mass, Hill radii, estimated RV semi-amplitudes and angular separations of the planet – star systems and potential planet – moon systems at both the full Hill radii (HR) and $\frac{1}{3}$ Hill radii ($\frac{1}{3}$HR).

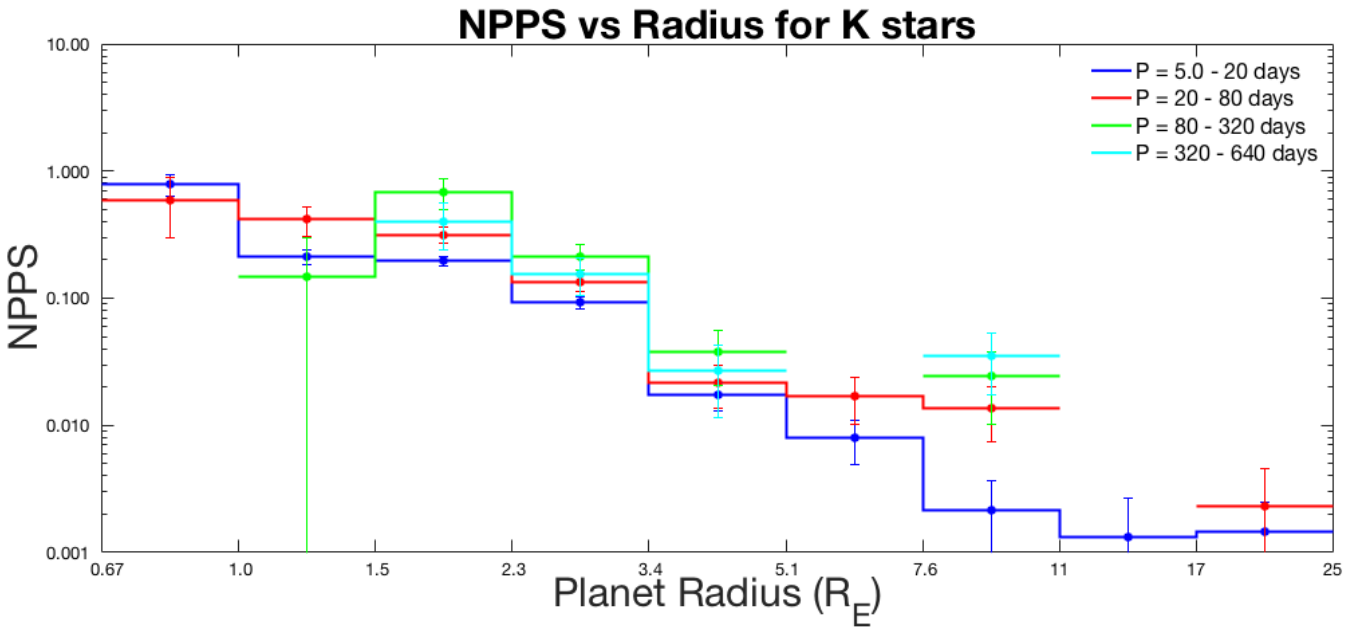

Figure 7. Number of Planets Per Star (NPPS) vs radius for K stars. Each line color represents a set range of periods. The data indicates that planets with radii between 1.5–5.1 $R_\oplus$ most commonly have orbital periods between 80–320 days. Also, for K stars, small planets are more abundant than giant planets in each orbital period bin.

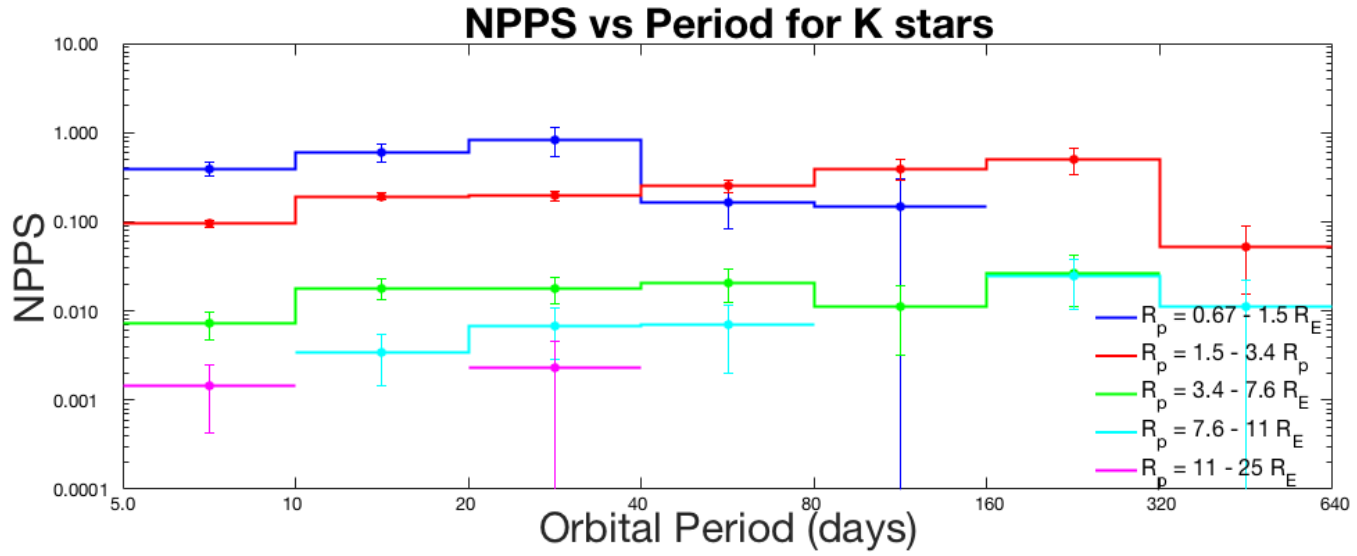

Figure 8. Number of Planets Per Star (NPPS) vs period for K stars. Each line color represents a set range of radii. Note there is a drop in the blue line representing the lowest mass planets between 0.67–1.5 $R_\oplus$ at an orbital period of 40 days. This corresponds to the limit of detection efficiency of *Kepler* for small planets and thus there is not sufficient data in this region to claim that this is a significant drop.

Tables 4 and 5 then present our calculations of Hill radii, angular separations of a potential planet–moon systems at the full Hill radius and RV semi-amplitudes for each exoplanet with a radius of $10R_\oplus$ or greater with our chosen quantified masses; 1 Saturn mass (M_{sat}), 1 Jupiter mass (M_J), and 13 Jupiter masses ($13M_J$).

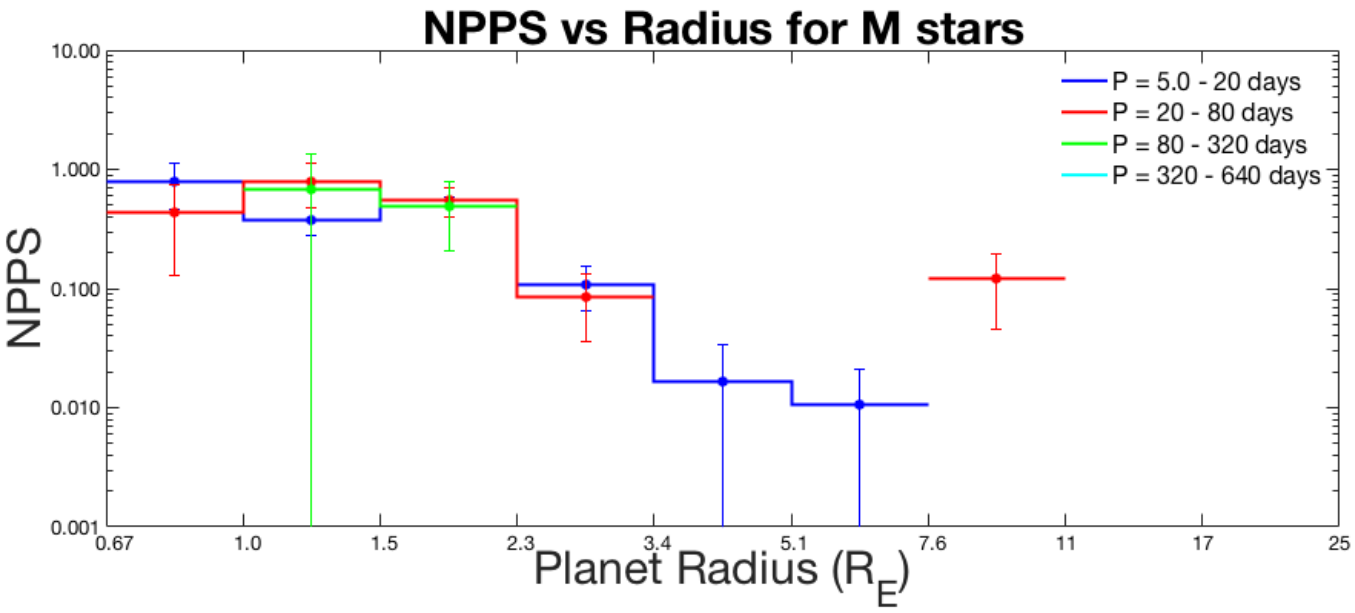

Figure 9. Number of Planets Per Star (NPPS) vs radius for M stars. Each line color represents a set range of periods. We observe a lack of any planets with $R_p > 11\ R_\oplus$. Planets with $R_p = 7.6$–$11\ R_\oplus$ tend to be found with orbital periods between 20–80 days.

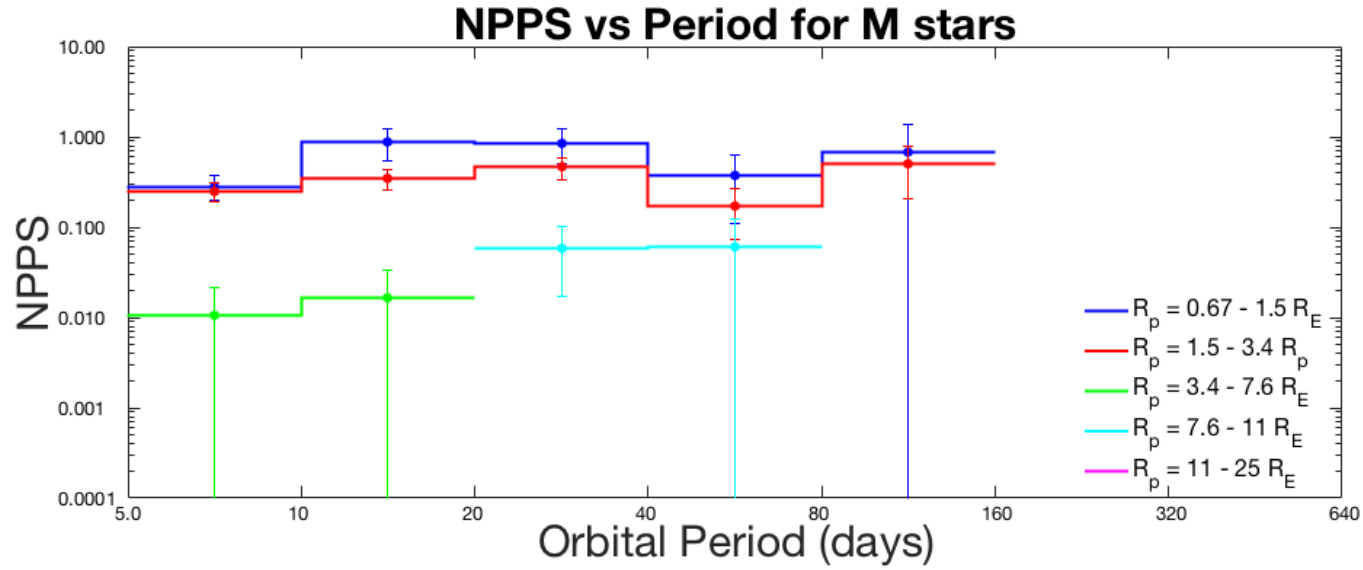

Figure 10. Number of Planets Per Star (NPPS) vs period for M stars. Each line color represents a set range of radii. We observe that small planets tend to be more abundant than giant planets in each orbital period bin. Note the drop in planets beyond an orbital period of 160 days corresponds with the limit of *Kepler* detection efficiency for these dim stars.

Table 2. Habitable Zone candidates with $R_p > 3\ R_\oplus$.

KOI name	Kepler	$T_{\rm eff}$	Period	a *	Planet Radius	Incident Flux	Stellar Mass	Distance	Magnitude
		K	days	AU	$R_\oplus$	$F_\oplus$	$M_\star$	PC	Kepler Band
K03086.01	–	5201 ± 83	174.732 ± 0.003	0.573	3 ± 0.235	1.61 ± 0.35	0.82 ± 0.05	1006 ± 84	15.71

Table 2 continued

Table 2 *(continued)*

KOI name	Kepler	$T_{\rm eff}$	Period	a *	Planet Radius	Incident Flux	Stellar Mass	Distance	Magnitude
		K	days	AU	$R_\oplus$	$F_\oplus$	$M_\star$	PC	Kepler Band
K06786.01	–	5883 ± 186	455.624 ± 0.026	1.153	3 ± 0.585	0.64 ± 0.33	0.99 ± 0.13	3192 ± 550	11.97
K02691.01	–	4735 ± 170	97.446 ± 0	0.373	3.05 ± 0.265	1.53 ± 0.49	0.73 ± 0.07	447 ± 50	14.98
K01581.02	896b	5510 ± 158	144.552 ± 0.003	0.516	3.06 ± 0.475	2 ± 0.85	0.88 ± 0.09	926 ± 170	15.48
K08156.01	–	6429 ± 182	364.982 ± 0.011	1.048	3.12 ± 0.69	1.74 ± 0.96	1.15 ± 0.16	978 ± 240	14.32
K07700.01	–	6382 ± 180	631.569 ± 0.013	1.491	3.13 ± 0.655	0.75 ± 0.4	1.1 ± 0.15	798 ± 177	14.00
K04016.01	1540b	4641 ± 79	125.413 ± 0	0.443	3.14 ± 0.125	1.19 ± 0.18	0.73 ± 0.04	293 ± 18	14.07
K05706.01	1636b	5977 ± 201	425.484 ± 0.009	1.155	3.2 ± 0.61	0.9 ± 0.46	1.13 ± 0.13	1589 ± 348	15.81
K02210.02	1143c	4895 ± 78	210.631 ± 0.002	0.648	3.23 ± 0.15	0.71 ± 0.11	0.82 ± 0.04	607 ± 38	15.20
K08276.01	–	6551 ± 183	385.859 ± 0.005	1.107	3.23 ± 0.705	1.93 ± 1.05	1.22 ± 0.17	944 ± 216	13.99
K04121.01	1554b	5275 ± 83	198.089 ± 0.002	0.631	3.24 ± 0.36	1.64 ± 0.47	0.86 ± 0.05	1164 ± 143	15.72
K05622.01	1635b	5474 ± 158	469.613 ± 0.014	1.117	3.24 ± 0.46	0.38 ± 0.15	0.85 ± 0.09	944 ± 160	15.70
K07982.01	–	6231 ± 207	376.38 ± 0.047	1.029	3.26 ± 0.665	1.17 ± 0.63	1.03 ± 0.13	1436 ± 333	15.63
K03946.01	1533b	6325 ± 79	308.544 ± 0.002	0.963	3.28 ± 0.565	2.82 ± 1.12	1.25 ± 0.11	734 ± 119	13.22
K08232.01	–	5573 ± 174	189.184 ± 0.004	0.610	3.31 ± 0.77	2.24 ± 1.32	0.85 ± 0.1	865 ± 212	15.05
K05625.01	–	5197 ± 181	116.454 ± 0.002	0.414	3.33 ± 0.375	2.07 ± 0.75	0.7 ± 0.07	894 ± 132	16.02
K02073.01	357d	5036 ± 200	49.5 ± 0	0.246	3.43 ± 2.04	6.57 ± 8.8	0.79 ± 0.04	771 ± 51	15.57
K02686.01	–	4658 ± 93	211.033 ± 0.001	0.627	3.43 ± 0.17	0.51 ± 0.09	0.74 ± 0.04	267 ± 17	13.86
K01855.01	–	4338 ± 125	58.43 ± 0	0.248	3.45 ± 0.3	1.92 ± 0.55	0.59 ± 0.06	298 ± 33	14.78
K02828.02	–	4817 ± 176	505.463 ± 0.008	1.153	3.46 ± 0.315	0.25 ± 0.08	0.8 ± 0.05	769 ± 95	15.77
K02926.05	–	3891 ± 78	75.731 ± 0.002	0.297	3.47 ± 0.19	0.74 ± 0.14	0.61 ± 0.03	425 ± 35	16.28
K08286.01	–	5440 ± 180	191.037 ± 0.013	0.634	3.54 ± 0.6	1.59 ± 0.75	0.93 ± 0.09	1654 ± 335	16.65
K01830.02	967c	5180 ± 103	198.711 ± 0.001	0.625	3.56 ± 0.215	1.06 ± 0.21	0.83 ± 0.05	502 ± 37	14.44
K00951.02	258c	4942 ± 200	33.653 ± 0	0.193	3.61 ± 2.43	12.16 ± 18.1	0.83 ± 0.05	1542 ± 431	15.22
K01986.01	1038b	5159 ± 82	148.46 ± 0.001	0.524	3.61 ± 0.205	1.56 ± 0.28	0.87 ± 0.04	606 ± 42	14.84
K01527.01	–	5401 ± 107	192.667 ± 0.001	0.622	3.64 ± 0.32	1.52 ± 0.39	0.86 ± 0.05	743 ± 71	14.88
K05790.01	–	4899 ± 82	178.267 ± 0.003	0.571	3.71 ± 0.21	0.81 ± 0.14	0.82 ± 0.04	643 ± 44	15.52
K08193.01	–	5570 ± 158	367.948 ± 0.005	0.996	3.72 ± 0.6	0.64 ± 0.28	0.97 ± 0.09	1116 ± 202	15.72
K08275.01	–	5289 ± 176	389.876 ± 0.007	1.002	3.76 ± 0.46	0.44 ± 0.17	0.89 ± 0.08	975 ± 152	15.95
K01070.02	266c	5885 ± 250	107.724 ± 0.002	0.457	3.89 ± 1.89	5.47 ± 6.24	0.95 ± 0.06	1562 ± 280	15.59
K07847.01	–	6098 ± 217	399.376 ± 0.069	1.103	3.93 ± 1.225	2.67 ± 2.04	1.12 ± 0.17	2190 ± 713	13.28
K00401.02	149d	5381 ± 100	160.018 ± 0.001	0.571	3.96 ± 0.68	2.08 ± 0.77	0.93 ± 0.05	541 ± 56	14.00
K01707.02	315c	5796 ± 108	265.469 ± 0.006	0.791	4.15 ± 0.96	1.75 ± 0.8	0.88 ± 0.06	1083 ± 147	15.32
K05581.01	1634b	5636 ± 171	374.878 ± 0.008	1.053	4.27 ± 1.125	1.5 ± 0.97	1.1 ± 0.13	1019 ± 272	14.51
K01258.03	–	5717 ± 165	148.272 ± 0.001	0.546	4.3 ± 0.75	2.52 ± 1.16	0.98 ± 0.11	1217 ± 245	15.77
K02683.01	–	5613 ± 152	126.445 ± 0	0.473	4.49 ± 0.635	2.52 ± 0.99	0.89 ± 0.1	947 ± 147	15.50
K00881.02	712c	5067 ± 102	226.89 ± 0.001	0.673	4.53 ± 0.26	0.73 ± 0.14	0.79 ± 0.04	854 ± 59	15.86
K01429.01	–	5644 ± 80	205.913 ± 0.001	0.679	4.68 ± 0.5	1.86 ± 0.5	0.98 ± 0.06	1232 ± 135	15.53
K00902.01	–	3960 ± 124	83.925 ± 0	0.303	4.78 ± 0.405	0.62 ± 0.18	0.53 ± 0.04	348 ± 43	15.75
K05929.01	–	5830 ± 158	466.003 ± 0.003	1.165	4.92 ± 0.875	0.59 ± 0.27	0.97 ± 0.12	780 ± 168	14.69
K00179.02	458b	6226 ± 118	572.377 ± 0.006	1.406	5.8 ± 0.905	1.15 ± 0.45	1.13 ± 0.09	904 ± 140	13.96
K03823.01	–	5536 ± 79	202.117 ± 0.001	0.667	5.8 ± 0.53	1.59 ± 0.38	0.96 ± 0.05	563 ± 57	13.92
K01058.01	–	3337 ± 86	5.67 ± 0	0.034	5.85 ± 2.015	3.22 ± 2.55	0.16 ± 0.07	32 ± 12	13.78
K00683.01	–	5799 ± 110	278.124 ± 0	0.842	5.86 ± 0.72	1.58 ± 0.51	1.03 ± 0.07	622 ± 73	13.71
K05375.01	–	5142 ± 150	285.375 ± 0.004	0.794	5.94 ± 4.05	7.56 ± 11.19	0.82 ± 0.21	1138 ± 769	13.86
K05833.01	–	6261 ± 174	440.171 ± 0.006	1.145	5.97 ± 1.53	2.97 ± 1.85	1.03 ± 0.16	809 ± 200	13.01
K02076.02	1085b	6063 ± 181	219.322 ± 0.001	0.739	6.11 ± 1.085	2.27 ± 1.08	1.12 ± 0.14	1314 ± 270	15.27
K02681.01	397c	5307 ± 100	135.499 ± 0.001	0.480	6.18 ± 0.56	1.83 ± 0.47	0.78 ± 0.05	983 ± 76	16.00
K05416.01	1628b	3869 ± 140	76.378 ± 0.002	0.295	6.28 ± 0.6	0.79 ± 0.26	0.59 ± 0.06	418 ± 56	16.60

Table 2 continued

Table 2 *(continued)*

KOI name	Kepler	$T_{\rm eff}$	Period	a *	Planet Radius	Incident Flux	Stellar Mass	Distance	Magnitude
		K	days	AU	$R_\oplus$	$F_\oplus$	$M_\star$	PC	Kepler Band
K01783.02	–	5791 ± 111	284.063 ± 0.002	0.845	6.36 ± 1.105	2.52 ± 1.07	1 ± 0.08	913 ± 157	13.93
K02689.01	–	5594 ± 186	165.345 ± 0	0.547	6.98 ± 1.175	1.94 ± 0.91	0.8 ± 0.08	1001 ± 191	15.55
K05278.01	–	5330 ± 187	281.592 ± 0.001	0.776	7.22 ± 0.885	0.61 ± 0.24	0.8 ± 0.08	911 ± 133	15.87
K03791.01	460b	6340 ± 190	440.784 ± 0.001	1.146	7.23 ± 2	2.14 ± 1.44	1.03 ± 0.15	917 ± 242	13.77
K01375.01	–	6018 ± 120	321.212 ± 0	0.945	7.25 ± 1.165	2.18 ± 0.87	1.09 ± 0.09	755 ± 129	13.71
K03263.01	–	3638 ± 76	76.879 ± 0	0.275	7.71 ± 0.83	0.4 ± 0.12	0.47 ± 0.05	220 ± 28	15.95
K01431.01	–	5597 ± 112	345.159 ± 0	0.975	7.79 ± 0.745	0.8 ± 0.22	1.03 ± 0.06	456 ± 48	13.46
K01439.01	849b	5910 ± 113	394.625 ± 0.001	1.109	7.79 ± 1.585	2.66 ± 1.28	1.16 ± 0.13	740 ± 147	12.85
K01411.01	–	5716 ± 109	305.076 ± 0	0.912	7.82 ± 1.045	1.54 ± 0.53	1.08 ± 0.07	537 ± 75	13.38
K00950.01	–	3748 ± 59	31.202 ± 0	0.150	8.31 ± 0.575	1.59 ± 0.32	0.46 ± 0.03	237 ± 21	15.80
K05071.01	–	6032 ± 211	180.412 ± 0.001	0.637	8.86 ± 1.73	2.78 ± 1.47	1.06 ± 0.14	1373 ± 301	15.66
K03663.01	86b	5725 ± 108	282.525 ± 0	0.836	8.98 ± 0.89	1.15 ± 0.31	0.97 ± 0.06	328 ± 35	12.62
K00620.03	51c	6018 ± 107	85.312 ± 0.003	0.384	9 ± 2.25	7.05 ± 8	1.05 ± 0.14	927 ± 205	14.67
K01477.01	–	5270 ± 79	169.498 ± 0.001	0.575	9.06 ± 0.59	1.29 ± 0.24	0.9 ± 0.05	1053 ± 78	15.92
K03678.01	1513b	5650 ± 186	160.885 ± 0	0.542	9.09 ± 2.53	3.4 ± 2.34	0.82 ± 0.09	410 ± 112	12.89
K08007.01	–	3391 ± 42	67.177 ± 0	0.218	9.66 ± 1.115	0.24 ± 0.07	0.3 ± 0.04	135 ± 18	16.06
K00620.02	51d	6018 ± 107	130.194 ± 0.004	0.509	9.7 ± 0.5	4.01 ± 4.56	1.05 ± 0.14	927 ± 205	14.67
K01681.04	–	3638 ± 80	21.914 ± 0	0.117	10.39 ± 1.26	2.01 ± 0.66	0.45 ± 0.05	203 ± 30	15.86
K00868.01	–	4245 ± 85	235.999 ± 0	0.653	10.59 ± 0.435	0.29 ± 0.05	0.67 ± 0.03	358 ± 22	15.17
K01466.01	–	4810 ± 76	281.563 ± 0	0.766	10.83 ± 0.535	0.49 ± 0.08	0.76 ± 0.04	855 ± 55	15.96
K00351.01	90h	5970 ± 119	331.597 ± 0	0.965	10.89 ± 1.61	1.76 ± 0.66	1.09 ± 0.08	809 ± 118	13.80
K00433.02	553c	5234 ± 103	328.24 ± 0	0.908	10.99 ± 0.77	0.6 ± 0.13	0.93 ± 0.05	706 ± 46	14.92
K05329.01	–	6108 ± 211	200.235 ± 0.001	0.686	10.99 ± 2.305	2.64 ± 1.47	1.07 ± 0.15	1207 ± 269	15.39
K03811.01	–	5631 ± 76	290.14 ± 0	0.843	11.58 ± 2.045	2.02 ± 0.82	0.95 ± 0.06	738 ± 130	13.91
K03801.01	–	5672 ± 76	288.313 ± 0.001	0.846	13.21 ± 2.185	1.93 ± 0.74	0.97 ± 0.07	1837 ± 318	16.00
K01268.01	–	5798 ± 78	268.941 ± 0.001	0.827	13.57 ± 2.305	2.53 ± 1	1.04 ± 0.08	1262 ± 219	14.81

* Semi major axis

Table 3. Radial Velocity, Hill Radius & Angular Separation Calculations for HZ Candidates with $R_p > 3\ R_\oplus$.

KOI name	Kepler	Planet Mass	Hill Radius	$\alpha'' Planet - Star$	$\alpha'' Moon(HR)$	$\alpha'' Moon(\frac{1}{3} HR)$	Radial Velocity
		$M_\oplus$	AU	μ arcsec	μ arcsec	μ arcsec	m/s
K03086.01	–	6.44 ± 0.98	0.0114 ± 0.0006	570 ± 48	11.3 ± 1.1	3.78 ± 0.37	0.84 ± 0.15
K06786.01	–	6.44 ± 2.44	0.0216 ± 0.0029	361 ± 62	6.77 ± 1.5	2.26 ± 0.49	0.54 ± 0.23
K02691.01	–	6.62 ± 1.12	0.0078 ± 0.0005	834 ± 93	17.4 ± 2.3	5.81 ± 0.75	1.13 ± 0.24
K01581.02	896b	6.66 ± 2.01	0.0102 ± 0.0011	558 ± 102	11 ± 2.4	3.67 ± 0.78	0.89 ± 0.29
K08156.01	–	6.88 ± 2.96	0.019 ± 0.0029	1070 ± 263	19.4 ± 5.6	6.44 ± 1.86	0.56 ± 0.27
K07700.01	–	6.92 ± 2.82	0.0275 ± 0.0039	1870 ± 414	34.5 ± 9.1	11.5 ± 3.03	0.48 ± 0.22
K04016.01	1540b	6.95 ± 0.54	0.0094 ± 0.0003	1510 ± 93	32 ± 2.2	10.6 ± 0.73	1.09 ± 0.11
K05706.01	1636b	7.18 ± 2.67	0.0214 ± 0.0028	727 ± 159	13.5 ± 3.4	4.47 ± 1.14	0.56 ± 0.23
K02210.02	1143c	7.3 ± 0.66	0.0134 ± 0.0005	1070 ± 67	22.1 ± 1.6	7.42 ± 0.54	0.9 ± 0.1
K08276.01	–	7.3 ± 3.1	0.0201 ± 0.003	1170 ± 268	21.3 ± 5.8	7.1 ± 1.94	0.56 ± 0.26
K04121.01	1554b	7.33 ± 1.59	0.0129 ± 0.001	543 ± 67	11.1 ± 1.6	3.69 ± 0.54	0.89 ± 0.2
K05622.01	1635b	7.33 ± 2.03	0.0229 ± 0.0023	1180 ± 201	24.3 ± 4.8	8.05 ± 1.59	0.67 ± 0.21
K07982.01	–	7.41 ± 2.94	0.0199 ± 0.0028	716 ± 166	13.9 ± 3.8	4.6 ± 1.25	0.65 ± 0.28
K03946.01	1533b	7.49 ± 2.51	0.0175 ± 0.002	1310 ± 212	23.8 ± 4.7	7.9 ± 1.57	0.61 ± 0.22
K08232.01	–	7.6 ± 3.45	0.0127 ± 0.002	706 ± 173	14.7 ± 4.3	4.86 ± 1.41	0.95 ± 0.46
K05625.01	–	7.68 ± 1.69	0.0092 ± 0.0007	463 ± 69	10.3 ± 1.7	3.47 ± 0.58	1.28 ± 0.34

Table 3 continued

Table 3 *(continued)*

KOI name	Kepler	Planet Mass	Hill Radius	$\alpha''Planet - Star$	$\alpha''Moon(HR)$	$\alpha''Moon(\frac{1}{3}HR)$	Radial Velocity
		$M_\oplus$	AU	μ arcsec	μ arcsec	μ arcsec	m/s
K02073.01	357d	8.08 ± 9.36	0.0053 ± 0.0021	319 ± 21	6.87 ± 2.8	2.33 ± 0.94	1.64 ± 1.91
K02686.01	–	8.08 ± 0.78	0.0139 ± 0.0005	2350 ± 150	52.1 ± 3.8	17.2 ± 1.26	1.06 ± 0.13
K01855.01	–	8.16 ± 1.38	0.0059 ± 0.0004	832 ± 92	19.8 ± 2.6	6.71 ± 0.87	1.9 ± 0.41
K02828.02	–	8.2 ± 1.45	0.025 ± 0.0016	1500 ± 185	32.5 ± 4.5	10.8 ± 1.5	0.76 ± 0.15
K02926.05	–	8.24 ± 0.88	0.0071 ± 0.0003	698 ± 58	16.7 ± 1.6	5.65 ± 0.52	1.74 ± 0.22
K08286.01	–	8.52 ± 2.81	0.0133 ± 0.0015	383 ± 78	8.04 ± 1.9	2.66 ± 0.62	0.99 ± 0.35
K01830.02	967c	8.6 ± 1.01	0.0137 ± 0.0006	1250 ± 92	27.3 ± 2.3	9.17 ± 0.79	1.07 ± 0.15
K00951.02	258c	8.81 ± 11.55	0.0042 ± 0.0019	125 ± 35	2.72 ± 1.5	0.91 ± 0.48	1.98 ± 2.6
K01986.01	1038b	8.81 ± 0.97	0.0113 ± 0.0005	864 ± 60	18.6 ± 1.5	6.27 ± 0.52	1.17 ± 0.15
K01527.01	–	8.93 ± 1.53	0.0136 ± 0.0008	837 ± 80	18.3 ± 2.1	6.06 ± 0.68	1.09 ± 0.21
K05790.01	–	9.23 ± 1.02	0.0128 ± 0.0005	888 ± 61	19.9 ± 1.6	6.69 ± 0.53	1.2 ± 0.16
K08193.01	–	9.27 ± 2.91	0.0211 ± 0.0023	892 ± 162	18.9 ± 4	6.27 ± 1.33	0.84 ± 0.29
K08275.01	–	9.44 ± 2.25	0.0221 ± 0.0019	1030 ± 160	22.7 ± 4	7.59 ± 1.35	0.9 ± 0.24
K01070.02	266c	10 ± 9.46	0.01 ± 0.0032	293 ± 53	6.4 ± 2.4	2.11 ± 0.78	1.39 ± 1.32
K07847.01	–	10.17 ± 6.18	0.023 ± 0.0048	503 ± 164	10.5 ± 4.1	3.52 ± 1.36	0.82 ± 0.53
K00401.02	149d	10.3 ± 3.45	0.0127 ± 0.0014	1060 ± 109	23.5 ± 3.6	7.76 ± 1.17	1.27 ± 0.43
K01707.02	315c	11.16 ± 5.03	0.0185 ± 0.0028	731 ± 99	17.1 ± 3.5	5.73 ± 1.16	1.21 ± 0.56
K05581.01	1634b	11.71 ± 6.01	0.0231 ± 0.0041	1030 ± 276	22.7 ± 7.3	7.55 ± 2.42	0.97 ± 0.52
K01258.03	–	11.85 ± 4.03	0.0125 ± 0.0015	448 ± 90	10.3 ± 2.4	3.45 ± 0.81	1.45 ± 0.54
K02683.01	–	12.75 ± 3.51	0.0115 ± 0.0011	499 ± 78	12.1 ± 2.2	4.01 ± 0.73	1.76 ± 0.55
K00881.02	712c	12.94 ± 1.45	0.0171 ± 0.0007	788 ± 55	20 ± 1.6	6.67 ± 0.54	1.59 ± 0.22
K01429.01	–	13.68 ± 2.85	0.0163 ± 0.0012	551 ± 60	13.2 ± 1.8	4.38 ± 0.58	1.5 ± 0.34
K00902.01	–	14.18 ± 2.34	0.0091 ± 0.0006	872 ± 108	26.2 ± 3.7	8.63 ± 1.21	3.18 ± 0.63
K05929.01	–	14.89 ± 5.16	0.029 ± 0.0035	1490 ± 322	37.2 ± 9.2	12.4 ± 3.07	1.25 ± 0.48
K00179.02	458b	19.68 ± 5.98	0.0365 ± 0.0038	1560 ± 241	40.4 ± 7.5	13.5 ± 2.52	1.4 ± 0.45
K03823.01	–	19.68 ± 3.5	0.0182 ± 0.0011	1180 ± 120	32.3 ± 3.8	10.8 ± 1.28	2.2 ± 0.43
K01058.01	–	19.96 ± 13.39	0.0017 ± 0.0004	1070 ± 407	53.7 ± 23.9	18.9 ± 8.45	23.89 ± 21.28
K00683.01	–	20.02 ± 4.79	0.0227 ± 0.0019	1350 ± 159	36.5 ± 5.3	12.2 ± 1.76	1.92 ± 0.5
K05375.01	–	20.49 ± 27.21	0.0232 ± 0.0105	697 ± 471	20.4 ± 16.6	6.76 ± 5.5	2.28 ± 3.14
K05833.01	–	20.66 ± 10.32	0.0311 ± 0.0054	1420 ± 350	38.4 ± 11.6	12.9 ± 3.88	1.7 ± 0.93
K02076.02	1085b	21.49 ± 7.43	0.0198 ± 0.0024	562 ± 116	15.1 ± 3.6	5.02 ± 1.2	2.12 ± 0.82
K02681.01	397c	21.91 ± 3.87	0.0146 ± 0.0009	488 ± 38	14.8 ± 1.5	4.98 ± 0.49	3.21 ± 0.63
K05416.01	1628b	22.51 ± 4.19	0.01 ± 0.0007	706 ± 95	23.9 ± 3.6	7.89 ± 1.19	4.84 ± 1.11
K01783.02	–	23 ± 7.78	0.0241 ± 0.0028	925 ± 159	26.4 ± 5.5	8.76 ± 1.82	2.24 ± 0.8
K02689.01	–	26.93 ± 8.83	0.0177 ± 0.002	546 ± 104	17.7 ± 3.9	5.89 ± 1.31	3.65 ± 1.31
K05278.01	–	28.52 ± 6.81	0.0256 ± 0.0022	852 ± 124	28.1 ± 4.8	9.33 ± 1.58	3.24 ± 0.91
K03791.01	460b	28.59 ± 15.4	0.0347 ± 0.0064	1250 ± 329	37.8 ± 12.2	12.6 ± 4.07	2.35 ± 1.36
K01375.01	–	28.72 ± 8.99	0.0281 ± 0.003	1250 ± 214	37.2 ± 7.5	12.4 ± 2.51	2.53 ± 0.85
K03263.01	–	31.88 ± 6.68	0.0112 ± 0.0009	1250 ± 159	50.8 ± 7.7	16.8 ± 2.53	7.96 ± 2.02
K01431.01	–	32.44 ± 6.04	0.0308 ± 0.002	2140 ± 225	67.6 ± 8.4	22.6 ± 2.8	2.9 ± 0.58
K01439.01	849b	32.44 ± 12.86	0.0336 ± 0.0046	1500 ± 298	45.4 ± 11	15.1 ± 3.66	2.56 ± 1.09
K01411.01	–	32.65 ± 8.5	0.0284 ± 0.0025	1700 ± 237	52.9 ± 8.7	17.7 ± 2.92	2.94 ± 0.81
K00950.01	–	36.19 ± 4.88	0.0064 ± 0.0003	633 ± 56	27 ± 2.7	8.87 ± 0.89	12.32 ± 2.01
K05071.01	–	40.35 ± 15.35	0.0215 ± 0.0029	464 ± 102	15.7 ± 4	5.25 ± 1.35	4.41 ± 1.87
K03663.01	86b	41.28 ± 7.97	0.0292 ± 0.002	2550 ± 272	89 ± 11.3	29.6 ± 3.75	4.09 ± 0.88
K00620.03	51c	41.43 ± 20.18	0.0131 ± 0.0022	414 ± 92	14.1 ± 3.9	4.75 ± 1.32	5.81 ± 3.02
K01477.01	–	41.9 ± 5.32	0.0207 ± 0.0009	546 ± 41	19.7 ± 1.7	6.55 ± 0.56	5.19 ± 0.76
K03678.01	1513b	42.14 ± 22.84	0.0202 ± 0.0037	1320 ± 361	49.3 ± 16.2	16.3 ± 5.38	5.66 ± 3.2
K08007.01	–	46.71 ± 10.5	0.0117 ± 0.001	1610 ± 214	86.5 ± 13.7	28.8 ± 4.56	16.25 ± 4.89
K00620.02	51d	47.04 ± 4.72	0.0181 ± 0.001	549 ± 121	19.5 ± 4.5	6.47 ± 1.48	5.73 ± 1.19
K01681.04	–	52.85 ± 12.48	0.0058 ± 0.0005	578 ± 87	28.6 ± 4.9	9.36 ± 1.62	20.56 ± 5.87
K00868.01	–	54.59 ± 4.37	0.0284 ± 0.0009	1830 ± 112	79.4 ± 5.5	26.6 ± 1.84	7.41 ± 0.77
K01466.01	–	56.7 ± 5.46	0.0323 ± 0.0012	896 ± 58	37.8 ± 2.8	12.6 ± 0.94	6.67 ± 0.78
K00351.01	90h	57.23 ± 16.48	0.0362 ± 0.0036	1190 ± 174	44.8 ± 7.9	15 ± 2.64	4.99 ± 1.54
K00433.02	553c	58.13 ± 7.93	0.0361 ± 0.0017	1290 ± 84	51.2 ± 4.1	17 ± 1.37	5.67 ± 0.87
K05329.01	–	58.13 ± 23.75	0.026 ± 0.0037	568 ± 127	21.5 ± 5.7	7.21 ± 1.91	6.06 ± 2.74
K03811.01	–	63.52 ± 21.85	0.0343 ± 0.004	1140 ± 201	46.4 ± 9.8	15.4 ± 3.26	6.36 ± 2.27
K03801.01	–	79.4 ± 25.58	0.0368 ± 0.004	461 ± 80	20 ± 4.1	6.7 ± 1.37	7.85 ± 2.65
K01268.01	–	83.1 ± 27.5	0.0356 ± 0.004	655 ± 114	28.2 ± 5.8	9.43 ± 1.95	8.01 ± 2.77

We plot a histogram of the effective temperatures of Kepler host stars to determine if there is a similar distribution of temperatures among both the HZ candidates and the full catalog.

Table 4. Radial Velocity Semi-amplitude calculations for Category 4 HZ candidates with $R_p > 10\ R_\oplus$.

KOI name	Kepler	Period	Planet Radius	Stellar Mass	RV (M_{sat})	RV (M_J)	RV ($13M_J$)
		Days	$R_\oplus$	$M_\star$	m/s	m/s	m/s
K01681.04		21.914 ± 0.0002	10.39 ± 1.26	0.45 ± 0.051	37.03 ± 5.94	123.73 ± 20.08	1621.95 ± 258.66
K00868.01		235.999 ± 0.0003	10.59 ± 0.435	0.666 ± 0.031	12.91 ± 0.86	43.13 ± 3.06	563.9 ± 38.53
K01466.01		281.563 ± 0.0004	10.83 ± 0.535	0.755 ± 0.036	11.2 ± 0.76	37.4 ± 2.71	488.67 ± 34.16
K00351.01	90h	331.597 ± 0.0003	10.89 ± 1.61	1.089 ± 0.084	8.3 ± 0.91	27.74 ± 3.11	361.88 ± 39.94
K00433.02	553c	328.24 ± 0.0004	10.99 ± 0.77	0.927 ± 0.045	9.28 ± 0.64	30.99 ± 2.28	404.54 ± 28.79
K05329.01		200.235 ± 0.0006	10.99 ± 2.305	1.072 ± 0.146	9.93 ± 1.91	33.17 ± 6.45	432.68 ± 83.35
K03811.01		290.14 ± 0.0003	11.58 ± 2.045	0.947 ± 0.064	9.53 ± 0.91	31.84 ± 3.16	415.53 ± 40.36
K03801.01		288.313 ± 0.0005	13.21 ± 2.185	0.969 ± 0.068	9.41 ± 0.94	31.42 ± 3.23	410.03 ± 41.29
K01268.01		268.941 ± 0.0005	13.57 ± 2.305	1.041 ± 0.075	9.18 ± 0.94	30.65 ± 3.23	399.95 ± 41.32

Table 5. Hill Radii calculations for Category 4 HZ candidates with $R_p > 10\ R_\oplus$.

KOI name	Kepler	Planet Radius	Hill Radius (M_{sat})	Hill Radius (M_J)	Hill Radius (13 M_J)	α'' (M_{sat}) [a]	α'' (M_J) [b]	α'' ($13M_J$) [c]
		$R_\oplus$	AU	AU	AU	μ arcsec	μ arcsec	μ arcsec
K01681.04		10.39 ± 1.26	0.007 ± 0.0003	0.0105 ± 0.0004	0.0246 ± 0.0009	28.6 ± 4.9	9.4 ± 1.6	578 ± 87
K00868.01		10.59 ± 0.435	0.0342 ± 0.0005	0.0511 ± 0.0009	0.1201 ± 0.002	79.4 ± 5.5	26.6 ± 1.8	1830 ± 112
K01466.01		10.83 ± 0.535	0.0384 ± 0.0006	0.0574 ± 0.001	0.135 ± 0.0023	37.8 ± 2.8	12.6 ± 0.9	896 ± 58
K00351.01	90h	10.89 ± 1.61	0.0429 ± 0.0011	0.0641 ± 0.0017	0.1506 ± 0.004	44.8 ± 7.9	15 ± 2.6	1190 ± 174
K00433.02	553c	10.99 ± 0.77	0.0425 ± 0.0007	0.0636 ± 0.0012	0.1495 ± 0.0026	51.2 ± 4.1	17 ± 1.4	1290 ± 84
K05329.01		10.99 ± 2.305	0.0306 ± 0.0014	0.0458 ± 0.0021	0.1076 ± 0.0049	21.5 ± 5.7	7.2 ± 1.9	568 ± 127
K03811.01		11.58 ± 2.045	0.0392 ± 0.0009	0.0586 ± 0.0014	0.1378 ± 0.0032	46.4 ± 9.8	15.4 ± 3.3	1140 ± 201
K03801.01		13.21 ± 2.185	0.039 ± 0.0009	0.0584 ± 0.0015	0.1372 ± 0.0033	20 ± 4.1	6.7 ± 1.4	461 ± 80
K01268.01		13.57 ± 2.305	0.0373 ± 0.0009	0.0557 ± 0.0014	0.131 ± 0.0033	28.2 ± 5.8	9.4 ± 2	655 ± 114

[a] Angular separation of exomoon at full Hill radius for $M_p = M_{\rm sat}$.

[b] Angular separation of exomoon at full Hill radius for $M_p = M_J$.

[c] Angular separation of exomoon at full Hill radius for $M_p = 13M_J$.

Figure 11 shows the stellar temperature distributions for both the HZ Kepler candidates (green) as well as the full Kepler catalog (gray). The histograms show that there is a similar distribution of temperatures among both the HZ candidates and the full catalog, with the HZ host star temperatures dropping off (around) 7000K. As the habitable zone of stars with greater effective temperatures will lie further away from the star, planets in this zone are harder to detect. Thus this drop is likely a false upper limit.

Using the calculations from our Tables above, we plot the Kepler magnitude of the host star of both the unconfirmed and confirmed HZ planets and their expected radial velocity signatures to determine the expected detectability of these planets.

Figure 12 shows the Kepler magnitude of the host star of both the unconfirmed and confirmed HZ planets and their expected radial velocity signatures.

We then provide a similar plot in Figure 13, this time plotting the Kepler magnitude of the host star of both the unconfirmed and confirmed HZ planets and their expected angular separations of a moon at the full Hill radius of the host planet.

Figure 14 shows the distribution of the estimated planet - moon angular separation at the full Hill radii of the candidate. It can be seen that the resolution required to image a moon is between 1 - 90 μ arcseconds with the moon positioned at its maximum stable distance from the planet. If a potential moon resides within $\frac{1}{3}$ Hill radius from the planet as expected, the resolution will need to improve as much again. Note these graphs do not take into account the separate calculations of angular separation for those planets $\geq 10R_\oplus$.

Figure 15 shows the distribution of the Hill radii of Kepler habitable zone planets $> 3R\oplus$. Potential moons of giant planets found in the habitable zone will likely have

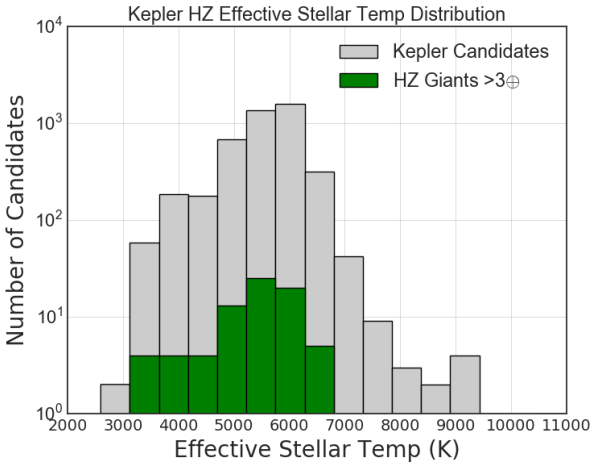

Figure 11. Stellar temperature distributions. Habitable zone Kepler candidates in green overlays the distribution of the full Kepler catalog in gray. The histograms show that there is a similar distribution of temperatures among both the HZ candidates and the full Kepler catalog. While the distribution of the habitable zone candidates drops off at 7000K, this could be a false upper limit as the habitable zone of stars with greater effective temperature lies further away from the star and current transit detection methods are less sensitive to planets at these longer orbits.

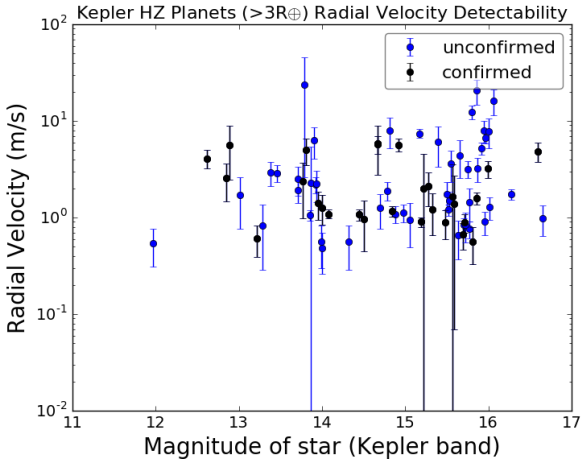

Figure 12. We plot the Kepler magnitude of the host star of both the unconfirmed and confirmed HZ planets and their expected radial velocity signatures to determine the expected detectability of these planets. We find that a large majority of the planets in our list have an estimated radial velocity semi amplitude between 1 and 10 m/s. As the *Kepler* telescope was focused on a field faint stars, the planets listed are at the limit of the capabilities of current RV detection instruments. Future radial velocity missions to follow up on these candidates should focus on those found closest to the top left corner of the graph, where the brightest stars host candidates with large RV semi amplitudes.

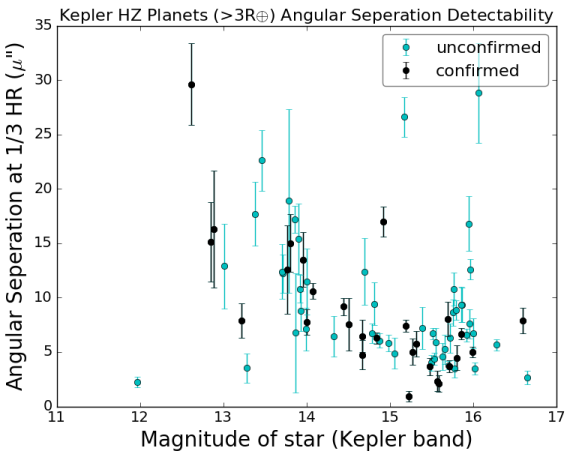

Figure 13. We plot the Kepler magnitude of the host star of both the unconfirmed and confirmed HZ planets and their expected Angular separation to determine the expected detectability of these planets. Confirmed candidates are noted by black dots and unconfirmed candidates by teal dots. Note the Y axis is the angular separation at $\frac{1}{3}$ Hill radius which we have taken as the typical distance of a stable moon. Future imaging missions will need the capabilities to resolve a separation between 1 35 μ arc seconds.

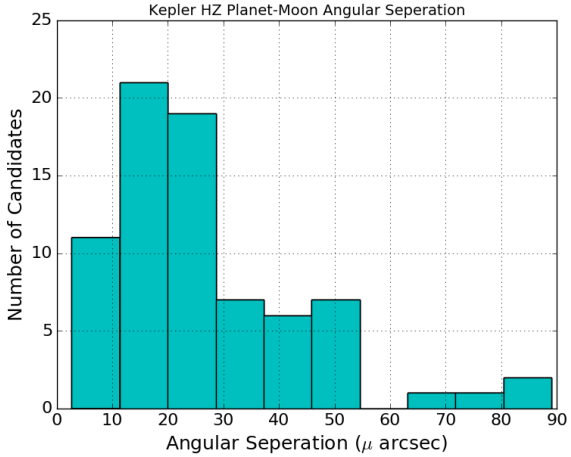

Figure 14. Here we show the distribution of Kepler habitable zone planets ($> 3R\oplus$) Planet - Moon angular separation, with moons positioned at the full Hill radii. Potential moons of giant planets found in the habitable zone will likely have a maximum angular separation from their host planet between 1 - 90 μ arc seconds. This information can be used for planning of imaging future missions if we assume Kepler candidates are representative of the entire population of stars and planets.

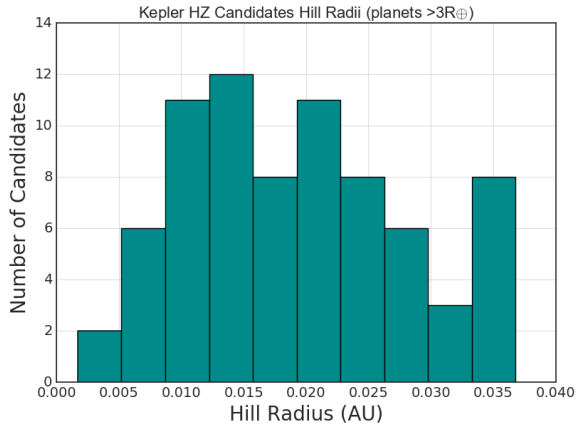

Figure 15. Here we show the distribution of Kepler habitable zone planets ($> 3R\oplus$) Hill radii. Potential moons of giant planets found in the habitable zone will likely have a maximum radius of gravitational influence between 5 - 35 milli AU. This information can be used for planning of imaging future missions as the Kepler candidates can be considered representative of the entire population of stars.

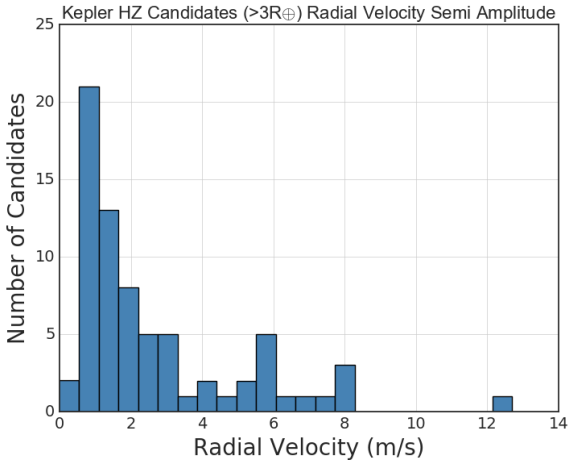

Figure 16. Here we show the distribution of Kepler habitable zone candidates ($> 3R\oplus$) estimated radial velocity semi amplitudes. As the giant planets we are investigating reside in the habitable zone of their star, the increased distance from the host star produces a relatively small RV semi amplitude, thus the majority of the candidates have estimated radial velocity semi amplitudes of <2 m/s.

a maximum radius of gravitational influence between 5 - 35 Milli AU. If we assume a similar distribution exists around the entire population of giant planets found in the HZ, we can use this information to calculate the expected angular separation of a moon around the closest giant HZ planets. This can then be used for planning of future imaging missions.

Finally, Figure 16 shows the distribution of the radial velocity semi amplitude of the HZ candidates. While we estimate the majority of candidates will have a signature <2 m/s, there are a number of planets that are likely to have significantly larger signatures and thus more easily detectable. However, as the Kepler stars are faint, even the largest of these signatures are on the limit of our current detection capabilities and so these planets will still be difficult to observe. Note this graph does not take into account the separate calculations of the radial velocity semi amplitude for those planets $\geq 10R_\oplus$.

5. DISCUSSION AND CONCLUSIONS

From our calculations in Section 3 we found the frequency of giant planets (R_p = 3.0–25 $R_\oplus$) in the OHZ is $(6.5 \pm 1.9)\%$ for G stars, $(11.5 \pm 3.1)\%$ for K stars, and $(6 \pm 6)\%$ for M stars. For comparison, the estimates of occurrence rates of terrestrial planets in the HZ for G-dwarf stars range from 2% (Foreman-Mackey et al. 2014) to 22% (Petigura et al. 2013) for GK dwarfs, but systematic errors dominate (Burke et al. 2015). For M-dwarfs, the occurrence rates of terrestrial planets in the HZ is ∼20% (Dressing & Charbonneau 2015). Therefore, it appears that the occurrence of large terrestrial moons orbiting giant planets in the HZ is less than the occurrence of terrestrial planets in the HZ. However this assumes that each giant planet is harboring only one large terrestrial exomoon. If giant planets can host multiple exomoons then the occurrence rates of moons would be comparable to that of terrestrial planets in the HZ of their star, and could potentially exceed them.

The calculations in Tables 3, 4 and 5 are intended for the design and observing strategies of future RV surveys and direct imaging missions. We found that a large majority of the planets in our list have an estimated RV semi-amplitude between 1 and 10 m/s. While currently 1 m/s RV detection is regularly achieved around bright stars, the *Kepler* telescope was focused on a field faint stars, thus the planets included in our tables are at the limit of the capabilities of current RV detection. Precision RV capability is planned for the forthcoming generation of extremely large telescopes, such as the GMT-Consortium Large Earth Finder (G-CLEF) designed for the Giant Magellan Telescope (GMT) (Szentgyorgyi et al. 2016), further increasing the capabilities towards the measurement of masses for giant planets in the HZ. Future RV surveys to follow up these candidates should focus on those candidates with the largest estimated RV semi-amplitudes orbiting the brightest stars.

Tidally heated exomoons can potentially be detected in direct imaging, if the contrast ratio of the satellite and the planet is favorable (Peters & Turner 2013). This is

particularly beneficial for low mass stars, where the low stellar luminosity may aid in the detection of a tidally heated exomoon. However, the small inner working angle for low-mass stars will be unfavorable for characterization purposes.

A new approach was proposed for detection and characterization of exomoons based on spectroastrometry (Agol et al. 2015). This method is based on the principle that the moon outshines the planet at certain wavelengths, and the centroid offset of the PSF (after suppressing the starlight with either a coronagraph or a starshade) observed in different wavelengths will enable one to detect an exomoon. For instance, the Moon outshines Earth at ∼2.7 μm. Ground-based facilities can possibly probe the HZs around M-dwarfs for exomoons, but large space-based telescopes, such as the 15m class LUVOIR, are necessary for obtaining sharper PSF and resolving the brightness.

If imaging of an exomoon orbiting a Kepler giant planet in the habitable zone is desired, instruments must have the capability to resolve a separation between $\sim 1 - 90$ μ arcseconds. The large distance and low apparent brightness of the Kepler stars makes them unideal for direct imaging. But if we assume the distribution of Hill radii (Figure 15) calculated to surround the Kepler giant HZ planets to be representative of the larger giant HZ planet population, then our closest giant HZ planets could have exomoons with angular separations as large as $\sim 1 - 35$ m arcseconds (assuming the closest giant HZ planets to reside between 1-10pc away).

Additional potential for exomoon detection lies in the method of microlensing, and has been demonstrated to be feasible with current survey capabilities for a subset of microlensing events (Liebig & Wambsganss 2010). Furthermore, the microlensing detection technique is optimized for star–planet separations that are close to the snow line of the host stars (Gould et al. 2010), and simulations of stellar population distributions have shown that lens stars will predominately lie close to the near-side of the galactic center (Kane & Sahu 2006). A candidate microlensing exomoon was detected by Bennett et al. (2014), suggested to be a free-floating exoplanet-exomoon system. However, issues remain concerning the determination of the primary lens mass and any follow-up observations that would allow validation and characterization of such exomoon systems.

There is great habitability potential for the moons of giant exoplanets residing in their HZ. These potentially terrestrial giant satellites could be the perfect hosts for life to form and take hold. Thermal and reflected radiation from the host planet and tidal effects increase the outer range of the HZ, creating a wider temperate zone in which a stable body may exist. There are, however, some caveats including the idea that giant planets in the HZ of their star may have migrated there (Lunine 2001; Darriba et al. 2017). The moon of a giant planet migrating through the HZ may only have a short period in which the moon is considered habitable. Also, a planet that migrates inwards will eventually lose its moon(s) due to the shrinking Hill sphere of the planet (Spalding et al. 2016). Thus any giant planet that is in the HZ but still migrating inwards can quickly lose its moon as it moves closer to the host star.

(Sartoretti & Schneider 1999) uncovered another factor potentially hindering the detection of these HZ moons when they found that multiple moons around a single planet may wash out any transit timing signal. And the small radius combined with the low contrast between planet and moon brightness mean transits are also unlikely to be a good method for detection.

The occurrence rates calculated in Section 3 indicate a modest number of giant planets residing in the habitable zone of their star. Once imaging capabilities have improved, the detection of potentially habitable moons around these giant hosts should be more accessible. Until then we must continue to refine the properties of the giant host planets, starting with the radial velocity follow-up observations of the giant HZ candidates from our list.

ACKNOWLEDGEMENTS

This research has made use of the NASA Exoplanet Archive and the ExoFOP site, which are operated by the California Institute of Technology, under contract with the National Aeronautics and Space Administration under the Exoplanet Exploration Program. This work has also made use of the Habitable Zone Gallery at hzgallery.org. The results reported herein benefited from collaborations and/or information exchange within NASA's Nexus for Exoplanet System Science (NExSS) research coordination network sponsored by NASA's Science Mission Directorate. The research shown here acknowledges use of the Hypatia Catalog Database, an online compilation of stellar abundance data as described in Hinkel14, which was supported by NASA's Nexus for Exoplanet System Science (NExSS) research coordination network and the Vanderbilt Initiative in Data-Intensive Astrophysics (VIDA). This research has also made use of the VizieR catalogue access tool, CDS, Strasbourg, France. The original description of the VizieR service was published in A&AS 143, 23.

REFERENCES

Agol, E., Jansen, T., Lacy, B., Robinson, T.D., Meadows, V. 2015, ApJ, 812, 1

Akeson, R.L., Chen, X.; Ciardi, D., et al. 2013, PASP, 125, 930

Barnes, J. W., O'Brien, D.P. 2002, ApJ, 575, 1087

Bennett, D.P., Batista, V., Bond, I.A., et al. 2014, ApJ, 785, 155

Burke, C.J., Christiansen, J.L., Mullally, F., et al. 2015, ApJ, 809, 8

Cameron, A.G.W., Ward,W.R. 1976, Abstracts of the Lunar and Planetary Science Conference, 7, 120

Canup, R.M., Ward, W.R. 2002, AJ, 124, 3404

Chen, J., Kipping, D. 2016, ApJ, 834, 1

Cumming, A., Butler, R.P., Marcy, G.W., et al. 2008, PASP, 120, 531

Darriba, L.A., de Ela, G.C., Guilera, O.M., Brunini, A. 2017, A&A, 607, A63

Diaz, R.F., Rey, J., Demangeon, O., et al. 2016, A&A, 591, A146

Dittmann, J.A., Irwin, J.M., Charbonneau, D., et al. 2017, Nature, 544, 333

Dressing, C., Charbonneau, D. 2013, ApJ, 767, 1

Dressing, C., Charbonneau, D. 2015, ApJ, 807, 1

Elser,S., Moore, B., Stadel, J., Morishima, R. 2011, Icarus, 214, 2, 357-365

Foreman-Mackey, D., Hogg, D.W., Morton, T.D. 2014, ApJ, 795, 1

Foreman-Mackey, D. Morton, T.D, Hogg, D.W., Agol, E., Schlkopfet, B. 2016, ApJ, 152, 206

Fressin, F., Torres, G., Charbonneau, D., et al. 2013, ApJ, 766, 2

Gillon, M., Triaud, A.H.M.J., Demory, B.O., et al. 2017, Nature, 542, 456

Gould, A., Dong, S., Gaudi, B.S., et al. 2010, ApJ, 720, 1073

Hartmann, W.K., Davis, D.R. 1975, Icarus, 24, 4, 504-515

Heller, R. 2012, A&A, 545, L8

Heller, R., Barnes, R. 2013, AsBio, 13, 18

Heller, R., Pudritz, R. 2013, ApJ, 806, 2

Heller, R., Marleau, G.-D., Pudritz, R.E. 2015, A&A, 579, L4

Hinkel, N.R., Kane, S.R. 2013, ApJ, 774, 27

Hinkel, N.R., Timmes, F.X., Young, P.A., Pagano, M.D., Turnbull, M.C. 2014, ApJ, 148, 54

Holt, T.R., Brown, A. J., Nesvorny, D., Horner, J., Carter, B. 2017, ApJ, submitted (arXiv:1706.01423)

Howard, A.W., Marcy, G.W., Bryson, S.T., et al. 2012, ApJS, 201, 15

Hsu, H.-W., Postberg, F., Sekine, Y., et al. 2015, Nature, 519, 207

Kaltenegger, L., Sasselov, D. 2011, ApJ, 736, 25

Kane, S.R., Sahu, K.C. 2006, ApJ, 637, 752

Kane, S.R., Gelino, D.M. 2012, PASP, 124, 323

Kane, S.R., Hill, M.L., Kasting, J.F., et al. 2016, ApJ, 830, 1

Kasting, J.F., Whitmire, D.P., Reynolds, R.T. 1993, Icarus, 101, 108

Kipping, D.M. 2009, MNRAS, 392, 181

Kipping, D.M., Fossey, S.J., Campanella, G. 2009, MNRAS, 400, 398

Kipping, D.M., Bakos, G.A., Buchhave, L., Nesvorn, D., Schmitt, A.R. 2012, ApJ, 750, 115

Kipping, D.M., Hartman, J., Buchhave, L., et al. 2013, ApJ770, 101

Kipping, D.M., Forgan, D., Hartman, J., et al. 2013, ApJ, 777, 134

Kipping, D.M., Nesvorn, D., Buchhave, L., et al. 2014, ApJ784, 28

Kipping, D.M., Schmitt, A.R., Huang, X., et al. 2015, ApJ, 813, 14

Kivelson, M.G., Khurana, K.K., Russell, C.T., et al. 1996, Nature, 384, 537

Koch, D.G., Borucki, W.J., Basri, G., et al. 2010, ApJ, 713, 2

Kopparapu, R.K. 2013, ApJL, 767, 1

Kopparapu, R.K. Ramirez, R., Kasting, J.F., et al. 2013, ApJ, 765, 131

Kopparapu, R.K., Ramirez, R., Schottel-Kotte, J., et al. 2014, ApJ, 787, L29

Liebig, C., Wambsganss, J. 2010, A&A, 520, A68

Lunine, J.I. 2001, PNAS, 98, 809

Morabito, L.A., Synnott, S.P., Kupferman, P.N., Collins, S.A. 1979, Science, 204, 972

Ochsenbein F., Bauer P., Marcout J. 2000, AAS Meeting Abstracts, 143, 221

Nesvorny, D., Alvarellos, J. L.A., Dones, L., Levison, H.F., 2003, The Astronomical Journal,126, 398-429

Peters, M.A., Turner, E.L. 2013, ApJ, 769, 2

Petigura, E.A., Howard, A.W., Marcy, G.W. 2013, PNAS, 110(48),19273-19278

Pollack, J. B., Burns, J. A., Tauber, M. E. 1979, Icarus, 37, 587

Porco, C. C., Helfenstein, P., Thomas, P. C., et al. 2006, Science, 311, 1393

Rowan, D., Meschiari, S., Laughlin, G., et al. 2016, ApJ, 817, 104

Sartoretti, P., Schneider, J. 1999, A&AS, 134, 553

Scharf, C.A. 2006, ApJ, 648, 1196
Spalding, C., Batygin, K., Adams, F.C. 2016, ApJ, 817, 1
Spergel, D. 2015, NASA reports
Szentgyorgyi, A., Baldwin, A., Barnes, S., et al. 2016, SPIE, 9908, 990822
Teachey,A., Kipping, D.M., Schmitt, A.R. 2017, ApJ, 155, 1
Williams, D.M., Kasting, J.F., Wade, R.A. 1997, Nature, 385, 234
Wittenmyer, R.A., Endl, M., Cochran, W.D., et al. 2006, AJ, 132, 177
Wittenmyer, R.A., Tinney, C.G., O'Toole, S.J., et al. 2011, ApJ, 727, 102
Wittenmyer, R.A., Tinney, C.G., Butler, R.P., et al. 2011 ApJ, 738, 81
Wittenmyer, R.A., Butler, R.P., Tinney, C.G., et al. 2016, ApJ, 819, 28
Zechmeister, M., Kürster, M., Endl, M., et al. 2013, A&A, 552, A78
Zollinger, R.R., Armstrong, J.C., Heller, R. 2017, MNRAS472, 1

Bibliography

Agol, E, Jansen, T, Lacy, B, Robinson, TD & Meadows, V 2015, 'The Center of Light: Spectroastrometric Detection of Exomoons', *The Astrophysical Journal*, vol. 812, no. 1

Astakhov, SA, Burbanks AD, Wiggins S & Farrelly D 2003, 'Chaos-assisted capture of irregular moons', *Nature*, vol. 423, pp. 6937

Barensten, G 2017, NASA Mission objectives - Kepler, viewed October 2017, <https://keplerscience.arc.nasa.gov/objectives.html>

Barnes, JW & O'Brien, DP 2002, 'Stability of Satellites around Close-in Extrasolar Giant Planets', *The Astrophysical Journal*, vol. 575, pp. 1087

Burrows, AS 2014, 'Highlights in the Study of Exoplanet Atmospheres', *Nature*, vol. 513, pp. 345-352

Cameron, AGW & Ward, WR 1976, 'The Origin of the Moon', *Abstracts of the Lunar and Planetary Science Conference*, vol. 7, pp. 120

Canup, RM & Ward, WR 2002, 'Formation of the Galilean Satellites: Conditions of Accretion', *The Astronomical Journal*, vol. 124, pp. 3404-3423

Chandler, CO, McDonald, I & Kane, SR 2015, 'The Catalog of Earth-Like Exoplanet Survey TArgets (CELESTA): A Database of Habitable Zones around Nearby Stars', *The Astrophysical Journal*, vol. 151, no. 3

Chen, J & Kipping, D 2016, 'Probabilistic Forecasting of the Masses and Radii of Other Worlds', *The Astrophysical Journal*, vol. 834, no. 1

Comins, N.F & Kaufmann, W.J 2012, *Discovering the Universe*, 9th edition, W. H. Freeman and Company, New York.

Elser, S, Moore, B, Stadel, J & Morishima, R 2011, 'How common are Earth–Moon planetary systems?', *Icarus*, vol. 214, no. 2, pp. 357-365

Fulton, JF, Petigura, EA, Blunt, S & Sinukoff, E 2018, 'RadVel: The Radial Velocity Modeling Toolkit', *PASP*, vol. 130, pp. 986

Harman, C 2015, Sonny Harman Images, viewed September 2017, <https://sites.psu.edu/ceh5286/images/>

Hartmann, WK & Davis, DR 1975, 'Satellite-sized planetesimals and lunar origin', *Icarus*, vol. 24, no. 4, pp. 504-515

Heller, R 2012. 'Exomoon Habitability Constrained by Energy Flux and Orbital Stability', *Astronomy & Astrophysics manuscript*, vol. 2012-4

Heller, R & Barnes, R 2012, 'Constraints on the Habitability of Extrasolar Moons', *IAU Symposium*, vol. 293

Heller, R & Barnes, R 2013, 'Exomoon Habitability Constrained By Illumination And Tidal Heating', *Astrobiology*, vol. 13, no. 1, pp. 18-46

Heller, R, Marleau, GD & Pudritz, RE 2015, 'The Formation of the Galilean Moons and Titan in the Grand Tack Scenario', *Astronomy and Astrophysics*, vol. 579, no. L4

Heller, R & Pudritz, R 2013, 'Water Ice Lines And The Formation Of Giant Moons Around Super-Jovian Planets', *The Astrophysical Journal*, vol. 806, no. 2

Heller, R & Zuluaga, JI 2013, 'Magnetic shielding of exomoons beyond the circumplanetary habitable edge', *The Astrophysical Journal Letters*, vol . 776, no. 2

Hill, ML, Kane, SR, Seperuelo Duarte, E, Kopparapu, RK, Gelino, DA & Wittenmyer, RA 2018, 'Exploring Kepler Giant Planets in the Habitable Zone', *The Astrophysical Journal*, Accepted for publication

Hinkel, NR & Burger, D 2014, 'Hypatia Catalog Database', *The Astrophysical Journal*, vol, 148, no. 3, pp. 54

Hinkel, NR & Kane, SR 2013, 'Habitability of Exomoons at the Hill or Tidal Locking Radius', *The Astrophysical Journal*, vol. 774, no. 1, pp. 27

Holt, TR, Brown, AJ, Nesvorny, D, Horner, J & Carter, B 2017, 'Cladistical analysis of the Jovian and Saturnian satellite systems', *The Astrophysical Journal*, submitted

Hsu, HW, Postberg, F, Sekine, Y, Shibuya, T, Kempf, S, Hor´anyi, M, Juh´asz, A, Altobelli, N, Suzuki, K, Masaki, Y, Kuwatani, T, Tachibana, S, Sirono, S, Moragas-Klostermeyer, G & Srama, R 2015, 'Ongoing Hydrothermal Activities within Enceladus', *Nature*, vol. 519, no. 1, pp. 207-10

International Astronomical Union, "Planet Definition" Questions & Answers Sheet 2006, visited March 2018, <https://www.iau.org/news/pressreleases/detail/iau0601/>

Kaltenegger, L & Sasselov, D 2011, 'Exploring the Habitable Zone for Kepler Planetary Candidates', *The Astrophysical Journal*, vol. 736, pp. 25

Kaltenegger, L, Traub, WA & Jucks, KW 2006, 'Spectral Evolution of an Earth-like Planet', *The Astrophysical Journal*, vol. 658, pp. 598-616

Kane, SR 2017, 'Worlds without Moons: Exomoon Constraints for Compact Planetary Systems', *The Astrophysical Journal Letters*, vol. 839, no. 2

Kane, SR & Gelino, DM 2012, 'The Habitable Zone Gallery', *PASP*, vol. 124, pp. 323-28

Kane, SR, Hill, ML, Kasting, JF, Kopparapu, RK, Quintana, EV, Barclay, T, Batalha, NM, Borucki, WJ, Ciardi, DR, Haghighipour, N, Hinkel, NR, Kaltenegger, L, Selsis, F & Torres, G 2016, 'A Catalog of Kepler Habitable Zone Exoplanet Candidates', *The Astrophysical Journal*, vol. 830, no. 1

Kane, SR, Kopparapu, RK & Domagal-Goldman, SD 2014, 'On The Frequency Of Potential Venus Analogs From Kepler Data', *The Astrophysical Journal*, vol. 794, no. 1

Kasting, JF, Whitmire, DP & Reynolds, RT 1993, 'Habitable zones around main sequence stars', *Icarus*, vol. 101, pp. 108

Kipping, DM 2009, 'Transit Timing Effects Due to an Exomoon', *MNRAS*, vol. 392, no. 1, pp. 181-89

Kipping, DM, Bakos, GA, Buchhave, LA, Nesvorny, D & Schmitt, A 2012, 'The Hunt for Exomoons with Kepler (HEK). I. Description of a New Observational Project', *The Astrophysical Journal*, vol. 750, no. 2

Kipping, DM, Forgan, D, Hartman, J, Nesvorny, D, Bakos, GA, Schmitt, A & Buchhave, LA 2013, 'The Hunt for Exomoons with Kepler (Hek): III. The First Search for an Exomoon around a Habitable-Zone Planet', *The Astrophysical Journal*, vol. 777, no. 1, pp. 134-50

Kipping, DM, Fossey, SJ & Campanella, G 2009, 'On the Detectability of Habitable Exomoons With kepler-Class Photometry', *MNRAS*, vol. 400, no. 1, pp. 398-405

Kipping, DM, Hartman, J, Buchhave, LA, Schmitt, A, Bakos, GA & Nesvorny, D 2013, 'The Hunt for Exomoons with Kepler (Hek). II. Analysis

of Seven Viable Satellite-Hosting Planet Candidates', *The Astrophysical Journal*, vol. 770, no. 2

Kipping, DM, Nesvorny, D, Buchhave, LA, Hartman, J, Bakos, GA & Schmitt, A 2014, 'The Hunt for Exomoons with Kepler (Hek): IV. A Search for Moons around Eight M-Dwarfs', *The Astrophysical Journal*, vol. 784, no. 1, pp. 28-41

Kipping, DM, Schmitt, A, Huang, CX, Torres, G, Nesvorny, D, Buchhave, LA, Hartman, J & Bakos, GA 2015, 'The Hunt for Exomoons with Kepler (Hek): V. A Survey of 41 Planetary Candidates for Exomoons', *The Astrophysical Journal*, vol. 813, no. 1

Kivelson, MG, Khurana, KK, Russell, CT, Walker, RJ, Warnecke, J, Coroniti, FV, Polanskey, C, Southwood, DJ, Schubert, G 1996, 'Discovery of Ganymede's magnetic field by the Galileo spacecraft', *Nature*, vol. 384, pp. 537-541

Kopparapu, RK 2015, Calculation of Habitable Zones, visited December 2017 <http://www.geosc.psu.edu//thicksimruk15/planets/>

Kopparapu, RK, Ramirez, R, Kasting, JF, Eymet, V, Robinson, TD, Mahadevan, S, Terrien, RC, Domagal-Goldman, S, Meadows, V & Deshpande, R 2013, 'Habitable Zones around Main-sequence Stars: New Estimates', *The Astrophysical Journal*, vol. 765, pp. 131

Kopparapu, RK, SchottelKotte, J, Ramirez, R, Kasting, JF, Domagal-Goldman, S & Eymet, V 2014, 'Habitable Zones Around Main-Sequence Stars: Dependence on Planetary Mass', *The Astrophysical Journal*, vol. 787, pp. L29

Liebig, C & Wambsganss, J 2010, 'Detectability of extrasolar moons as gravitational microlenses', *Astronomy and Astrophysics*, vol. 520, no. A68

Mayor, M & Queloz, D 1995, '51 Pegasi', *Nature*, vol. 378, pp. 6555

Morabito, LA, Synnott, SP, Kupferman, PN & Collins, SA 1979, 'Discovery of Currently Active Extraterrestrial Volcanism', *Science*, vol. 204, pp. 4396

NASA Exoplanet Archive 2017, visited May 2018 <http://www.exoplanetarchive.ipac.caltech.edu>

Nesvorny, D, Alvarellos, JLA, Dones, L & Levison, HF 2003, 'Orbital and Collisional Evolution of the Irregular Satellites', *The Astronomical Journal*, vol. 126, pp. 398-429

Ochsenbein, F, Bauer, P & Marcout, J 2000, 'The VizieR Database of Astronomical Catalogues', *AAS Meeting Abstracts*, vol. 143, pp. 221

Perryman, M 2011, *The Exoplanet Handbook*, Cambridge University Press

Peters, MA & Turner, EL 2013, 'On the Direct Imaging of Tidally Heated Exomoons', *The Astrophysical Journal*, vol. 769, no. 2

Phys.org 2013, Magnetic shielding of exomoons: to be or not to be, visited 18 May 2018 <https://phys.org/news/2013-09-magneticshielding-exomoons.html>

Planet Hunters 2018, The Science, visited January 2018 <http://www.planethunters.org/#/science>

Pollack, JB, Burns, JA & Tauber, ME 1979, 'Gas drag in primordial circumplanetary envelopes - A mechanism for satellite capture', *Icarus*, vol. 37, pp. 587

Porco, CC, Helfenstein, P, Thomas, PC, Ingersoll, AP, Wisdom, J, West, R, Neukum, G, Denk, T, Wagner, R, Roatsch, T, Kieffer, S, Turtle, E, McEwen, A, Johnson, TV, Rathbun, J, Veverka, J, Wilson, D, Perry, J, Spitale, J, Brahic, A, Burns, JA, DelGenio, AD, Dones, L, Murray, CD, Squyres, S 2006, 'Cassini Observes the Active South Pole of Enceladus', *Science*, vol. 311, pp. 1393

Rodgers, LA 2015, 'Most 1.6 Earth-radius Planets are Not Rocky', *The Astrophysical Journal*, vol. 801, no. 1, pp. 13

Sartoretti, P & Schneider, J 1999, 'On the detection of satellites of extrasolar planets with the method of transits', *Astronomy & Astrophysics Supplement*, vol. 134, pp. 553-560

Scharf, CA 2006, 'The Potential for Tidally Heated Icy and Temperate Moons around Exoplanets', *The Astrophysical Journal*, vol. 648, no. 2, pp. 1196

Sheppard, SS 2017, The Jupiter Satellite and Moon Page, visited April 2018 <http://www.dtm.ciw.edu/users/sheppard/satellites/>

Szentgyorgyi, A, Baldwin, A, Barnes, S, Bean, J, Ben-Ami, S, Brennan, P, Budynkiewicz, J, Chun, MY, Conroy, C, Crane, JD, Epps, H, Evans, I, Evans, J, Foster, J, Frebel, A, Gauron, T, Guzm´an, J, Hare, T, Jang, B, Jang, JG, Jordan, A, Kim, J, Kim, KM, Mendes Mendes de Oliveira, C, Lopez-Morales, M, McCracken, K, McMuldroch, S, Miller, J, Mueller, M, Sok Oh, J, Onyuksel, C, Ordway, M, Park, BG, Park, C, Park, SJ, Paxson, C, Phillips, D, Plummer, D, Podgorski, W, Seifahrt, A, Stark, D, Steiner, J, Uomoto, A, Walsworth, R & Yu, YS 2016, 'The GMT-Consortium Large Earth Finder (G-CLEF): an optical Echelle spectrograph for the Giant Magellan Telescope (GMT)', *SPIE*, vol. 9908

Teachey, A, Kipping, DM & Schmitt, AR 2017, 'HEK VI: On the Dearth of Galilean Analogs in Kepler and the Exomoon Candidate Kepler-1625b I', *The Astrophysical Journal*, vol. 155, no. 1

Weiss, LM & Marcy, GW 2014, 'The Mass-Radius Relation for 65 Exoplanets Smaller than 4 Earth Radii', *The Astrophysical Journal*, vol. 783, no. 1, pp. 7

Williams, DM, Kasting, JF & Wade, RA 1997, 'Habitable Moons around Extrasolar Giant Planets', *Nature*, vol. 385, no. 1, pp. 234-36

Wolfgang, A, Rodgers, LA & Ford, EB 2016, 'Probabilistic Mass-Radius Relationship for Sub-Neptune-Sized Planets', *The Astrophysical Journal*, vol. 825, no. 1, pp. 14

Wolszczan, A & Frail, DA 1992, 'A Planetary System around the Millisecond Pulsar PSR1257 + 12', *Nature*, vol. 355, pp. 145-147

Yaqoob, T 2011, *Exoplanets and alien Solar systems*, New Earth Labs, Baltimore

Zollinger, RR, Armstrong, JC & Heller, R 2017, 'Exomoon Habitability and Tidal Evolution in Low-Mass Star Systems', *MNRAS*, vol. 472, no. 1